THE
PHYSICAL REVIEW
A Journal of Experimental and Theoretical Physics Established by E. L. Nichols in 1893
VOL. 54, NO. 8 OCTOBER 15, 1938 SECOND SERIES

The Scattering and Photoelectric Absorption of High Voltage X-Rays in Nitrogen

HAROLD C. TRUEBLOOD AND DONALD H. LOUGHRIDGE
University of Washington, Seattle, Washington
(Received June 20, 1938)

A study of the expansion chamber tracks of 810 kv x-radiation passing through nitrogen shows that the angular distribution of total electrons emitted is in good agreement with the Klein-Nishina formula when allowance is made for the presence of photoelectrons. The latter are distinguished from recoils by the criterion of the maximum Compton energy. Electrons having energies greater than the Compton energy for the corresponding angle of emission were classified as photoelectrons while those having smaller energies were either photo- or recoil electrons. The ratio of recoils to photoelectrons is of the order of 100 in contrast to the theoretical value of about 5000. The angle of bipartition for photoelectrons is about 48° for 360 kev and about 20° for 650 kev photoelectrons.

CONSIDERABLE experimental work has been done on the scattering and photoelectric absorption of low voltage x-rays,[1–4] but relatively little work has been done in the region of high voltage x-rays.[5] The latter region is of special interest because it affords an opportunity to test more fully the present quantum theory of the interaction of radiation and matter. According to present theory[6, 7] the photoelectric absorption of high voltage x-rays in light elements is practically zero, while pair production has not begun. Thus, practically all of the absorption should be due to incoherent scattering, and both the angular distribution of the emitted electrons and the absorption cross section should be given by the Klein-Nishina formula.

The present investigation lies in the region of 100–800 kev, and includes a determination of the energy of recoil electrons as a function of the angle of emission and a determination of the angular distribution of photoelectrons as a function of the energy. Also, a preliminary value of σ/τ (the ratio of the number of recoil electrons to the number of photoelectrons) is obtained.

[1] Hewlett, Phys. Rev. **17**, 284 (1921); Phys. Rev. **19**, 265 (1922); Phys. Rev. **20**, 688 (1922). Hahn, Phys. Rev. **46**, 149 (1934).
[2] Bothe, Zeits. f. Physik **20**, 237 (1923); Bless, Phys. Rev. **30**, 871 (1927).
[3] Bubb, Phys. Rev. **23**, 137 (1924). Compton and Simon, Phys. Rev. **25**, 309 (1925); Proc. Nat. Acad. Sci. **11**, 303 (1925); Phys. Rev. **26**, 289 (1925). Ikeuti, Comptes rendus **180**, 1257 (1925). Nuttall and Williams, Phil. Mag. **1**, 1217 (1926). Kirchner, Physik. Zeits. **27**, 385 (1926); Physik. Zeits. **27**, 799 (1926); Ann. d. Physik **81**, 1113 (1926); Ann. d. Physik **83**, 969 (1927).
[4] Eggleston and Martin, Proc. Roy. Soc. **162**, 95 (1937).
[5] Read and Lauritsen, Phys. Rev. **45**, 433 (1934). Read, Proc. Roy. Soc. **152**, 402 (1935). Cuykendall, Phys. Rev. **50**, 105 (1936).
[6] Klein and Nishina, Zeits. f. Physik **52**, 853 (1929). Heitler, *Quantum Theory of Radiation* (Oxford Press).
[7] Sauter, Ann. d. Physik **11**, 454 (1931).

Discussion of Theory

Probability of electron emission

Using relativistic wave equations and Born's approximation which can be applied for light elements, Sauter[7] obtained for photoelectric emission the result

$$\frac{\varphi_k}{\varphi_0}=\frac{3}{2}\frac{Z^2}{137}\left(\frac{\mu}{k}\right)^5(\gamma-1)^{\frac{3}{2}}\left[\frac{4}{3}+\frac{\gamma(\gamma-2)}{\gamma+1}\times\left(1-\frac{1}{2\gamma(\gamma^2-1)^{\frac{1}{2}}}\log\frac{\gamma+(\gamma^2-1)^{\frac{1}{2}}}{\gamma-(\gamma^2-1)^{\frac{1}{2}}}\right)\right], \quad (1)$$

where ϕ_k is the cross section for the photoelectric emission of K-electrons, $\phi_0=(8\pi r^2)/3$ is the cross section for classical scattering, Z is the atomic number, μ is the rest energy of an electron, k is the energy of the incident photon, and

$$\gamma=1/(1-\beta^2)^{\frac{1}{2}}=(k+\mu)/\mu$$

is the ratio of the total energy (kinetic energy $+mc^2$) of the electron to the rest energy. Since the K shell contains two electrons and experiment shows that these contribute about 80 percent of the photoelectric effect,[8] one may obtain the approximate total photoelectric cross section by doubling the value obtained from Eq. (3) and multiplying by a factor of 5/4.

The cross section for incoherent scattering can be calculated in a similar manner, except that in this case two light quanta are involved and the process is of the second order. If the energy of the primary quanta is much greater than the binding energy of the electrons, the scattering electrons can be considered as free. By the use of relativistic equations, Klein and Nishina[6] have obtained the following formula for the scattering cross section of free electrons:

$$d\varphi_s=\frac{r_0^2\,d\Omega_\varphi}{2}\frac{k^2}{k_0^2}\left(\frac{k_0}{k}+\frac{k}{k_0}-\sin^2\varphi\right), \quad (2)$$

where $d\phi_s$ is the differential scattering cross section, r_0 is the classical radius of an electron, $d\Omega_\varphi$ is the differential solid angle, k_0 and k are the energies of the incident and scattered quanta, and ϕ is the angle through which a quantum is deflected. If this equation is integrated over all angles, one obtains for the total cross section

$$\frac{\varphi_s}{\varphi_0}=\frac{3}{4}\left\{\frac{1+\alpha}{\alpha^3}\left[\frac{2\alpha(1+\alpha)}{1+2\alpha}-\log(1+2\alpha)\right]+\frac{1}{2\alpha}\log(1+2\alpha)-\frac{1+3\alpha}{(1+2\alpha)^2}\right\}, \quad (3)$$

where ϕ_0 is again the classical cross section for scattering and $\alpha=k_0/\mu=h\nu_0/mc^2$.

Angular distribution of recoil electrons

The angular distribution of recoil electrons may be obtained from Eq. (2). This equation as it stands represents the relative number of photons that are scattered into a solid angle $d\Omega_\varphi$ at an angle ϕ with the direction of the incident beam. One may now substitute for $d\Omega_\varphi$ the quantity $2\pi\sin\phi\,d\phi$ and obtain the total (relative) number of photons scattered between the angles ϕ and $\phi+d\phi$. From the well-known theory of the Compton effect one obtains

$$E_{\text{kin}}=h\nu-h\nu'=h\nu\frac{\alpha\ \text{vers}\ \varphi}{1+\alpha\ \text{vers}\ \varphi};$$
$$\therefore\quad \frac{h\nu'}{h\nu}=\frac{k}{k_0}=\frac{1}{1+\alpha\ \text{vers}\ \varphi} \quad (4)$$

and with this further substitution for k/k_0, Eq. (2) becomes

$$d\varphi_s=r_0^2\pi\sin\varphi\,d\varphi\left(\frac{1}{1+\alpha\ \text{vers}\ \varphi}+\frac{1}{(1+\alpha\ \text{vers}\ \varphi)^3}-\frac{\sin^2\varphi}{(1+\alpha\ \text{vers}\ \varphi)^2}\right). \quad (5)$$

If ϕ is expressed in terms of θ by means of the Compton theory, then Eq. (5) shows the total number of electrons ejected between the angles θ and $\theta+d\theta$, and this quantity divided by $2\pi\sin\theta\,d\theta$ gives the number of recoil electrons per unit solid angle. The final result is

$$\frac{d\varphi_s}{d\Omega_\theta}=\frac{r_0^2(1+\alpha)^2(2-\sin 2\theta)}{2a^2\cos^3\theta}\times\left[\frac{a}{a+2\alpha}+\left(\frac{a}{a+2\alpha}\right)^3-\frac{4(a-1)}{(a+2\alpha)^2}\right], \quad (6)$$

[8] Rutherford, Chadwick, and Ellis, *Radiations from Radioactive Substances* (Cambridge University Press) p. 464.

TABLE I. *Ratio of total scattering to the photoelectric absorption.*

$h\nu$ (KEV)	σ/τ
350	2260
510	4875
650	8100

where $a=(1-\alpha)^2\tan^2\theta-1$. If $d\varphi/d\Omega_\theta$ is evaluated for various angles θ, a graph of the results will show the angular distribution of the recoil electrons in a plane cross section along the incident beam of radiation. Such a curve, computed for 510 kev, is shown in Figs. 6 and 7, where the area under the theoretical curve has been adjusted to be equal to that under the experimental curve so as to refer to equal numbers of tracks in both cases.

Theoretical values of σ/τ, or the ratio of the total scattering per atom to the photoelectric absorption, may be obtained by means of Eq. (1), (3)

$$\frac{\sigma}{\tau}=\frac{Z\left(\frac{\varphi_s}{\varphi_0}\right)}{\frac{5}{2}\left(\frac{\varphi_k}{\varphi_0}\right)}=\frac{Z\left[\frac{3}{4}\left\{\frac{1+\alpha}{\alpha^3}\left(\frac{2\alpha(1+\alpha)}{1+2\alpha}-\log(1+2\alpha)\right)+\frac{1}{2\alpha}\log(1+2\alpha)-\frac{1+3\alpha}{(1+2\alpha)^2}\right\}\right]}{\frac{5}{2}\left[\frac{3}{2}\frac{Z^5}{137}\left(\frac{\mu}{k}\right)^5(\gamma^2-1)^{\frac{1}{2}}\left\{\frac{4}{3}+\frac{\gamma(\gamma-2)}{\gamma+1}\left(1-\frac{1}{2\gamma(\gamma^2-1)^{\frac{1}{2}}}\log\frac{\gamma+(\gamma^2-1)^{\frac{1}{2}}}{\gamma-(\gamma^2-1)^{\frac{1}{2}}}\right)\right\}\right]}. \tag{7}$$

A few values for nitrogen are shown in Table I. In making comparisons with our experiments, the 510 kev value will be used, since this lies near the maximum[9] of the energy spectrum of the 800 kv x-ray tube.

EXPERIMENTAL PROCEDURE

The interaction of high voltage x-rays with nitrogen was studied by means of a 6″ automatic cloud chamber. A sylphon tube, the bottom of which was closed with a brass spinning, formed the lower portion of the chamber, and when compressed air was admitted to the brass casting surrounding the sylphon, the sylphon was compressed the desired amount. Then at the proper instant, a valve was opened by an electromagnet, thus allowing the air to escape and the chamber to expand. The expansions and all other events occurring during the operation of the chamber were controlled by a motor-driven commutator arranged so that the expansions occurred every half minute.

Nitrogen was introduced into the chamber by allowing it to bubble slowly through 95 percent ethyl alcohol, and the alcohol that distilled over into the chamber was used to form the condensation on the ions.

An 800 kv x-ray tube was located in the room above the cloud chamber apparatus, and radiation from this tube passed through a $\frac{3}{4}''\times13''$ hole in a lead cylinder in the three-foot thick concrete floor of that room and then down into a lead tunnel located above the cloud chamber. In this tunnel, the x-rays were further collimated so that the beam passing through the chamber was $\frac{1}{4}''$ in diameter. A solenoid operated lead shutter prevented the radiation from entering the chamber except during a very small interval at the time of the expansion. Soft radiation was removed from the beam of x-rays by a $\frac{1}{2}''$ lead filter, and a special filter located immediately above the chamber removed the K-radiation of lead. The x-rays entered the chamber through a Cellophane window $\frac{5}{16}''$ in diameter. In order to accommodate the vertical beam of radiation, the chamber was used in the vertical position. A pair of Helmholtz coils was used to produce a magnetic field so that one could determine the energies of the emitted electrons.

Photographs were obtained by a single Sept camera (f: 3.5 lens) placed directly in front of the cloud chamber, and sufficient illumination was provided by two 2000-w Movieflood lamps and a set of hollow cylindrical glass lenses filled with benzene. The photographs were reprojected to

[9] Determined by Mr. John Rose, physicist of the Swedish Hospital, Seattle Washington, by means of total absorption measurements in water and lead. A similar result was obtained by Donald H. Loughridge in preliminary measurements with a crystal spectrograph. The maximum intensity of the x-rays was found to occur near 500 kv.

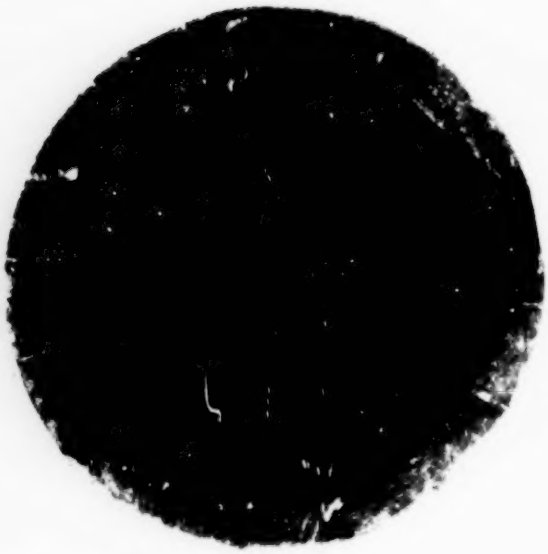

FIG. 1. Photoelectron track 673 kev showing change in curvature due to close collision.

normal size on a ground glass screen and could be viewed easily from the rear. In order to avoid distortion of the tracks, the optical system in the reprojecting apparatus was identical to that with which the photographs were taken.

The current through the Helmholtz coils was measured about every twelve pictures, and the peak voltage across the x-ray tube was kept constant at 810 kv. The magnetic field had been previously calibrated by means of a small search coil, and the x-ray tube peak voltage had been measured with a rotary voltmeter.[10]

The curvatures of the tracks were measured by comparison with a set of curves having known radii of curvature which varied from 1 to 15 cm in steps of 0.1 cm and the initial directions of the tracks were measured by means of a protractor with divisions every 5°.

In order to be satisfactory for measurement, a track must begin within the x-ray beam and not less than $\frac{1}{8}''$ from the walls of the chamber. The track must have a reasonably definite point of origin, a definite initial direction, and a constant radius of curvature. It must also remain within the beam of light, the mean thickness of which was about $\frac{1}{2}''$ ($\frac{3}{8}''$ at the x-ray beam). Some tracks showed definite changes in curvature due to collisions of the electron with other particles (Fig. 1); these tracks could be measured if the curvature remained constant along a sufficient length of track.

[10] Henderson, Goss, and Rose, Rev. Sci. Inst. **6**, 63 (1935).

Discussion of Results

Maximum energy of electrons

If one plots the total number of tracks in each 50 kv interval against the corresponding energy, one obtains the curve shown in Fig. 2. This curve has a definite bend near 600 kv, and the portion above 650 kv is a straight line while that below 550 kv has only a small curvature. If the latter portion of the curve is extended down to the energy axis, the cut-off value is found to be 625 kv which is very near the maximum energy of the Compton recoil electrons. One may thus infer that the electrons are of two types: photoelectrons which have a maximum kinetic energy of 820 kev and recoil electrons with a maximum kinetic energy of 625 kev. Both of these energies are very near the theoretical values of 810 kev and 612 kev.

According to the Compton theory, the energy of a recoil electron is a definite function of its angle of emission. This relationship has been verified experimentally in the region of 100 kv x-rays and the present data extend this region to 810 kv. The maximum recoil energy for *any particular direction of emission* can be obtained by plotting only these tracks which occur within 5° of that direction (i.e., in a 10° interval) and drawing a curve similar to that in Fig. 2. A number of these curves are shown in Figs. 3, 4, and 5 and the maximum energies for angles up

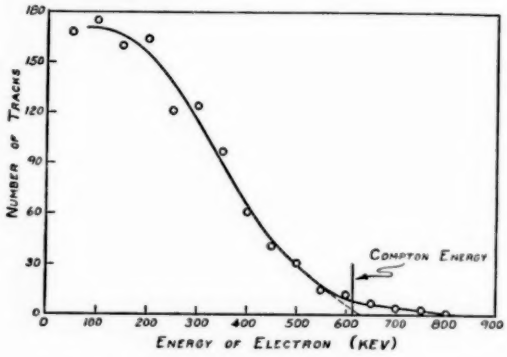

FIG. 2. Total energy distribution.

to 52° check the theoretical values within a few percent.

Angular distribution

If the total number of electrons emitted in each 5° angle is plotted as a function of the angle, one obtains the curve shown in Fig. 6. The smooth curve in the same figure represents the angular distribution of the recoil electrons according to the Klein-Nishina formula. Both curves are for a plane cross section along the incident beam of radiation. Although one is not strictly justified in drawing a curve through each experimental point where the statistical fluctuations may be large, such a curve has been drawn in order to show more clearly the general trend of the experimental results. In Fig. 6 the peak of the experimental curve corresponds rather closely to that of the Klein-Nishina curve, but at 15° the experimental curve rises above the theoretical curve and a little beyond 60° it crosses below again. The sharpness of the experimental peak is to be expected from the experimental set-up. Only one camera was used, and the thickness of the photographic plane was a little less than half an inch. Thus a track which appears to have an initial angle of 0° might actually have an angle of 5° measured in a direction perpendicular to the plane. The tracks with small initial angles should therefore be concentrated near 0°, while tracks with large initial angles should be displaced only slightly toward the smaller angles. The portion of the experimental curve beyond 60° contains only a small number of tracks, and due to statistical fluctuations should not be expected to conform closely with theory. The excessive number of tracks between 15° and 60° however, cannot be explained on the basis of experimental procedure, since the experimental displacement is toward smaller angles instead of larger, and statistical fluctuations should be as much below the curve as above.

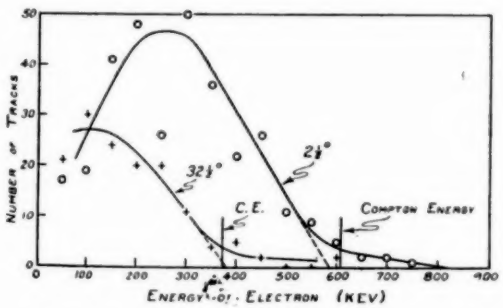

FIG. 3. Energy distribution at 2½° and 32½°.

In order to explain this excessive emission, there seem to be two alternatives: either the Klein-Nishina formula is not correct in this region or a considerable number of photoelectrons are present. Of these two alternatives, the latter seems the more probable.

According to quantum mechanical theory, the angle of bipartition, or the angle such that equal numbers of electrons are ejected on either side, for photoelectrons is given by the relation[11]

$$\cos\theta_b=\beta=\frac{\{h\nu(h\nu+2mc^2)\}^{\frac{1}{2}}}{h\nu+mc^2}. \tag{8}$$

If $h\nu=510$ kev (or mc^2), then $\theta_b=30$ percent, and if $h\nu=100$ kev, $\theta_b=57°$. Since the radiation used in the present experiment ranges from 100 to 800 kv with a maximum intensity near 500 kv, the angle of bipartition is of the right order of magnitude to produce the observed effect.

The initial angle was found by measuring the angle of a line tangent to the track at the point of

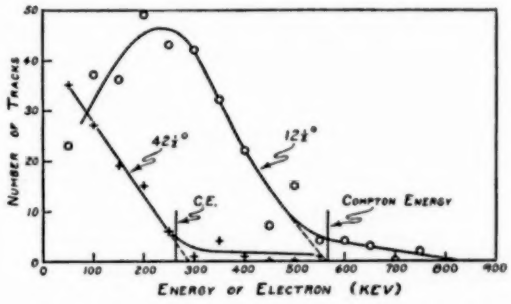

FIG. 4. Energy distribution at 12½° and 42½°.

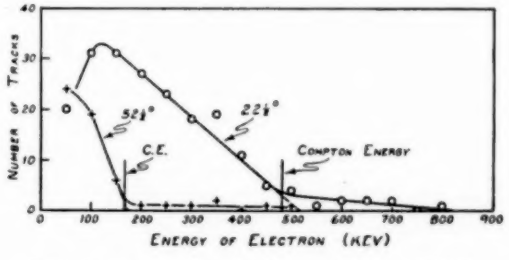

FIG. 5. Energy distribution at 22½° and 52½°.

[11] This equation was derived for small values of β and hence is not strictly true when β is large, although Sauter has shown that it is nearly correct for values of β as high as 0.52.

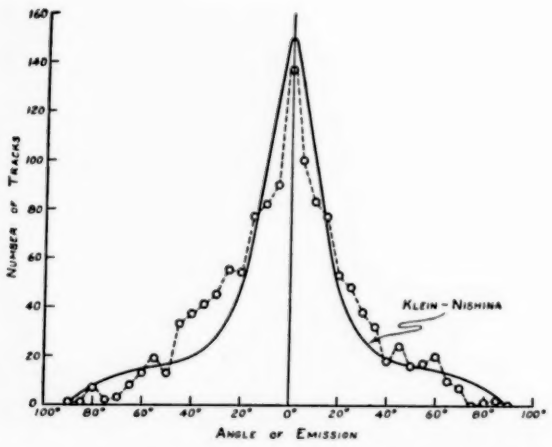

FIG. 6. Angular distribution. (With magnetic field.)

origin. In order to determine whether the presence of a magnetic field (thus producing curved tracks) caused a systematic error in the measurement of the angles, about 400 photographs were taken without the magnetic field. The tracks were then straight instead of curved and were a little easier to measure. This set of data (821 tracks) is plotted in Fig. 7 and again compared with the Klein-Nishina curve. The experimental curve obtained without the magnetic field is similar to that obtained with the magnetic field, thus showing that no systematic error is present.

The principal difference between the experimental curves in Figs. 6 and 7 is that the shoulder of the latter curve is distinctly lower. In Fig. 6 the excessive emission begins at 15°, while in Fig. 7 it does not begin until 20°. If the excessive emission is due to photoelectrons, this effect may be explained by the experimental conditions under which the two sets of data were obtained. The first set of data was obtained by measuring both the angle and the curvature of a track, while the second set was obtained by measuring the angle only. Since a larger proportion of high energy tracks are satisfactory for measurement of curvature than are low energy tracks, and satisfactory conditions for the measurement of angle are about the same in each case, the second set of data contains a larger proportion of low-energy tracks. The angle of bipartition for low-energy photoelectrons is large, thus tending to spread out the angular distribution curve toward higher angles.

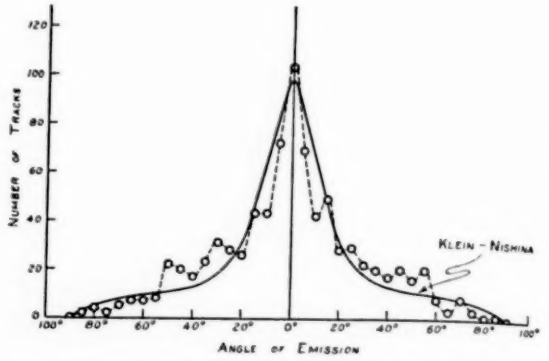

FIG. 7. Angular distribution. (Without magnetic field.)

Maximum value of σ/τ

Photoelectrons and recoil electrons can be identified only by their energies. The kinetic energy of a photoelectron (neglecting the binding energy) is equal to the energy of the incident quantum of radiation, while the kinetic energy of a recoil electron is given by the Compton theory. Thus, if monochromatic radiation were used, the photoelectrons and the recoil electrons would be separated into two distinct groups. However, in the present experiment, the incident radiation has a continuous spectrum and such a distinct separation of the two types of emitted electrons is not possible. In this case, one can obtain only a partial separation. The maximum energy of the radiation is 810 kev and from the Compton theory one may compute the corresponding maximum energy of the recoil electrons. Any electron which has a kinetic energy greater than the maximum Compton energy for its particular angle of emission may therefore be classified as a photoelectron, and any electron which has a smaller energy may be either a photoelectron or a recoil electron.

If T represents the total number of emitted electrons and T_1 the known number of photoelectrons, then the maximum value of σ/τ, or the ratio of the number of recoil electrons to the number of photoelectrons, is given by the equation

$$\sigma/\tau=(T-T_1)/T_1. \tag{9}$$

The results of the first set of data (about 2600 photographs from which were obtained 966 tracks) indicated the presence of a much larger number of photoelectrons than had been expected

from theory. (Eq. (7).) Later the experiment was repeated, and the second set of data (about 1100 photographs from which were obtained 216 tracks) indicated an even lower value of σ/τ. Both sets of data were then rechecked, and all tracks that may have been due to photoelectrons were carefully remeasured.

Of the electrons in the first set of data that apparently had energies greater than the maximum Compton energy, 12 were retained as photoelectrons because no reason could be found for classifying them otherwise, 27 seemed to be photoelectrons but were slightly doubtful, and 30 were doubtful. A similar grouping of the second data gave 8, 10, and 8.

In computing the value of σ/τ, only the first two of these groups were used, that is, only those photoelectrons about which there can be scarcely any question. In Fig. 8 we have plotted the respective energies of these photoelectrons against their energies and show by the full line the maximum Compton recoil energy as a function of angle. All of the electrons in the first group have measured energies at least 10 percent greater than the maximum Compton energy (well above the probable error), while those in the second group have energies at least 3 percent greater. In both groups, about one-fourth of the electrons have energies more than double the corresponding Compton values.

The number of photoelectrons obtained in this manner does not necessarily give the true proportion, since more of the high energy tracks are satisfactory for measurement than low-energy tracks. In order to overcome this difficulty, in the second set of data, all of the tracks which began within the x-ray beam were counted, but were unsatisfactory for precise measurement. However, if all of these tracks were assumed to be due to recoil electrons, the value of σ/τ would probably be too high. Therefore, in order to obtain an experimental value which would be closer to the true value, the energies of the unmeasured tracks were estimated by inspection and divided into three groups—0–75 kev, 75–375, and 375 kev or more. Since the filtration used ($\frac{1}{2}$" lead plus a special filter to absorb the K-radiation of lead) effectively cut out the radiation below 100 kev, all the electrons in the first estimated group were assumed to be of the recoil type. The second energy range contained a large number of accurately measured tracks and of these only a small proportion were due to photoelectrons, while the third energy range contained a smaller number of accurately measured tracks of which a considerably larger proportion were due to photoelectrons. The number of photoelectrons in the second and third energy ranges of the estimated tracks were then assumed to occur in the same proportion as in the corresponding energy range of the accurately measured tracks. The unmeasured tracks in the first set of data were not counted, but were assumed to occur in the same proportion as those in the second set of data. In these data, the numbers of estimated tracks in the three respective groups were 555, 429, and 50, while the total number of accurately measured tracks was 216.

The maximum value of σ/τ was computed from Eq. (9), where T is the sum of the measured

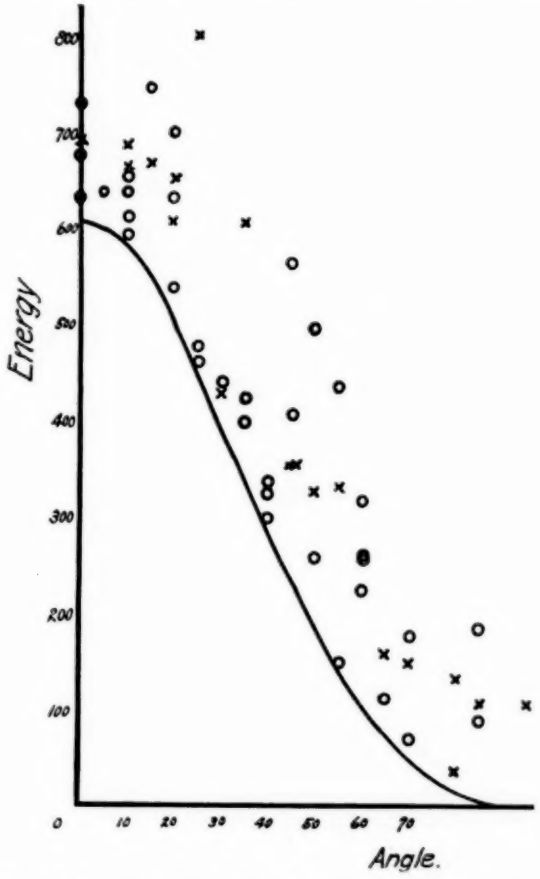

FIG. 8. Energy distribution of photoelectrons. o—second group. x—first group. Full line curve gives Compton upper energy limit for recoils.

and the estimated tracks and T_1 is the sum of the photoelectrons actually counted and those estimated from the tracks which were unsatisfactory for exact measurement. If only those photoelectrons in Group I are considered, the maximum value of σ/τ is 113, while if both groups are considered, the value is 40. Under the assumption that the estimated tracks contain no photoelectrons (all recoil electrons) the corresponding values of σ/τ are 342 and 117. Thus the maximum experimental value of σ/τ for a plane cross section is of the order of 100, which is to be compared with the theoretical value of 4875.

A number of errors are inherent in the experimental procedure, but all of these tend to make the value of σ/τ even smaller. These errors are due to two major causes: the thickness of the photographic plane and the difference between the angular distribution of the photoelectrons and recoil electrons. Since the thickness of the photographic plane is nearly half an inch, the measured tracks do not lie strictly in a plane but rather in a shallow box. The measured angles therefore tend to be a little smaller than the actual angles, and hence the maximum Compton energy for any given electron tends to be too large, thus reducing the number of photoelectrons and making σ/τ too large. Also, the energy which one measures is that due to the component of velocity in the plane of the photograph, and this energy is slightly smaller than the actual energy, which again reduces the number of photoelectrons and makes σ/τ too large.

The difference in angular distribution may be represented by the angle of bipartition. This angle for recoil electrons is always 0°, while that for photoelectrons is given by the relation $\cos\theta_b=\beta$. For 510 kv, θ_b is approximately 30°. In order to visualize the angular distributions more clearly, consider the diagram in Fig. 9. For purpose of discussion, let the recoil electrons be ejected only within the solid cone R and let the photoelectrons be ejected only between the two larger cones P. If now a planar shell cuts through these figures along their common axis, the shell will cut out a volume r_1 from the solid cone and a volume p_1 between the two other cones. Let r be the total volume of R and p the total volume of P. Then from geometrical considerations,

$$r_1/r>p_1/p;\quad\therefore\quad r_1/p_1>r/p.$$

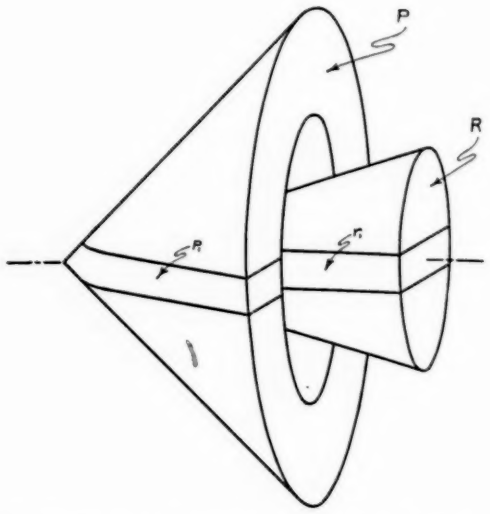

FIG. 9. Illustration of angular distribution. Photoelectron cones, P, and recoil cones, R.

Therefore the value of σ/τ (proportional to r_1/p_1) measured in the planar shell is greater than σ/τ measured in the total volume. As the thickness of the shell increases, σ/τ_s approaches σ/τ_v. In the present case, the actual thickness of the shell is nearly half an inch, and hence the measured value of σ/τ is greater than that in the total volume and less than that in a thin shell. Since the theoretical value of 4875 is for the total volume while the experimental value of 100 is for a thick shell, the experimental value must be made smaller in order to be comparable with theory.

The major experimental error in addition to that in measuring the tracks was the variation of the magnetic field. The current through the Helmholtz coils was ordinarily about 25 to 26 amp. and the variation from the mean during a fifteen-second reading was usually less than 0.5 amp., but occasionally the current would drop as much as 1 or 2 amp. However, in a total of more than 300 readings, only 5 times was the current observed to drop as much as 10 percent, and the lowest of these was 15.1 percent (from 25.9 to 22.0 amp.). This would cause an error of about 22 percent in the measurement of the energy. However, even if the measurement of the energy were continuously 25 percent too high, more than half of the photoelectrons would still remain.

Further evidence for a low value of σ/τ is obtained from measurements of the energy alone

(Fig. 2) and measurements of the angle alone (Figs. 6 and 7). In Fig. 2, the slope of the curve beyond 650 kv indicates the presence of a considerable number of photoelectrons at lower energies, while in Figs. 6 and 7 the excessive emission between 10° and 60° also indicates the presence of a considerable number of photoelectrons. These three curves are entirely independent of one another and are consistent in indicating the same result.

Angular distribution of the photoelectrons

Because of the limited number of photoelectron tracks, one cannot make a precise determination of the angle of bipartition for any given energy. However, one can obtain a good approximation by grouping the tracks into larger intervals of both angle and energy and then comparing the experimental angle of bipartition thus obtained with the theoretical angle corresponding to the mean value of the energy. Such a determination, even though approximate, will extend the region in which these data are known from about 88 kev[4] to 650 kev.

In the present data (see Fig. 10) the photoelectrons were divided into two energy ranges—200 to 500 kev with a mean value of 364 kev (22 tracks), and 500 to 800 kev with a mean value of 650 kev (23 tracks). Photoelectrons with energies below 200 kev were not considered because they were near to the region which had previously been investigated. The interval of angle was taken as 10°, or the sum of two adjacent 5° intervals plotted at the mean. The experimental points plotted in Fig. 10 thus represent at each angle the total number of tracks in the given energy range which have an initial angle in a 10° interval. Since these experimental data are for a planar shell rather than a spherical volume, the relative total number of photoelectrons emitted at each angle may be obtained by multiplying the experimental value at a given angle θ by the sine of that angle. The relative curves for a spherical volume are shown in the same figure. Since both curves are nearly symmetrical, the angle of bipartition is nearly equal to the angle of the maximum.

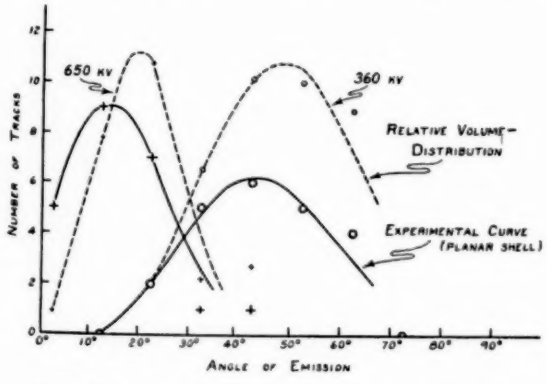

FIG. 10. Angular distribution of photoelectrons.

According to quantum mechanical theory, the angle of bipartition θ_b for photoelectrons is given to the first order approximation by the expression

$$\cos \theta_b = \beta. \tag{10}$$

Sauter[7] has shown that although this expression was obtained by neglecting higher powers of β, it differs very little from a more exact calculation of $\cos \theta_b$ for values of β as high as 0.52 (88 kev). By means of a nonrelativistic calculation, the following expression was obtained:[7]

$$\cos \theta_b = \frac{v/c}{1+h\nu/2mc^2}, \tag{11}$$

where the velocity v of the photoelectrons is to be computed nonrelativistically. The latter equation has been verified experimentally up to 88 kev,[4] but it cannot be used in the present case where the relativity correction is large.

For 360 kev and 650 kev radiation, the angles of bipartition calculated from Eq. (10) are, respectively, 36° and 26°. These are to be compared with the experimental values of 48° and 20°. Because of the method of separating the photoelectrons, the experimental angle of 48° is probably too high. Only those photoelectrons which have energies greater than the Compton energy can be counted, and with low energy electrons, this method favors large angles. For example, the data include four photoelectrons with an energy of about 250 kev; one of these has an initial angle of 50° and the other three an angle of 60°. There may be other photoelectrons with the same energy at smaller angles, but none can be counted below 45° because the Compton energy at this angle is 236 kev. Thus the apparent angle of bipartition may be shifted toward large angles. On the other hand, the experimental angle of 20° may be too low, because in this case (high energy electrons) nearly all of the electrons

are counted, but the thickness of the photographic plane favors small angles.

If one considers the experimental difficulties, the values of 48° and 20° for 360 kev and 650 kev radiation are in reasonably good agreement with theory.

The Klein-Nishina formula

The present experimental data offer no conclusive evidence in regard to the exactness of the Klein-Nishina formula. Read and Lauritsen found that for a range of 50 to 20 x-units (the wave-length of 500 kev radiation is 24.7 x-units) the *total* absorption coefficients of carbon and aluminum are within 1 percent of the Klein-Nishina value, and they state that their maximum likely error is 3 percent. Since a measure of the total absorption is a measure of the total number of photons removed from the incident beam, it is also a measure of the total number of electrons taking part in the interaction (if one assumes no coherent scattering). Thus, if only recoil electrons are emitted and the Klein-Nishina formula is correct, a measure of the total absorption should check the Klein-Nishina formula exactly. However, if the error in this experiment were as much as 3 percent, three photoelectrons in a total of 100 could be present and still not be detected. This corresponds to a σ/τ value of about 30. Consequently an experiment of this type cannot distinguish between the theoretical value of σ/τ of about 5000 which one gets from Eq. (9), and a value as low as 30. According to the present results, the value of σ/τ for 500 kev x-rays in nitrogen is of the order of 100 and is probably less than this; however, just how much less cannot be determined with the present data. If σ/τ is less than 30, the Klein-Nishina value may be too high.

The authors wish to express their appreciation to the Swedish Hospital of Seattle for facilities extended.

OCTOBER 15, 1938 PHYSICAL REVIEW VOLUME 54

Initial Recombination of Ions

L. ONSAGER
Sterling Chemistry Laboratory, Yale University, New Haven, Connecticut

(Received August 19, 1938)

The probability that a pair of ions of given initial separation will recombine with each other is computed from the laws of Brownian motion, which is the proper procedure whenever the Langevin factor equals unity, as in gases at high pressures. In the absence of forces other than the Coulomb attraction, the probability of escape equals the reciprocal of the Boltzmann factor. This result includes the correlation between temperature and pressure coefficients of the ionization by light particles previously predicted by Compton, Bennett and Stearns, if one allows their basic hypothesis about the laws which govern the initial separation of the ions. The effect of an electric field is to increase the fraction of escaping ions by a factor which in the incipient stage of the effect is proportional to the field intensity and independent of the initial distance, although it depends on the orientation of an ion pair. The predicted increase of the ionization current is a little more than one percent for every 100 volts/cm, which accounts for the observed effects of fields exceeding 1500 volts/cm. A reasonable amount of columnar recombination would help to explain the proportionately greater effects of weak fields. The inferred initial separations of the ions are apparently compatible with present knowledge of electron scattering and attachment.

IT stands to reason that an electron, ejected by a photon or by collision with a charged particle, if not removed too far before it becomes attached to a molecule or otherwise slowed down to thermal velocities, may recombine with its parent ion. The possibility of such *initial recombination* was pointed out long ago by Rutherford.[1] In recent years particular attention has been paid to the possible effect of this process upon the ionization of air by particles of low ionizing power (cosmic rays, β-(γ-) rays).

[1] E. Rutherford, *Radioactivity* (1904), p. 33.

Compton, Bennett and Stearns[2] were indeed able to correlate the effect of temperature with that of pressure; but the observed increase of the ionization with the collecting field belies their prediction that fields of much less than 40,000 volts/cm would hardly interfere with the initial recombination. From a rigorous analysis of the Brownian motion problem involved, I have been led to a different conclusion.

At present, initial recombination is not as confidently assumed as *columnar recombination* ("en colonnes"), which involves all the ions in the track left by one ionizing particle. Jaffé,[3] who carried out an approximate computation of the latter effect, found that it accounts very well for the much less complete collection of ions in the case of α-rays, as compared with β-rays at the same gas pressure. He was not, however, entirely satisfied with his attempts to correlate the collected amounts of ionization caused by β-rays for different gas pressures. While the discrepancies which aroused his suspicion have only been confirmed by subsequent experiments, recent authors have at times given less weight to them.[4]

The theories of initial and columnar recombination are related, for both processes depend on the initial distances of separation of ions of opposite sign. As yet, our best information about this question is inference from the collection of ions. However, granted a good guess about the distribution of initial distances, the extent of recombination can be computed from the laws of diffusion and migration.

The theory of columnar recombination leads to a nonlinear system of differential equations, and Jaffé's approximate solution is not easily improved.

The theory of initial recombination reduces to a problem of Brownian motion of *one particle* under the action of the collecting field together with the Coulomb attraction, with the combined potential (in polar coordinates r, Θ)

$$w=-\epsilon X r\cos\Theta-(\epsilon^2/Dr)$$
$$=kT(-2\beta r\cos\Theta-(2q/r)). \quad (1)$$

The equation of Brownian motion

$$\partial f/\partial t=kT(\omega_1+\omega_2)\times$$
$$\times\operatorname{div}(\exp(-w/kT)\operatorname{grad} f\exp(w/kT)), \quad (2)$$

with the potential w of Eq. (1), I have studied before in order to compute the ionization of weak electrolytes in strong fields,[5, 6] and I have shown that velocity of ionization is increased by an external field, in the ratio:

$$K(X)/K(0)=F(2\beta q)$$
$$=J_1(4(-\beta q)^{\frac{1}{2}})/2(-\beta q)^{\frac{1}{2}}. \quad (3)$$

The theory of (general) recombination on the basis of Eq. (2) is equivalent to Langevin's well-known treatment,[7] and leads to his formula for the coefficient of recombination in terms of the mobilities of the ions,

$$\alpha=4\pi\epsilon^2(\omega_1+\omega_2)/D, \quad (4)$$

independent of the field. The verification of Eq. (4) affords a general criterion for the applicability of Eq. (2); thus it is indicated that our considerations will be valid in gases for pressures above a few atmospheres.

The derivation of Eq. (3) involved the solution of Eq. (2) for the case stationary flow with a source at the origin and a sink for $r=\infty$. The problem of initial recombination involves the case of a source at a general point (r, Θ) with sinks at origin and infinity:

$$f(\infty, \Theta)=0,$$
$$f(0, \Theta)<\infty. \quad (5)$$

The solution to this problem—the Green function of Eq. (2)—is rather complicated.[6] Fortunately, as an equation for $f\exp(w/kT)$, Eq. (2) is self-adjoint in 3 dimensions, and considering the symmetry of its Green function, one can show that the chance φ for any ultimate fate of the ion must itself satisfy the differential equation

$$\operatorname{div}(\exp(-w/kT)\operatorname{grad}\varphi)=0, \quad (6)$$

which admits the trivial solution $\varphi=1$ (certainty). In the following, we shall understand by $\varphi(r, \Theta)$ the probability that an ion pair of initial separation r at an angle Θ with the "downstream" direction of the field will escape initial recombi-

[2] A. H. Compton, R. D. Bennett and J. C. Stearns, Phys. Rev. **39**, 873 (1932).
[3] G. Jaffé, Ann. d. Physik IV, **42**, 303 (1913).
[4] H. Zanstra, Physica **2**, 817 (1935).
[5] L. Onsager, J. Chem. Phys. **2**, 599 (1934).
[6] L. Onsager, Diss. Yale, 1935.
[7] P. Langevin, Ann. chim. phys. VII, **28**, 433 (1903).

nation. Obviously, the boundary conditions are

$$\varphi(0, \Theta)=0, \qquad \varphi(\infty, \Theta)=1. \tag{7}$$

In the absence of a collecting field ($\beta=0$), the required solution is simply the reciprocal of the Boltzmann factor:

$$\varphi=e^{w/kT}=e^{-2q/r}. \tag{8}$$

At the corresponding stage of their considerations, Compton, Bennett and Stearns[2] introduced the assumption that the effect of the density ρ upon the distribution $f_0(r)$ of initial displacements can be described by a simple scale-factor:

$$f(\rho, r)=\rho^3 F(\rho r). \tag{9}$$

Combining this hypothesis with Eq. (8) we obtain for the total current of escaping ions

$$I=I_0\int_0^\infty e^{-2q/r}F(\rho r)4\pi\rho^2 r^2 d(\rho r)=I_0 g(2q\rho). \tag{10}$$

As reasonable as Eq. (9) is the assumption that the temperature does not enter as an independent parameter in the function F. On this basis, one obtains a correlation between pressure and temperature coefficients of the ionization current, identical with that previously derived by Compton, Bennett and Stearns. The result expressed by Eq. (10) differs from theirs in certain restrictions imposed on the type of function g, so as to prevent negative values of the corresponding range-function $F(t)$. Thus their suggestion

$$g(z)=a(a^2+z^2)^{-\frac{1}{2}},$$

is not admissible because it would imply

$$4\pi F(t)=at^{-4}J_0(a/t).$$

However, it seems possible to describe the available data by reasonable image-functions $F(t)$. The simple pair

$$F(t)=(\kappa^3/4\pi t^3)^{\frac{1}{2}}e^{-\kappa t},$$

$$g(2q\rho)=(1+(8\kappa q\rho)^{\frac{1}{2}})e^{-(8\kappa q\rho)^{\frac{1}{2}}},$$

might be of some interest, although the maximum of this g is not quite flat enough.

While Eq. (9) is probably a good approximation to the truth, it is hard to believe that the effect of the Coulomb field on the diffusion of the electrons before their attachment to molecules would be altogether negligible, and if not, the simple relations given here would seem to require corrections.

Our results so far contain little that is new, and involve assumptions about the initial separations of ions—for without such assumptions, Eq. (8) is rather barren of predictions. Our predictions about the effect of the collecting field will be more independent in this regard, and to the same extent, their experimental verification will test only our reasoning and general picture.

A solution of Eq. (6) with boundary conditions given by Eq. (7) is now required for the general case $\beta>0$. We are fortunate enough to find the labor all done. It turns out that a previously published solution[5] of Eq. (2), when divided by the Boltzmann factor, satisfies the boundary conditions for $1-\varphi$. Thus we obtain

$$\varphi(r, \Theta)=e^{-\beta r(1+\cos\Theta)}\times\int_{s=2q/r}^\infty J_0(2(-\beta r(1+\cos\theta)s)^{\frac{1}{2}})e^{-s}ds \tag{11}$$

$$=e^{-(2q/r)-\beta r(1+\cos\Theta)}\sum_{m,\ n=0}^{\infty}\beta^{n+m}\times(1+\cos\Theta)^{n+m}(2q)^m r^n/m!(m+n)!.$$

The double series can be obtained by omitting all negative powers of r from the complete Laurent expansion of $\exp((2q/r)+\beta r(1+\cos\Theta))$. The corresponding representation of φ by a contour integral might be useful in connection with analytic range-functions $F(\rho r)$.

According to Eq. (11), the *relative* effect of the collecting field reaches its maximum for *small* initial separations r, in which case

$$e^{2q/r}\varphi(r, \Theta)\to J_0(4(-\beta q)^{\frac{1}{2}}\cos\tfrac{1}{2}\Theta). \tag{12}$$

The variation of φ with r is best brought out by expansion in powers of q as follows

$$e^{2q/r}\varphi(r, \Theta)=1+(2q/r)(1-e^{-\beta r(1+\cos\Theta)})+O(\beta^2), \tag{13}$$

where the factor implied by $O(\beta^2)$ has an upper bound independent of r and Θ. Expansion in

power series of the field intensity yields

$$e^{2q/r}\varphi = 1+2\beta q(1+\cos\Theta)+O(\beta^2), \quad (14)$$

where the approximation is no longer uniform in r;—naturally $\varphi<1$. Even with this reservation, it is remarkable enough that in the limit represented by Eq. (14), the relative effect of the field is independent of the distance r, although it depends on the direction Θ.

In comparing these predictions with experience, we may rely on the diffusion of the electrons before capture to produce a practically isotropic distribution of directions. Hence, in the approximation expressed by Eq. (14), the yield of ions escaping initial recombination will be

$$I(X)/I(0) = 1+2\beta q = 1+9.64|X|/DT^2. \quad (15)$$

For $D=1$, $T=300$ we get

$$2\beta q = 1.07\times10^{-4}|X|.$$

The predicted effects are somewhat larger than those recently observed by Broxon and Merideth[8] for field intensities from 1500 to 4500 volts/cm in air at pressures of 20–200 atmospheres. The deficiency is greater the lower the pressure, and might well be ascribed to saturation in the sense of Eq. (13). On the other hand, the field effects observed by Broxon and Merideth for the range 10–1000 volts/cm are substantially greater than those expected for initial recombination alone. It should be observed that the theory permits but little leeway in this direction, dependent on the greater values of q and β for ions carrying more than a single charge,[5] and allowance for a reasonable proportion of these hardly makes a difference. The discrepancy varies about linearly with the logarithm of the field intensity, which is precisely what one should expect if *some columnar recombination takes place*. For pressures of 100–200 atmospheres and electric fields of the order 1000 volts/cm, the number of ions thus removed would amount to 20 ± 10 percent of those which escape initial recombination. Attractive though this explanation is, I hesitate to accept it as final because the expected variation with the lineal density of ions in the "columns" (for which the total current is an independent measure) refuses to appear in the data. The latter circumstance might perhaps be better explained by simultaneous ejection of several electrons to form a cluster of ions; but I am not ready to support this hypothesis either without more direct evidence.

This and some other puzzling details will hardly affect the conclusion that initial recombination is the most important process which interferes with the collection of ions at high pressures, except in the case of heavy ionizing particles. The theory developed here is of course widely applicable to phenomena of ionization, whether by α-rays, β-rays, other ionizing particles, or ordinary photons, wherever this type of recombination occurs as a prominent or minor factor. The agent which liberates the original electrons is not as important as their opportunity for subsequent energy losses and attachment to molecules; in this respect, different types of environment offer enormous variations.

In the particular case of air, it is known that the oxygen molecules are responsible for the attachment of the electrons. It is gratifying that the median diffusion range of the ejected electrons before attachment, as inferred from the observations in connection with the present theory,—of the order 5×10^{-6} cm at 100 atmospheres pressure—seems compatible with our knowledge about the interaction between electrons and oxygen molecules.[9]

[8] J. W. Broxon and G. T. Merideth, Phys. Rev. **54**, 1 (1938).

[9] F. Bloch and N. E. Bradbury, Phys. Rev. **48**, 689 (1935).

The Fine Structures of Hα and Dα Under Varying Discharge Conditions

ROBLEY C. WILLIAMS*
Cornell University, Ithaca, New York

(Received July 11, 1938)

The fine structures of Hα and Dα have been observed under varying conditions of excitation in the discharge tube with pure hydrogen and pure deuterium maintained in each case at near liquid-air temperature, and with the aid of a Zeiss triple-prism spectrograph and a pair of Hilger quartz interferometer plates. The interference patterns obtained upon the photographic plates were analyzed with a Moll microphotometer. The microphotometer curves were reduced to intensity curves and to linear dispersion curves in the usual manner. From the final reduced curves analyses were made of the intensities and positions of the fine structure components. Within the limits of error of the observations the positions of the fine structure components were found to be invariant with changing discharge conditions. The average interval between the two main components of the complex was found to be 0.319 cm^{-1} for Hα and 0.321 cm^{-1} for Dα. The second and third most intense components were optically resolved from each other in Dα but not in Hα. The average interval between these components was found to be 0.130 cm^{-1}. According to theory these intervals are respectively 0.328 cm^{-1} and 0.108 cm^{-1}.

INTRODUCTION

THE first recorded observation of the complex character of Hα was made in 1887 by Michelson and Morley. They examined the visibility of the fringes of Hα as formed by a Michelson interferometer, and concluded that the line possessed a doublet structure. The magnitude of this doublet interval has been reported by numerous investigators with values that differ widely.

In 1913 Bohr developed a theory for hydrogen, according to which the transitions of an electron from a quantized circular orbit having a quantum number 3 to one having a quantum number 2 is responsible for the Hα emission. On this simple basis this transition would occur in only one way and the line would have no structure.

Refinements of the quantum theory and the advent of the relativistic wave mechanics have now resulted in a consistent picture of the formation of Hα, from which it is predicted that this line should consist of five components. Expressions for the relative positions and intensities of these components have been derived by Heisenberg and Jordan,[1] Darwin,[2] and Dirac.[3] Computations of their relative intensities have been made by Sommerfeld and Unsöld,[4] Kupper,[5] and Saha and Banerji.[6]

The theoretical predictions agree in assigning to Hα a fine structure as illustrated in Fig. 1. (The components are assigned numbers in the order of their intensities, and these numbers will be used in further reference to them.) Since deuterium is an isotope of hydrogen, the fine structure of Dα is presumably the same, at least to a first approximation, as that of Hα. Fig. 2 shows the theoretical fine structure intensity pattern that should result for Dα at a temperature of 100°K, if it is assumed that the line width is due solely to Doppler broadening. This is the chief factor affecting the shape of the spectral lines of either Hα or Dα, since it is many times as great as the natural widths of the energy levels involved.

The pattern presented by the complex of the fine structure components of Hα and Dα, as observed with high optical resolution, is generally called the *doublet* pattern. The two components chiefly responsible for the familiar doublet appearance are called the *major* components in this paper, while the three less intense ones are called *minor* components. The interval between the intensity maxima of the doublet pattern is called the doublet interval, or *peak-to-peak interval*. The intervals predicted by theory are those between the centers of the components, and are referred to as the *component-to-component* intervals. The doublet interval and the interval between the major components will usually differ slightly, because of the overlapping minor components. The term "center of gravity" is not

* Now at the Observatory of the University of Michigan.
[1] Heisenberg and Jordan, Zeits. f. Physik **37**, 263 (1926).
[2] Darwin, Proc. Roy. Soc. **A116**, 227 (1927).
[3] Dirac, Proc. Roy. Soc. **A117**, 610 (1928).
[4] Sommerfeld and Unsöld, Zeits. f. Physik **38**, 237 (1926).
[5] Kupper, Ann. d. Physik **86**, 511 (1928).
[6] Saha and Banerji, Zeits. f. Physik **68**, 704 (1931).

used in this paper, since there is usually no measurable point in an intensity complex corresponding to the ordinary definition of that term.[7]

Several investigations have been pursued in recent years with the object of checking experimentally the theoretical predictions of the positions and intensities of the fine structure components of both Hα and Dα. Since clear resolution has been obtained only for the two major components, comparable values can be listed only for the measured *doublet* interval. Table I lists the results of the more recent investigations.

Experimental Procedure

A hydrogen discharge tube was used in which the pressure and current density could be measured, as well as the potential difference across the portion of the discharge from which the light was taken. It was believed that these three variables would have the chief influence, if any, upon the component separations and intensities, although the effect of the addition of a large percentage of helium gas to the pure hydrogen gas, and the effect of a longitudinal magnetic field were also investigated. A primary consideration in this investigation was to insure that enough plates be taken for each discharge condition to eliminate the possibility of any real variations being masked by accidental errors of measurement. Since each plate contained enough fringes to allow six independent determinations of the peak-to-peak interval to be made, it was decided that four plates for each discharge condition would be sufficient. Three values of pressure in the discharge tube were selected, and for each value of the pressure, two values of the current density. Nearly the same pressure and current density values were used for both pure hydrogen gas and pure deuterium gas.

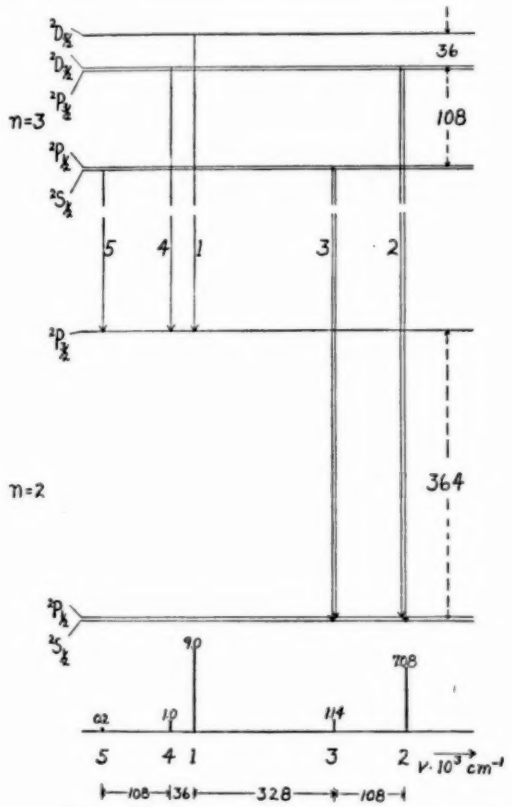

Fig. 1. Theoretical fine structure of Hα.

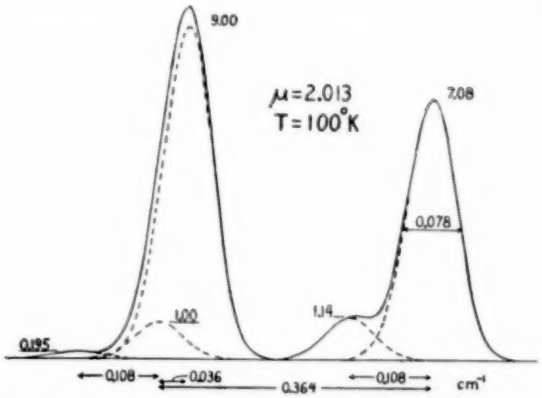

Fig. 2. The fine structure intensity pattern of Dα at a temperature of 100°K. The pattern is drawn from the theoretical positions and intensities of the components.

The source of radiation was a liquid-air-cooled, modified Wood tube of 8 mm internal diameter which is described in detail in an earlier publication.[8] Two electrodes were inserted through the glass at the ends of the U-section from one side of which the light was taken in order to allow the potential difference across this part of the tube to be measured. An electrostatic voltmeter was used to measure the potential difference, and consequently the discharge was not appreciably affected while the readings were being taken.

The discharge tube was connected through a liquid-air trap to a McLeod gauge by means of

[7] See Williams and Gibbs, Phys. Rev. **45**, 475 (1934) for a discussion of the distinction between the position of the center of gravity and the position of the maximum intensity of a complex spectral pattern.

[8] Williams and Gibbs, Phys. Rev. **45**, 475 (1934).

TABLE I. *Recent measurements of the doublet interval in* Hα *and* Dα.

INVESTIGATOR	YEAR	DOUBLET INTERVAL IN cm^{-1} Hα	Dα
Houston and Hsieh[1]	1934	0.312	
Williams and Gibbs[2]	1934	0.304	0.317
Kopfermann[3]	1934		0.323
Spedding, Shane and Grace[4]	1934	0.314	0.318
Williams and Gibbs (Unpublished)	Dec. 1934	0.314	0.318
Heyden[5]	1937		0.331

[1] Houston and Hsieh, Phys. Rev. **45**, 263 (1934).
[2] Williams and Gibbs, Phys. Rev. **45**, 475 (1934).
[3] Kopfermann, Naturwiss. **22**, 218 (1934).
[4] Spedding, Shane and Grace, Phys. Rev. **47**, 38 (1935).
[5] Heyden, Zeits. f. Physik **106**, 499 (1937).

which the pressures in the tube were determined. Both hydrogen and deuterium were available in very nearly 100 percent concentrations, and reservoirs containing these were attached either separately or jointly to the discharge tube through two stopcocks. The pressure of the gas in the tube could be regulated very easily, and maintained over a long period at any desired value.

The source of excitation was a 20,000 volt Thordarson transformer with a variable resistance in series with the primary. An a.c. milliammeter was placed in the secondary circuit in series with the tube, so that the current values could be recorded. Thus it is seen that the three important variables: pressure, current density, and potential gradient were known for every discharge condition.

The optical equipment was a triple-prism spectrograph made by Zeiss, with a Hilger quartz Fabry-Perot étalon placed in the parallel beam of the collimator. Eastman 4-C photographic plates were used, which proved to be relatively fast and almost entirely free from grain. It was the general experience that more trouble was caused in the microphotometering process by dust settling on the plates while drying than by plate grain. The Eberhard effect was eliminated practically by using fine-grain plates and agitated development, and by keeping the density of the photographic image moderately low.

In order to calibrate the plates for their density-intensity relation, an arrangement was provided for impressing intensity marks upon each plate. This was done by placing in front of the slit a box containing an electric lamp, and having a window covered with two layers of ground glass. The intensity of illumination on the plate was controlled by varying the slit widths. This method is a standard one[9] and needs no justification other than to point out that the slit readings must be reduced by 0.02 mm to allow for the diffraction losses at the slit jaws, and that slit readings less than 0.06 mm should not be used. For the readings lower than this, the intensity is not proportional to the slit readings as corrected above. When the slit openings are large there is considerable overlapping of regions of the spectrum fairly far apart, and if the spectral intensity distribution in the region used is far from uniform, serious error can be introduced by using too wide a slit. In the spectral region used for intensity marks in this investigation ($\lambda 6600 - \lambda 6300$) the combined effects of intensity-lamp energy distribution, transmission of the spectrograph, and sensitivity of the plate produced a region of nearly uniform effective sensitivity, and consequently little error was introduced by using a slit as wide as 1 mm.

Plates were taken of Hα and Dα at pressures of 1.2×10^{-1}, 3.1×10^{-1}, and 2.5 mm of mercury. For each pressure, plates were taken for two values of the current density: 15 and 40 ma/cm^2. It was found that a discharge could not be maintained at a pressure appreciably below 1.2×10^{-1} mm, and for a pressure greater than 2.5 mm the α-lines were so weak that usable pictures could not be obtained. Exposures varied from 2 to 55 minutes. The nominal étalon spacing was 5 mm for the Hα and the Dα plates, and was obtained with great accuracy from interference fringes of neon lines.

In analyzing an intensity complex, a proper choice of étalon separation is most important. Inasmuch as both the resolving and dispersive power of the interferometer increases with increasing plate separation, as large a value as possible of this quantity should be used. But if so large a spacing is used that the fringes begin to overlap, the resultant confusion of intensities makes the analysis most difficult. Accordingly a separation was selected just large enough that the intensity complex of a given interference order does not overlap appreciably on the pattern of the next order. In the case of Hα

[9] G. R. Harrison, J. Opt. Soc. Am. **24**, 59 (1934).

FIG. 3. Interferometer fringes of Dα obtained with a 5 mm étalon spacing.

and Dα, the total measurable width of the complex is about 0.750 cm^{-1} and 0.650 cm^{-1} respectively. An étalon separation of 5 mm results in a $\Delta\nu$ between orders of 1.0 cm^{-1}. Hence the Hα or Dα patterns will not overlap on adjacent interference orders, and the intensity of the fringe pattern will approach zero very closely between orders. The result of this selection is shown in Fig. 3, which is a photograph of a fringe pattern of Dα. Fig. 4 shows a microphotometer record of such a pattern. As can readily be seen, the intensity pattern is at the constant value zero for a considerable interval on both sides of the complex. Of course, a 5 mm étalon does not have the optical resolving power of a 7.8 mm étalon as used by other investigators. But for a reflectivity of 90 percent from the silvered plates, the resolving power of a 5 mm étalon is at least 400,000. Because of the broadening of the Hα and Dα fringes by thermal agitation in the discharge, however, the maximum resolving power that can be obtained for Dα is about 150,000, and for Hα, about 90,000. Hence a highly silvered 5 mm étalon has a resolving power considerably in excess of the necessary minimum.

MEASUREMENT OF THE PEAK-TO-PEAK INTERVALS

The interval between components 1 and 2 of the Hα or Dα intensity complex was determined by measuring the peak-to-peak interval, and then applying certain corrections made necessary by the overlapping minor components. The separation in cm^{-1} in the fringe system of a Fabry-Perot étalon between two fringes is $\Delta\nu=\Delta p/2d\cos\theta$, where Δp is the difference in order of interference between the two fringes, d is the spacing of the étalon plates in cm, and θ is the mean angle that the fringes make in the case of close fringes with the center of the fringe system as viewed from the camera objective. Since d and θ are known or can be measured, $\Delta\nu$ is determined after Δp is known. The dispersion of the Fabry-Perot étalon fringe system is not linear, but varies in such a way that the linear distance on the photographic plate between a fringe and the center of the fringe system is very nearly proportional to the square root of the order difference between the fringe and the center of the system.

Actually, however, the relation connecting orders of interference with radii of fringes is not an exact square-root relation, because of possible optical distortions in the optical system. An accurate, although laborious, method of determining the Δp between two fringes of the same integral order of interference is to use an equation of the type

$$y=A+Bx+Cx^2+Dx^3+\cdots,$$

where y represents the order of interference of a certain wave-length λ_1, counted from an arbitrary zero fringe, and x the corresponding linear distance on the plate of the fringe measured from the same zero. Three fringes of λ_1, are selected at a time, and the three constants A, B and C determined. It has been found by repeated trial that the value D is negligible with the Zeiss spectrograph used. With the constants determined for a set of three orders of interference, the fractional order of interference (Δp) between λ_1 and another fringe of a slightly differing wavelength can be determined by solving for y in the above equation.

This method supposes the experimental curve connecting order number with fringe diameter to be parabolic in short sections, when the value of

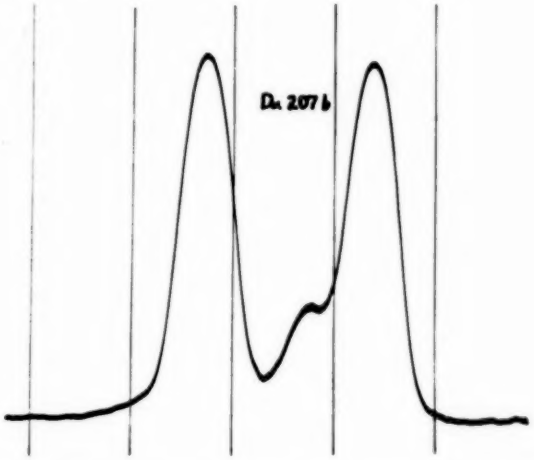

FIG. 4. Microphotometer tracing of part of the fringe pattern shown in Fig. 3.

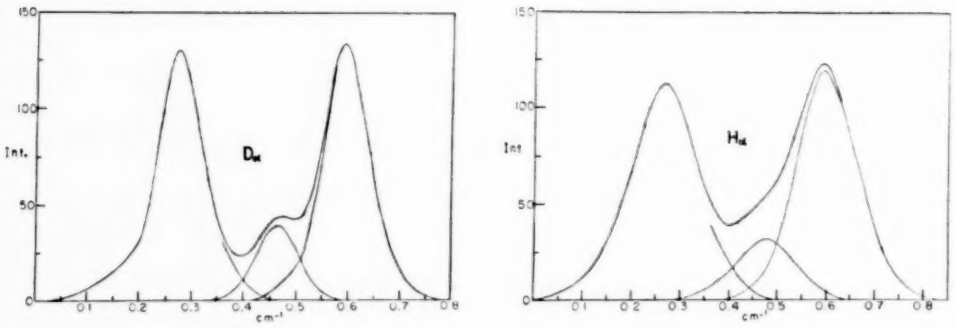

FIG. 5. Typical intensity curves obtained for Hα and Dα.

D is neglected, but allows the equation of the parabola to change at every set of three fringes used. Less serious error will be introduced by this method of computing, in case the fringe system is not strictly parabolic, than will be introduced in computing by the so-called "standard" method, or by the one suggested by Tolansky.[10]

The fringe radii were determined by measuring their diameters and dividing by two. A Moll microphotometer was used as a measuring engine, and diameter readings taken at the position of maximum deflection of the galvanometer. This method of measurement proved surprisingly accurate as judged by the smallness of accidental errors, chiefly owing to the fine grain of the plates and the proper exposures of the photographic images.

Reduction of Microphotometer Curves to Intensity Curves

From each series of five plates taken under identical discharge conditions, two sets of fringes were selected to be microphotometered. The fringe selected was number 3 in most cases, since it was found that the intensity distribution along the length of the slit image was sensibly constant at fringe 3. Microphotometer records were obtained in the usual fashion. The same width of thermocouple slit was used that was used in the measurement of the peak-to-peak intervals. The microphotometer curves were retraced by use of an enlarging camera on cross-section paper. The density-intensity curve was placed on the same sheet of paper, and the reductions to intensity curves made. These curves were corrected to linear dispersion in the usual fashion, and resulting typical curves for Hα and Dα are shown in Fig. 5.

Component-to-Component Intervals

The purpose of plotting true intensity curves of the Hα and Dα complexes is to determine values of relative intensities, and to determine line shapes, from both of which corrections for displacements may be computed to apply to the measured peak-to-peak interval in order to yield the major component-to-component interval. The problem of corrections is the most critical one in the determination of component intervals, and unfortunately is a problem not susceptible to precise nor definite calculation. The corrections can be arrived at only after certain rather limited assumptions are made which are not directly open to test.

The method of analyzing the curves so as to obtain the corrections to the measured peak-to-peak intervals is fairly completely described in a previous article,[11] and was modified in the present research only in one major respect: Inasmuch as the Dα patterns showed a resolution of components 2 and 3, the intensity complexes of this isotope were analyzed first. This increased resolution has made possible for the first time the direct measurement of the interval between components 2 and 3. The interval so found for Dα was used in the analysis of the patterns of Hα, since these components were not resolved for the latter isotope. This differs from the previous work, in which this interval was taken as about 0.108 cm^{-1}, from theoretical considerations.

The general results of this investigation are

[10] Tolansky, J. Sci. Inst. **8**, 223 (1931).

[11] Williams and Gibbs, Phys. Rev. **45**, 475 (1934).

TABLE II. *Component separations in* Hα.

Plate No.	Pressure (mm Hg)	Current Density (A/cm^2)	P.D. (V/cm)	Doublet Interval (cm^{-1})	Half-Int. Breadth (cm^{-1})	Intensities Relative to Theory		Corrections				Intervals
								Comp. 1		Comp. 2		
						I_1	I_2	(cm^{-1})	Due to	(cm^{-1})	Due to	Comp. 1 to 2 (cm^{-1})
201*a*	0.12	0.015	20–30	0.3153	0.150	0.67	1.70	−0.0039	4	+0.0050	3	
201*b*				0.3130				+0.0010	3			0.316
201*c*				0.3148				−0.0039	4	0.0045	3	
201*e*				0.3140	0.150	0.70	1.60	+0.0010	3			
202*b*	0.12	0.040	20–40	0.3149	0.160	0.70	1.45	−0.0039	4	0.0045	3	
202*c*				0.3178				+0.0012	3			0.318
202*d*				0.3162	0.155	0.70	1.43	−0.0041	4	0.0042	3	
202*e*				0.3183				+0.0011	3			
204*a*	0.31	0.015	20–25	0.3090	0.165	0.79	1.80	−0.0041	4	0.0082	3	
204*b*				0.3108				+0.0015	3			0.316
204*c*				0.3108	0.165	0.79	1.80	−0.0041	4	0.0082	3	
204*d*				0.3113				+0.0015	3			
205*a*	0.31	0.040	24	0.3134								
205*b*				0.3136	0.165	0.82	1.85	−0.0041	4			0.319
205*c*				0.3153				+0.0015	3	0.0082	3	
205*d*				0.3119								
203*a*	2.50	0.040	100	0.3096	0.180	0.90	1.90	−0.0042	4	0.0090	3	
203*b*				0.3060				+0.0028	3			0.315
203*c*				0.3074	0.190	0.88	1.75	−0.0043	4	0.0100	3	
203*d*				0.3077				+0.0030	3			

TABLE III. *Component separations in* Dα.

Plate No.	Pressure (mm Hg)	Current Density (A/cm^2)	P.D. (V/cm)	Doublet Interval (cm^{-1})	Half-Int. Breadth (cm^{-1})	Intensities Relative to Theory		Corrections				Intervals	
								Comp. 1		Comp. 2			
						I_1	I_2	(cm^{-1})	Due to	(cm^{-1})	Due to	Comp. 2 to 3 (cm^{-1})	Comp. 1 to 2 (cm^{-1})
210*a*	0.14	0.015	20–30	0.3224	0.120	0.74	2.3	−0.0038	4	+0.0015	3	0.134	
210*b*				0.3224									0.321
210*c*				0.3229	0.120	0.72	2.2	−0.0038	4	0.0015	3	0.132	
210*d*				0.3260									
209*a*	0.14	0.030	20–40	0.3218	0.125	0.75	2.1	−0.0038	4	0.0020	3	0.133	
209*b*				0.3220									0.320
209*c*				0.3230	0.125	0.75	1.9	−0.0037	4	0.0011	3	0.135	
209*d*				0.3221									
207*a*	0.31	0.015	20	0.3217	0.120	0.79	2.2	−0.0038	4	0.0015	3	0.135	
207*b*				0.3212									0.319
207*c*				0.3221	0.115	0.82	2.4	−0.0038	4	0.0012	3	0.126	
207*d*				0.3212									
206*a*	0.31	0.040	24	0.3205	0.127	0.89	2.0	−0.0038	4	0.0020	3	0.135	
206_1				0.3208									0.319
206*b*				0.3200	0.125	0.87	1.8	−0.0038	4	0.0019	3	0.136	
206*c*				0.3226									
208*b*	2.50	0.040	100	0.3179	0.155	0.94	2.4	−0.0041	4	0.0045	3	0.136	
								+0.0008	3				
208*c*				0.3177									0.319
208*d*				0.3186	0.146	0.97	2.6	−0.0041	4	0.0035	3	0.137	
								+0.0008	3				
208*e*				0.3171									

contained in Tables II and III. Column 1 is plate number, and columns 2, 3 and 4 give the pressure, the current density, and the potential gradient in the discharge tube. Column 5 contains the measured peak-to-peak intervals in cm^{-1}. Each entry in column 5 is an average of the measurements of 6 fringes. Column 6 gives the half-intensity breadth in cm^{-1}, computed for those plates whose fringes were subjected to an intensity analysis. Column 7 contains the intensities of components 1 and 3, in terms of their theoretical intensities. Component 2 has here been taken arbitrarily as having standard intensity. Column 8 lists the corrections in cm^{-1} that are applied to the positions of the peaks to obtain positions of maxima of major components. These are listed in two sub-columns as corrections to peak 1, and corrections to peak 2. There is also listed after each correction the minor component to whose effect the correction is due. Column 9 gives the measured interval in cm^{-1} between the centers of components 2 and 3 for Dα. The last column contains the final value for the separation in cm^{-1} between the centers of component 1 and component 2. This column is, of course, the sum of column 5 and column 8.

Before discussing the results of the investigation the assumptions underlying the measurements and the probable upper limits of error will be noted. The chief source of error in the measurements is the evaluation of the corrections. The peak-to-peak interval can be measured with the photometric comparator to an estimated maximum error of 0.0005 cm^{-1} in the mean from a set of four plates. The mean is apparently affected only by accidental errors of measurement, for no systematic differences can be regularly observed from fringe to fringe, or from plate to plate.

The corrections necessary to reduce the position of an intensity peak to the center of the component almost directly under it are dependent upon four factors: The relative intensity of all components, the separations of the components, the value of the half-intensity breadth, and the similarity to a Doppler curve of the actual intensity curve of a component. It is assumed that the components are single in structure, all have approximately the same half-intensity breadth, and all have a shape somewhat similar to that of a Doppler curve.

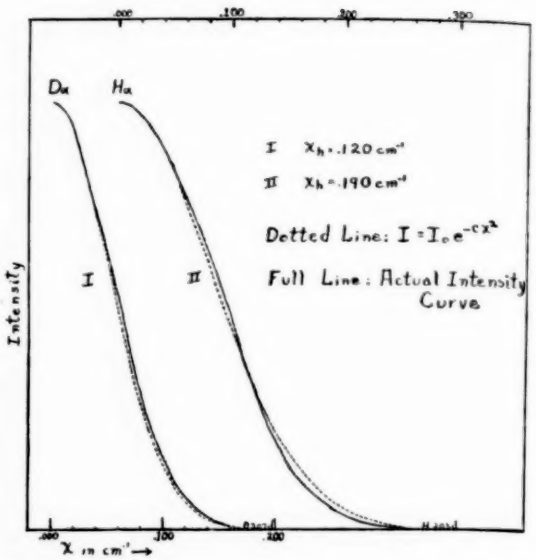

FIG. 6. A comparison of the intensity curves of the high frequency sides of Hα and Dα with Doppler curves of the same half-intensity breadth.

The intensities and positions of components 2 and 3 for Dα are obtained by symmetry and subtraction, as mentioned previously. With the above assumptions granted, these values for Dα are quite accurate. The positions and intensities of these components for Hα are based on the hypothesis that the interval from component 2 to component 3 is the same for Hα as for Dα. The assigned position of component 4 relative to component 1 for both Hα and Dα is a pure assumption that the theoretical value is reasonably correct. The intensity of this component is taken as the theoretical intensity relative to component 2, which has been arbitrarily considered as standard.

Neither the position nor intensity of component 5 would have any appreciable effect on the position of the intensity peaks, if the actual position and intensity of this component are even approximately those predicted by theory.

The assumption of singleness and similarity of all five components cannot be tested. The similarity of the actual curve to the theoretical Doppler curve has been tested by comparing the undisturbed, high frequency side of the Hα and Dα complexes with a Doppler curve of the same half-intensity breadth. The result of this is shown in Fig. 6. Comparisons are here shown for the smallest and the largest half-intensity breadth met with in this research. It is seen

that the two curves are practically the same, particularly near their tops. It must be remembered that the slope of these curves enters into the corrections, and in places where the slope is almost zero the percent difference in slope between the theoretical and actual curve could be quite large. In the region of small values of the slope near the top of the curves the slope is approximately proportional to the displacement from the center of the component. Hence a 100 percent deviation of the true slope from the Doppler curve slope would introduce an error of ± 0.007 cm^{-1} in the correction of peak 2 and a ± 0.003 cm^{-1} in the correction of peak 1 for Hα, and considerably less than half these values for Dα. The actual corrections for peaks 1 and 2 are opposite in sign, however, and thus it would seem that the net maximum error due to this cause would be on the order of ± 0.004 cm^{-1} for Hα and ± 0.002 cm^{-1} for Dα.

The errors in the corrections to peak 1 would be largely due to the error introduced in the placing of component 4 relative to component 1, and in assigning to it a theoretical intensity. The magnitude of the errors of the corrections, for both Hα and Dα, can be estimated from Table IV, where corrections are computed for various assumed values of the ratio of intensity of component 1 to component 4, and of the interval between components 1 and 4. The single-lined rectangle represents the most likely range of values, and it can be seen that the maximum error would probably be not over ± 0.002 cm^{-1} for either Hα or Dα.

TABLE IV. *Corrections to Component 1 due to Component 4. (Various hypotheses relative to intensity and separation are used.)*

I_1/I_4		For half-width = 0.160 cm^{-1} (H) For half-width = 0.115 cm^{-1} (D)						
4	H	0.0053	0.0055	0.0059	0.0064	0.0068	0.0070	0.0070
	D	0.0052	0.0056	0.0063	0.0068	0.0071	0.0074	0.0075
5	H	0.0044	46	49	51	54	55	56
	D	0.0044	47	51	55	58	60	61
6	H	0.0038	40	42	44	46	47	47
	D	0.0039	42	45	47	49	50	52
7	H	0.0033	34	36	38	40	41	41
	D	0.0034	36	39	41	43	44	45
8	H	0.0029	31	32	34	35	36	36
	D	0.0031	33	35	37	38	39	40
9	H	0.0027	27	28	29	30	32	32
	D	0.0028	30	31	32	33	35	36
10	H	0.0023	24	25	26	27	28	28
	D	0.0025	27	28	29	31	32	33
Separation of I_1 and I_4 in cm^{-1}		0.030	0.032	0.034	0.036	0.038	0.040	0.042

A possible source of error in the measurement of the separation of the components of Dα would be the presence of an appreciable quantity of ordinary hydrogen in the discharge. A plate was taken to determine the relative abundance of hydrogen and deuterium. With a discharge current sufficient to expose Dα in one second without the étalon in place, Hα did not appear on the plate in a two-minute exposure. Evidently, then, the concentration of Hα was considerably less than 1 percent. The pure deuterium gas used was graciously given to Cornell University by Professor H. C. Urey of Columbia University, and the completion of this research was made possible largely through his generosity.

On combining all these estimates and assumptions, the probable *maximum* error for the interval between components 1 and 2 is about ± 0.005 cm^{-1} for Hα and ± 0.003 cm^{-1} for Dα. The interval between components 2 and 3 of Dα is probably known to the same degree of accuracy; namely, about ± 0.003 cm^{-1}. It is for the reason that the correction errors are so potentially large that no estimation of the relatively small probable error based solely on peak-to-peak measurement is given.

The most striking aspect of the data in Tables II and III is the large percent deviation from theory in the interval from component 2 to component 3. This interval should be 0.108 cm^{-1} by theory, and thus a deviation of about 20 percent is indicated. The other measurable interval is the main interval between components 1 and 2. The most likely statement that can be made at this time regarding this important interval is that it is sensibly invariant with changing discharge conditions for either Hα or Dα, that the Hα interval seems consistently about 0.002 cm^{-1} less than the Dα interval, and that either interval is about 0.009 cm^{-1} to 0.011 cm^{-1} less than the theoretically predicted one.

The results of this investigation indicate one reason for the chief discrepancies of the work of some of the previous investigators, including the previous work of the author. Without exception the assumption has always been made that

component 3 was in its theoretical position, because until the present research, this component had never been resolved from component 2. (Resolution is here defined as that degree of separation of two components such that the resultant intensity complex has two maxima and a minimum.) But component 3 is actually considerably removed from its theoretical position, and its intensity is far greater than predicted. Consequently, corrections based on the theoretical position and intensity of the component will be different from the corrections based on its observed position and intensity.

The relative intensities of the components listed in Tables II and III are seen to vary rather greatly from the theoretical predictions in agreement with the results of previous investigators. It is interesting to note that component 1 can be either more intense or less intense than component 2, but that it never quite reaches its theoretical relative intensity. Component 3 has an intensity relative to component 2 always considerably larger than it should have according to theory.

The most recent work on the structure of Dα is that reported by Maria Heyden in 1937.[12] An interval of 0.3312 cm^{-1} is found between component 2 and the "Schwerpunkt" of components 1 and 4, which compares favorably with the predicted interval of 0.3321 cm^{-1}. From the microphotometer records reproduced in this paper it is difficult to determine whether or not component 3 is resolved, because of the very large grain of the plates. It is unfortunate that no examples of the resolution of components 2 and 3 are shown, as would be expected on those plates for which half-intensity breadths of less than 0.080 cm^{-1} are reported. As is shown in Fig. 2, a half-intensity breadth of 0.078 cm^{-1} results in a clear resolution even in the case of theoretical positions and intensities.

TABLE V. *Test for lack of symmetry of hyperfine structure.*

PLATE	PRESSURE (mm Hg)	CURRENT DENSITY (A/cm^2)	PEAK-TO-PEAK INTERVAL (cm^{-1})	
211*a*	0.31	0.030	0.3200	Magnetic field
211*b*	0.31	0.030	0.3206	Magnetic field
211*a*	0.31	0.030	0.3215	No magnetic field
211*b*	0.31	0.030	0.3213	No magnetic field

[12] Maria Heyden, Zeits f. Physik **106**, 499 (1937).

POSSIBLE CAUSES OF DEVIATION FROM THEORY

It was suggested by Professor H. Bethe that possibly the hyperfine structure of the Hα and Dα lines would be large enough to account for the observed deviations from theory. If the hyperfine structure splittings are unsymmetrical with respect to the fine structure levels and are sufficiently large, a shift of the peak of the observed intensity pattern from that of the theoretical pattern would result. Bethe[13] shows that the hyperfine structure splittings for the $2s\ ^2S_{\frac{1}{2}}$ level is equal to

$$\frac{8\alpha^2}{3}\,\frac{g(i)(i+\frac{1}{2})}{1838}\,\frac{Z^3R}{n^3},$$

where $g(i)$ is the nuclear splitting factor believed to be 2 for deuterium, and i is the nuclear spin quantum number.

If a magnetic field is impressed, the hyperfine structure levels will be perturbed. If the magnetic field is strong enough, the fine structure levels will also be perturbed, and the normal Zeeman triplet structure will result. However, it is possible to keep the magnetic field weak enough (60–100 gauss) not to perturb the fine structure levels appreciably, and yet be strong enough to alter completely the hyperfine structure levels. If the hyperfine structure levels are unsymmetrically placed, this complete alteration should affect the observed intensity pattern.

To test whether or not an unsymmetrical hyperfine structure existed the apparatus was so modified that a magnetic field of about 100 gauss could be impressed along the axis of the discharge tube. This was done by wrapping wire around the tube, connecting to a source of direct current, and immersing the tube and wire in the liquid air. Two plates were taken of Dα operating under ideal discharge conditions, and on each plate there was an interference pattern photographed with and without the magnetic field. If the hyperfine structure is important in shifting the peaks, the peak-to-peak interval should differ noticeably between the two cases. The results of these measurements are given in Table V. It is seen that the peak-to-peak intervals differ only slightly, and certainly the

[13] Bethe, *Handbuch der Physik*, Vol. 24, p. 273.

change is far too small to account for the observed deviations from theory. It may be safely said that the hyperfine structure is not an important factor in the observed fine structure pattern of Dα. A paper by Bechert and Meixner[14] has appeared which shows that there should be neither fine structure nor hyperfine structure differences between Hα and Dα, and consequently the magnetic field result for Dα can be safely assumed to hold for Hα. Furthermore, this paper shows that the hyperfine structure splitting should be symmetrical about the position of the fine structure components, so that no shift in the position of the intensity peaks due to hyperfine structure is to be expected.

At the suggestion of Professor J. Franck the possible effect of weak-field Stark-effect was considered. For an electric field sufficiently weak that the Stark-effect splitting is small compared with the separations of the fine structure levels, it has been calculated[15, 16] that each fine structure level is split up into $2J+1$ equidistant levels. The separation of these levels from each other is proportional to the first power of the electric field, as long as the field is small. Bethe[17] gives an equation relating field-strength and Stark-effect splittings, which shows that in order to produce a splitting of an amount that would appreciably distort the fine structure complex, a field of 100 volts per cm is required. There is little possibility that the potential difference across the discharge tube causes a field large enough to explain the observed discrepancies, since potential gradients generally existing in the discharge tube were less than 50 volts per cm.

In order to test whether or not there existed interionic fields of sufficient magnitude to produce the observed discrepancies, a series of plates were taken with the same pressure and widely differing current densities. Current densities as high as 0.050A/cm² and as low as 0.005A/cm² were taken. Within an estimated experimental error of 2 percent, the interval between components 2 and 3 did not change with current density, but continued to remain at about 0.130 cm^{-1}. This indicates that either Stark-effect is not responsible for the observed deviations from theory, or that the particular kinds of fields involved do not change much with changing current densities.

Observations with Helium in the Discharge Tube

It was considered barely possible that the presence of helium in the discharge tube would so modify the ionic field that appreciable differences could be observed between the fine structure pattern of pure deuterium and that of deuterium when helium was present. There exists a slight evidence of this in the results of Spedding, Shane and Grace, who found for 2 plates a 3 percent larger interval between components 1 and 2, when helium was abundantly present in the discharge tube, than they found for their other 3 plates when pure hydrogen and deuterium were present.

A source of He was provided, and although the nitrogen always present in commercial He could be removed by a liquid-air-cooled charcoal trap, the ordinary hydrogen also present could not be removed without difficulty. Consequently, a 3 mm étalon was used to avoid distortion of the Dα pattern by that of Hα. The deuterium was admitted only as an impurity in the He gas in the discharge, but due to their low excitation potential, the Balmer lines came out with great brilliance. The hydrogen molecular spectrum was almost entirely suppressed. Plates were taken of the fine structure pattern, with and without He present, and with the constant current density value of 19 ma/cm². These plates were measured on the microphotometer, and no change in interval between components 1 and 2 could be detected, within an estimated average error of ½ percent. Consequently, the apparent change of interval with He present, indicated by the results of Spedding, Shane and Grace, was not substantiated.

Acknowledgment

The advice and active cooperation of Professor R. C. Gibbs in directing this research are gratefully acknowledged.

[14] Bechert and Meixner, Ann. d. Physik **22**, 525 (1935).
[15] Rojansky, Phys. Rev. **33**, 1 (1929).
[16] Schlapp, Proc. Roy. Soc. **119**, 313 (1928).
[17] Bethe, *Handbuch der Physik*, Vol. 24, p. 416.

Determination of e/m from the $H\alpha - D\alpha$ Interval

ROBLEY C. WILLIAMS*
Cornell University, Ithaca, New York
(Received July 11, 1938)

Photographs were taken with a 3 mm étalon of the interference pattern of $H\alpha$ and $D\alpha$ from a discharge in the two gases mixed in equal proportions. The interval between the intensity peaks due to the low frequency major components of the two isotopes was measured with the microphotometer used as a comparator. Corrections were made to the observed positions of the intensity peaks to change them to the positions of the centers of the components. These corrections were based on the intensities, positions, and half-intensity breadths of the components as experimentally determined, and upon certain assumptions relative to the shape of the components. An interval between components of 4.14700 ± 0.0004 cm^{-1}, when reduced to vacuum, was obtained. By combining this with recently determined values of the atomic weights of hydrogen and deuterium as reported by Livingston and Bethe, the wave number of $H\alpha$ as determined by Houston, and the physical Faraday as computed by Birge, a value of $1.7579 \pm 0.0004 \times 10^7$ e.m.u./gram is obtained for the value of e/m.

HISTORICAL

VALUES of e/m determined by measuring the difference in wave number between two spectrum lines have been reported by several investigators within recent years. W. V. Houston[1] determined e/m spectroscopically in 1927, using the intervals between the λ4686 line of ionized helium and $H\alpha$, as well as $H\beta$. He obtained by this method a value of $e/m = 1.7606 \pm 0.001 \times 10^7$ e.m.u./gram, which Birge later changed to $1.7603 \pm 0.001 \times 10^7$ e.m.u./gram upon detecting a slight error in Houston's calculations. In 1933 Gibbs and Williams[2] determined the value of e/m provisionally by measuring the interval between similar components of the $H\alpha$ and $D\alpha$ lines, and obtained a value of $1.757 \pm 0.001 \times 10^7$ e.m.u./gram. Kinsler and Houston[3] in 1934 obtained a value of $1.7570 \pm 0.0007 \times 10^7$ e.m.u./gram for e/m from the Zeeman patterns of zinc, cadmium and helium. In 1935 Shane and Spedding[4] used the $H\alpha$–$D\alpha$ interval to obtain a value reported as $1.7579 \pm 0.0003 \times 10^7$ e.m.u./gram. Houston[5] has recently determined a provisional value of 1.760 ± 0.0015 e.m.u./gram for e/m, based upon a Fourier analysis of the fine structure patterns of $H\alpha$ and $D\alpha$.

DETERMINATION OF e/m FROM THE $H\alpha$–$D\alpha$ INTERVAL

The equations used for determining the mass of the electron in atomic weight units, and e/m are derived in a previous publication[6] and are given here

$$m = \frac{H^+D^+(\nu_D - \nu_H)}{D^+\nu_H - H^+\nu_D} \tag{1}$$

and

$$e/m = \frac{F(D^+\nu_H - H^+\nu_D)}{H^+D^+\Delta\nu_{H-D}}, \tag{2}$$

where F is the Faraday, ν_H and ν_D the wave numbers of like components of hydrogen and deuterium lines, and H^+ and D^+ the atomic weights of the hydrogen and deuterium nuclei.

The advantage of using the two isotopes of hydrogen for the determination of e/m is at once apparent: $\Delta\nu_{H-D}$ is the only quantity to be measured, while the atomic constants and the wave numbers are known to a relatively high degree of precision.

EXPERIMENTAL

By means of the discharge tube, spectrograph and interferometer described in the preceding paper, interference fringes were obtained of $H\alpha$ and $D\alpha$. The gas in the tube was maintained at approximately half hydrogen and half deuterium, with a total pressure of about 3.1×10^{-1} mm of mercury, and a current density of about 20

* Now at the Observatory of the University of Michigan.
[1] Houston, Phys. Rev. **30**, 608 (1927).
[2] Gibbs and Williams, Phys. Rev. **44**, 1029 (1933).
[3] Kinsler and Houston, Phys. Rev. **45**, 104 (1934); **46**, 533 (1934).
[4] Shane and Spedding, Phys. Rev. **47**, 33 (1935).
[5] Houston, Phys. Rev. **51**, 446 (1937).
[6] Gibbs and Williams, Phys. Rev. **44**, 1029 (1933).

FIG. 1. Interferometer fringes of H and D obtained with a 3-mm étalon spacing.

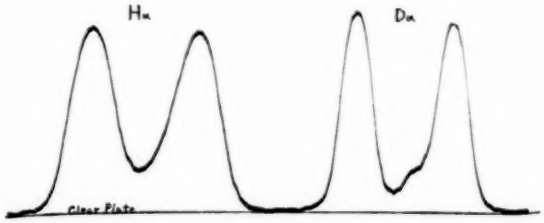

FIG. 2. Microphotometer tracing of the fringe pattern shown in Fig. 1.

ma/cm². Five excellent plates were taken with the aid of a 3-mm étalon spacing.

The choice of the proper optical equipment for the analysis of Hα and Dα on the same plate must be in the nature of a compromise. One possibility is to use a primary instrument of great dispersion, so that the spectrum lines of Hα and Dα are separated sufficiently to prevent the interference patterns overlapping. This was done by Shane and Spedding. The most serious objection to this type of apparatus is its lack of speed. This lack of speed, which is likely to introduce distortions because the optical apparatus and source cannot readily be maintained in the same adjustment for the necessary time, can be overcome by a much lighter coating of silver on the étalon plates, but this leads to a greatly reduced optical resolution. The second possibility is to use a lower-dispersion primary instrument, and an étalon spacing of approximately 3 mm. This spacing causes a given Dα fringe to be overlapped about two and a half orders from the Hα fringe of the same order, but does not cause the Hα and Dα patterns to be confused. Fig. 1 is a reproduction of such a fringe system. Fig. 2 shows that the intensity of the pattern drops truly to zero between each Hα and Dα fringe. The resolving power of a 3-mm étalon silvered to reflect over 90 percent is over 250,000, while the temperature broadening of even Dα makes a resolving power much greater than this relatively unimportant. This point is illustrated in the half-intensity breadths obtained for Dα with a 3-mm and a 5-mm étalon spacing. The former spacing yielded a half-intensity breadth of about 0.120 cm^{-1}, and the latter spacing gave a breadth between 0.115 cm^{-1} and 0.120 cm^{-1}.

The peak-to-peak separations of peak 1 of Hα and Dα were measured in the manner indicated in the preceding article. The fractional Δp interval between the two similar peaks was determined, and to this number the integer 2 was added, since it was known that the fringes overlap approximately two and a half orders of interference.

The $\Delta\nu$ interval was found by dividing $2+\Delta p$ by the customary denominator $2d\cos\theta$. By use of a standard neon spectrum, the étalon spacing was determined with an accuracy of about 1 part in 1,000,000. Neon fringes were taken with each plate of Hα and Dα.

The $\cos\theta$ factor was carefully accounted for. At the center of the interference pattern, the $\Delta\nu$ between orders is strictly equal to $1/2d$, but as the distance from the center increases, the $\Delta\nu$ decreases as $1/\cos\theta$. Hence in computing the $\Delta\nu$ between the peaks of a pattern, the measured Δp must be divided by $2d$ times the cosine of the angle made by the peaks in question. This angle is the angle whose tangent is the radius of the fringe divided by the focal length of the camera lens of the spectrograph.

RESULTS

The observed values of Δp between peak 1 of Hα and peak 1 of Dα are listed in Table I, by plate number and by fringe number. (To each

TABLE I. *Observed values of Δp between peak 1 of* Hα *and peak 1 of* Dα.

PLATE NUMBER	FRINGE 2	FRINGE 3	FRINGE 4	2d (cm)
212*a*		0.48926 0.48854	0.48800	0.600163
212*b*	0.48748	0.48710 0.48743	0.48804	0.600163
212*c*	0.48807	0.48842 0.48870	0.48827	0.600163
212*d*		0.48871 0.48845	0.48829	0.600163
212*e*	0.48677	0.48977 0.48899	0.48926	0.600163
	$\cos\theta =$ 0.99987	$\cos\theta =$ 0.99976	$\cos\theta =$ 0.99962	

TABLE II. *Values of $\Delta\nu$, the frequency difference between peak 1 of Hα and peak 1 of Dα.*

PLATE NUMBER	FRINGE 2	3	4
212*a*		4.14863 cm^{-1} 4.14743	4.14711 cm^{-1}
212*b*	4.14521 cm^{-1}	4.14503 4.14558	4.14718
212*c*	4.14619	4.14723 4.14770	4.14756
212*d*		4.14772 4.14728	4.14756
212*e*	4.14403	4.14948 4.14818	4.14981

fractional Δp the integer 2 must be added since the fringes are overlapped two and a half orders of interference.)

At the right-hand side of the table are listed the $2d$ values for each plate, and at the bottom is listed the cos θ value for each fringe. Dividing each $2+\Delta p$ by the proper $2d\cos\theta$, gives the values of $\Delta\nu$ in cm^{-1} shown in Table II.

The average peak-to-peak interval is:

$$\Delta\nu \text{ (air)} = 4.14716 \pm 0.0004 \text{ cm}^{-1}$$

and $$\Delta\nu \text{ (vac.)} = 4.14610 \pm 0.0004 \text{ cm}^{-1}.$$

To this interval a correction must be made because of the differential effects in the case of Hα and Dα of components 3 and 4 on the position of the center of component 1. The intensity ratio of component 1 and the disturbing components, and the magnitude of these corrections are listed in Table III. These corrections are based on the following assumptions and hypotheses: (1) The intensity distribution in each component is that given by Doppler broadening, and is the same for all components. (2) The position of component 4 is that determined by theory. (3) The position of component 3 in Hα is the same as that found by analysis for Dα. The differential correction is in such a direction as to increase the measured peak-to-peak interval of Hα and Dα.

Adding this amount to the average $\Delta\nu$ (vac.) just obtained, there results the completely corrected $\Delta\nu$ (vac.) value of the separation of the $2p\ ^2P_{3/2}-3d\ ^2D_{5/2}$ component of Hα from the corresponding component of Dα. This is:

$$\Delta\nu \text{ (vac.)} = 4.14700 \pm 0.0004 \text{ cm}^{-1}.$$

The values of and authorities for the atomic constants used in computing the atomic weight of the electron, m, from Eq. (1), and e/m from Eq. (2) are these:

$\nu_{H\alpha}$(vac.) = 15233.094 cm^{-1}	Houston[7]
$H^+ = 1.00813 - 0.00055$	Livingston and Bethe[8]
$D^+ = 2.01473 - 0.00055$	Livingston and Bethe[8]
$F = 9651.3 \pm 8$ abs. coulombs	

(F has been adjusted to the atomic mass scale, and is based upon an O^{16}/O^{18} ratio of 537.)

Substituting these values in Eq. (1) we obtain the value of the mass of the electron in atomic weight units:

$$m = 5.4902 \pm 0.0005 \times 10^{-4}.$$

The e/m ratio is determined by dividing the value of the Faraday by the atomic weight of the electron:

$$e/m = 9651.3/5.4902 = 1.7579 \pm 0.0004 \times 10^7 \text{ e.m.u./gram.}$$

The probable error of the determination of the Hα–Dα interval is ± 1 part in 10,000, and that of the Faraday is ± 1 part in 12,000. The effect of the probable errors of the atomic masses and the absolute wave number of Hα is negligible. Upon combining the two significant probable errors, a value of ± 0.0003 e.m.u./gram is obtained for e/m. This has been increased to ± 0.0004 e.m.u./gram to allow for any constant error. The uncertainties in the *corrections* of the component positions are not included in the adopted probable error.

After making slight changes[9] in the value of $R_{He} - R_H$ as used by Houston, adjusting the value of F to the physical mass scale as used in the present paper, and changing to the most recently reported[8] atomic mass values, Houston's earlier value of e/m becomes $1.7600 \pm 0.001 \times 10^7$ e.m.u./gram.

TABLE III. *Magnitude of the corrections to the frequencies of Hα and Dα.*

	Hα	Dα
Half-intensity width	0.165 cm^{-1}	0.120 cm^{-1}
I_1/I_4	7	6–7
I_1/I_3	3.5	3.5
Correction due to component 4	−0.0041 cm^{-1}	+0.0038 cm^{-1}
Correction due to component 3	+0.0012 cm^{-1}	0.0000 cm^{-1}
Net correction	−0.0029 cm^{-1}	+0.0038 cm^{-1}
Differential correction (+ increases interval)	+0.0009 cm^{-1}	

[7] Houston, Phys. Rev. **30**, 608 (1927).
[8] Livingston and Bethe, Rev. Mod. Phys. **9**, 373 (1937).
[9] Williams and Gibbs, Phys. Rev. **45**, 491 (1933).

TABLE IV. *Corrections to component 1 due to component 3 for* Hα.

I_1/I_3	$X_k=0.150$ cm^{-1}			I_1/I_3	$X_k=0.160$ cm^{-1}			I_1/I_3	$X_k=0.170$ cm^{-1}		
3	0.0006	0.00075	0.0011	3	0.0009	0.0012	0.0017	3	0.0013	0.0018	0.0025
4	0.0004	0.0006	0.00085	4	0.0007	0.0009	0.0014	4	0.0011	0.0014	0.0020
5	0.0003	0.00045	0.00065	5	0.00055	0.0007	0.0011	5	0.0010	0.0013	0.0016
Separation of I_1 and I_3 in cm^{-1}	0.200	0.190	0.180		0.200	0.190	0.180		0.200	0.190	0.180

Upon correcting to *vacuum* the measured $\nu_{H\alpha}-\nu_{D\alpha}$ interval as reported by Shane and Spedding and with the above-mentioned atomic mass values, their value for e/m becomes $1.7581\pm0.0003\times10^7$ e.m.u./gram.

In his latest report on this subject Dunnington[10] has announced a highly definitive value of $1.7597\pm0.0004\times10^7$ e.m.u./gram for e/m_0 which he obtained from magnetic deflection methods. The precision of his measurements and the extreme care taken by him to correct for numerous sources of error lend considerable weight to his determination.*

CRITICAL EXAMINATION OF POSSIBLE ERRORS

In the evaluation of e/m spectroscopically by use of hydrogen and deuterium, the errors in the constants used are probably relatively small compared to the error in the measured $\Delta\nu$ between the similar components of Hα and Dα.

The most accurate value is that of $\nu_{H\alpha}$, obtained by Houston in 1927. Even granting that this value is in error[9] by 0.0027 cm^{-1} the resultant percent error is negligibly small.

It now appears that the proton and deuteron mass values have become well established and are known to an accuracy considerably beyond that of the measured interval.

The observations on the fringe diameters of the interference patterns seem to be free from any chance of systematic errors. Errors in the screw of the microphotometer would introduce only differential effects, since absolute wave numbers are not being measured, but only the difference of two nearly equal wave numbers. That the actual determination of the points of maximum intensity of the fringes can be done with great accuracy is attested by the very small probable error of ±0.0004 cm^{-1} in the peak-to-peak measurements, and the maximum spread of the observations of about ±0.006 cm^{-1}.

The recent correction of the Faraday to fit the physical scale of masses is an important contribution to the accuracy of the calculations of e/m. The probable error of the Faraday value remains the same as before, about ±8 parts in 100,000.

All of the above-mentioned sources of error are probably smaller than that introduced by the correction of the positions of peak 1 in Hα and Dα. In the preceding paper there is a resumé of the conditions and assumptions underlying the type of correction. By reference to Table III in that paper, which shows the corrections of peak 1 due to the influence of component 4, it is seen that by adopting any reasonable value for I_1/I_4 and for the separation of component 4 from component 1, the *differential* correction between Hα and Dα ranges between 0.0002 cm^{-1} and 0.0004 cm^{-1}.

From Table IV it is seen that the range of corrections probable for peak 1 due to component 3 for Hα is from 0.0005 cm^{-1} to 0.0018 cm^{-1}. The correction due to component 3 is entirely negligible for Dα. The net differential correction, between Hα and Dα, to the position of peak 1 is estimated at +0.0009 cm^{-1} for the most probable value, but could conceivably be as high as +0.0015 cm^{-1} or as low as +0.0002 cm^{-1}. In the former case, e/m would have the value of 1.7576×10^7 e.m.u./gram, and in the latter case it would be 1.7582×10^7 e.m.u./gram.

At the beginning of this research it was thought that the value of e/m might possibly appear to vary with changing discharge conditions, even when the interval between the $2p\,^2P_{3/2}-3d\,^2D_{5/2}$ components (components 1) of Hα and Dα were measured. Five plates, called series H-D213, were taken with the discharge tube operating under the extreme conditions of 2.5 mm of Hg pressure, and a current density of 60 ma/cm^2. The average peak-to-peak separation of peak 1

[10] Dunnington, Phys. Rev. **52**, 475 (1937).

* *Note added in proof:* In a recent paper, Phys. Rev. **54**, 193 (1938) A. E. Shaw reports upon the use of crossed electric and magnetic fields, from which he obtains $e/m_0=1.7571\pm0.0013\times10^7$ e.m.u./gram.

was found to be 2.48666 orders of interference for these plates, compared with an average interval of 2.48832 orders of interference for the normal discharge conditions. This indicates that the peaks were about 0.003 cm^{-1} closer together for the 213 series than for the 212 series. However, the net corrections to the positions of peak 1 in the 213 series are $+0.0016$ cm^{-1} for Hα and $+0.0029$ cm^{-1} for Dα. This means that the differential correction is 0.0045 cm^{-1} in size, and in such direction to increase the Hα–Dα interval. The net result of this is that the Hα–Dα interval for the high pressure, high current density plates was found to be about 0.0015 cm^{-1} greater than for the plates taken under normal conditions. However, the corrections for the 213 series are much more uncertain than those for the 212 series because of the much larger half-intensity breadths of the fringes in the former case.

Component 2, resulting from a $2p\,^2P_{1/2}-3d\,^2D_{3/2}$ and a $2s\,^2S_{1/2}-3p\,^2P_{3/2}$ transition, was not used in this research, but instead the $2p\,^2P_{3/2}-3d\,^2D_{5/2}$ component was used. This was done for these reasons: The last-named component arises from a single transition and consequently is not split by a weak-field Stark effect, nor has it a large hyperfine structure splitting. Bechert and Meixner[11] show that the fine structure and hyperfine structure patterns of Hα and Dα should be identical; accordingly we should not expect any relative shift of component 1 in the fine structure patterns of the two isotopes.

[11] Bechert and Meixner, Ann. d. Physik **22**, 525 (1935).

Summary

Calculations of the value of e/m, based upon the interval between the $2p\,^2P_{3/2}-3d\,^2D_{5/2}$ components of Hα and Dα, result in a value of $1.7579\pm0.0004\times10^7$ e.m.u./gram. The new value of the Faraday, based on the physical scale, and the new scale of atomic weights are used in the evaluation.

From a careful consideration of the possible sources of error resulting from the measurement of the interval, it is felt that the value of e/m as determined from the Dα and Hα interval cannot be greater than 1.7583 nor smaller than 1.7575×10^7 e.m.u./gram.

The mass of the electron in atomic weight units is found to be $5.4902\pm0.0005\times10^{-4}$.

Acknowledgment

It is again a pleasure to acknowledge the active interest of Professor R. C. Gibbs in directing this research and assisting in the preparation of these papers.

OCTOBER 15, 1938 PHYSICAL REVIEW VOLUME 54

A Method of Calculating Fluctuations

Raymond Ellickson*
University of Chicago, Chicago, Illinois
(Received July 11, 1938)

A general method for the solution of fluctuation problems is described. A generating function for the differential equations that are satisfied by the probabilities in question is defined and the problem is reduced to the determination of the generating function. The general method for its determination is given and the results are applied to fluctuation problems in pair-production and radioactive disintegration. The method of finding the mean, mean square, and standard deviation from the generating function without reference to the form of the distribution itself is applied to the examples. The problem of fluctuations in chain and branch radioactive disintegrations is solved without restrictions on the size of the disintegration constants involved.

Introduction

In experiments on radioactivity, cosmic rays, energy loss of electrons, etc., fluctuations play an important part. In some cases it is relatively easy to take these fluctuations into account, for example, those that follow the Poisson law. The Poisson law can be derived from the more general binomial law[1] if the restriction is made

* Now at Brooklyn Polytechnic Institute.

[1] L. I. Schiff, Phys. Rev. **50**, 88 (1936).

that the probability, q, of the elementary event in question is so small that the product Nq remains finite as N becomes large, N being the total number of individuals under consideration.

For a large number of individuals that can fall in any one of a large number of divisions, the law can be derived directly, without reference to the binomial law, subject to the following more general conditions:[2]

1. The chance of falling in a division is the same for each individual.
2. The fact that an individual has fallen in a division does not affect the chance of other individuals falling therein.
3. The chance of an individual falling in it is the same for each division.

Although not a part of the general conditions, in radioactive problems the number of atoms of the parent substance must remain essentially constant throughout the experiment. If this is not the case, the probable number of disintegrations will be a function of the time and subject to fluctuations itself.

Examples of fluctuation problems that do not meet these conditions, and therefore are not governed by the Poisson law, are the number of particles in a cosmic-ray shower and chain or branch radioactive disintegration. In this paper a method is given for calculating fluctuations for some problems that are not subject to the Poisson law. The method is a very general one and can easily be extended to cover many similar problems. It is often possible to obtain the complete solution by using it, although there are some problems (e.g. Furry's Problem *B*) for which it is not possible to carry out all the steps without undue labor.

Illustration of the Method

While the method to be used is very general, it is easier to explain it in connection with special examples. One such example is Furry's Problem *A*,[3] which is an idealization of the problem of the fluctuations in the number of particles in cosmic-ray showers: The probability that in traversing thickness dt one particle is converted into two is just dt. If one particle enters a sheet of thickness t, what is the probability $P(n, t)$ that n particles will emerge? The probabilities in question satisfy the system of differential equations

$$(d/dt)P(n, t) = -nP(n, t) + (n-1)P(n-1, t) \quad (1)$$

with the boundary conditions

$$P(1, 0) = 1; \quad P(n, 0) = 0, \quad n \neq 1. \quad (2)$$

These equations can be solved, as Furry has done, by successive integration and application of the boundary conditions, or one may define a generating function[4]

$$Q(x, t) = \sum_{n=0}^{\infty} x^n P(n, t) \quad (3)$$

and attempt to determine it. Since

$$(\partial/\partial x)Q(x, t) = \sum_{n=0}^{\infty} nx^{n-1}P(n, t)$$

it follows from Eqs. (1) and (3) that

$$(\partial/\partial t)Q(x, t) = (x^2 - x)(\partial/\partial x)Q(x, t) \quad (4)$$

with the boundary condition

$$Q(x, 0) = x. \quad (5)$$

Having determined $Q(x, t)$, $P(n, t)$ can be found by series expansion. Other quantities of interest can be found from $Q(x, t)$ without determining the P's; thus the mean number

$$\langle n \rangle = \sum_{n=0}^{\infty} nP(n, t) = [(\partial/\partial x)Q(x, t)]_{x=1}, \quad (6)$$

and the mean square

$$\langle n^2 \rangle = \sum_{n=0}^{\infty} n^2 P(n, t) = [(\partial/\partial x)x(\partial/\partial x)Q(x, t)]_{x=1}. \quad (7)$$

The mean square can also be found from Eq. (6) and the relation

$$\langle n^2 \rangle - \langle n \rangle = \sum_{n=0}^{\infty} n(n-1)P(n, t) = [(\partial^2/\partial x^2)Q(x, t)]_{x=1}.$$

The standard deviation, probable error, and probable percentage error can be found from Eqs. (6) and (7). Thus, in cases where the series expansion for the $P(n, t)$ is difficult to carry out,

[2] D. J. Struik, J. Math. Phys. M. I. T. **9**, 151 (1930).
[3] W. H. Furry, Phys. Rev. **52**, 269 (1937).
[4] R. H. Fowler, *Statistical Mechanics*, 2d edition (Macmillan, 1936), pp. 36–46.

one can find the values of the quantities mentioned above using only the generating function, without finding the actual distribution.

Determination of the Generating Function

The method of determining the generating function, Q, will be given for a case somewhat more general than Eq. (4), in order that the results may be applied to the problems to be taken up later.

In general one has to solve a linear partial differential equation of the form

$$\partial Q/\partial t = X(\partial Q/\partial x) + Y(\partial Q/\partial y) + \cdots, \quad (8)$$

where X, Y, $\cdots$ are functions of x, y, $\cdots$, subject to the boundary condition

$$Q(0, x, y, \cdots) = F(x, y, \cdots). \quad (9)$$

To such a partial differential equation is associated the set of ordinary differential equations[5]

$$\begin{aligned} d\xi/dt &= X(\xi, \eta, \cdots), \\ d\eta/dt &= Y(\xi, \eta, \cdots), \\ &\cdots\cdots\cdots \end{aligned} \quad (10)$$

Their general solution is of the form

$$\begin{aligned} \xi &= f_1(t, x, y, \cdots), \\ \eta &= f_2(t, x, y, \cdots), \\ &\cdots\cdots\cdots \end{aligned} \quad (11)$$

where x, y, $\cdots$ appear as constants of integration, and the f's are chosen so that

$$\begin{aligned} x &= f_1(0, x, y, \cdots), \\ y &= f_2(0, x, y, \cdots), \\ &\cdots\cdots\cdots \end{aligned}$$

If the solution of Eq. (10) is known, that of Eqs. (8) and (9) is[6]

$$Q(t, x, y, \cdots) = F[f_1(t, x, y, \cdots), f_2(t, x, y, \cdots), \cdots], \quad (12)$$

which is the solution required.

Application to the Problem of Pair Production

One can now apply the results of the last section to the solution of Furry's Problem A.

From Eqs. (4), (8), and (10)

$$d\xi/dt = \xi^2 - \xi.$$

Integrating and setting $\xi = x$ at $t = 0$:

$$\xi = xe^{-t}/(xe^{-t} - x + 1) = e^{-t}\sum_{n=0}^{\infty} x^n(1 - e^{-t})^{n-1}. \quad (13)$$

The boundary condition $Q(x, 0) = x$ requires that $Q = \xi$, and comparing Eq. (13) with (3) it is evident that

$$P(n, t) = e^{-t}(1 - e^{-t})^{n-1}.$$

From Eqs. (6) and (13), the mean number of particles at depth t is

$$\langle n \rangle = e^t.$$

Therefore

$$P(n, t) = (\langle n \rangle)^{-1}[1 - (\langle n \rangle)^{-1}]^{n-1},$$

which is the solution obtained by Furry. From Eq. (7), the mean square is

$$\langle n^2 \rangle = 2e^{2t} - e^t.$$

The square of the standard deviation is then

$$\sigma_n^2 = \langle n^2 \rangle - (\langle n \rangle)^2 = e^t(e^t - 1).$$

In a Poisson distribution σ_n^2 is proportional to the mean number; in this problem it is roughly proportional to the square of the mean number, a substantial difference.

Another problem treated by Furry, Problem B, is stated as follows: The probability that in dt an electron produces a photon is dt, the electron itself continuing its course; the probability that in dt a photon produces a pair of electrons is $r\,dt$, the photon being absorbed. If one electron enters a sheet of thickness t, what is the probability, $P(n, t)$ that n electrons emerge?

Defining $p(n, m, t)$ as the probability that n electrons and m photons emerge, one has the differential equations

$$\begin{aligned} (d/dt)p(n, m, t) &= -(n + mr)p(n, m, t) \\ &+ np(n, m-1, t) + (m+1)rp(n-2, m+1, t) \end{aligned} \quad (14)$$

and the additional relation

$$P(n, t) = \sum_{m=0}^{\infty} p(n, m, t).$$

[5] Courant and Hilbert, *Methoden der Mathematischen Physik*, Vol. II (Julius Springer, 1927), p. 25.

[6] Heinrich Weber, *Die Partiellen Differential Gleichungen der Mathematischen Physik* (Friedrich Vieweg und Sohn, 1900), p. 147.

Defining the generating function

$$Q(x, y, t)=\sum_{n=0}^{\infty}\sum_{m=0}^{\infty}x^n y^m p(n, m, t),$$

one gets the equation

$$\partial Q/\partial t=x(y-1)(\partial Q/\partial x)+r(x^2-y)(\partial Q/\partial y)$$

and from Eq. (10)

$$d\xi/dt=\xi(1-\eta),$$
$$d\eta/dt=r(\eta-\xi^2).$$

These equations are not readily integrable so that in this case the method fails to give a useful result.

However, one can easily solve a problem that is essentially equivalent to the case $r=\infty$. It may be formulated as follows: The probability that an electron creates a pair in thickness dt is just dt, the electron continuing its course. If one electron enters a sheet of thickness t, what is the probability $P(n, t)$ that n particles emerge? Then the system of differential equations is

$$(d/dt)P(n, t)=-nP(n, t)+(n-2)P(n-2, t),$$

with the generating function

$$Q(x, t)=\sum_{n=0}^{\infty}x^n P(n, t).$$

One obtains, as before

$$\partial Q/\partial t=(x^3-x)(\partial Q/\partial x)$$

and

$$d\xi/dt=\xi^3-\xi.$$

Integrating by partial fractions

$$\xi=xe^{-t}[1-x^2(1-e^{-2t})]^{-\frac{1}{2}},$$

$$=e^{-t}\sum_{n=0}^{\infty}(-1)^n\binom{-\frac{1}{2}}{n}x^{2n+1}(1-e^{-2t})^n,$$

$$=\sum_{n=0}^{\infty}x^{2n+1}P(2n+1, t),$$

where $\binom{-\frac{1}{2}}{n}$ is the binomial coefficient. Therefore

$$P(2n+1, t)=(-1)^n\binom{-\frac{1}{2}}{n}e^{-t}(1-e^{-2t})^n;$$

from the conditions of the problem, $P(2n, t)=0$. The mean number

$$\langle n\rangle=e^{2t},$$

and therefore

$$P(2n+1, t)=(-1)^n\binom{-\frac{1}{2}}{n}(\langle n\rangle)^{-1}[1-(\langle n\rangle)^{-1}]^n.$$

The mean square and square of the standard deviation are

$$\langle n^2\rangle=3e^{4t}-2e^{2t},$$
$$\sigma_n{}^2=2e^{2t}(e^{2t}-1).$$

Application to Simple Radioactive Decay

As a first example of a somewhat different type of problem, consider the decay of a radioactive substance whose decay constant is λ. If $\langle n\rangle$ is the probable number of atoms present at time t, and ν the probable number at $t=0$,

$$(d/dt)(\langle n\rangle)=-\lambda\langle n\rangle,\quad \langle n\rangle=\nu e^{-\lambda t}.$$

To study the fluctuations of n about the probable value, we need to determine $P(n, t)$, the probability that there are just n atoms present at time t. These functions satisfy the differential equations,

$$(d/dt)P(n, t)=-\lambda nP(n, t)+\lambda(n+1)P(n+1, t). \quad (15)$$

To determine them completely their value at $t=0$, $P(n, 0)$, must be known. The generating function for Eq. (15) satisfies the equations

$$\partial Q/\partial t=\lambda(1-x)(\partial Q/\partial x),$$

$$Q(x, 0)=\sum_{n=0}^{\infty}x^n P(n, 0).$$

The appropriate solution of the associated ordinary differential equation is

$$\xi=(x-1)e^{-\lambda t}+1,$$

and therefore

$$Q(x, t)=\sum_{n=0}^{\infty}\xi^n P(n, 0).$$

In general, the values of $P(n, 0)$ will not be

known; however, one may assume that $P(n, 0)$ has a maximum for some value of n approximately equal to ν. If this maximum is sharp and ν is large, the generating function may be approximated by

$$\begin{aligned} Q(x, t) &= \xi^{\nu} \\ &= [1+e^{-\lambda t}(x-1)]^{\nu} \\ &= (a+bx)^{\nu}, \end{aligned}$$

where $b=1-a=e^{-\lambda t}$.

From this, it readily follows that

$$P(n, t)=\binom{\nu}{n}(1-b)^{\nu-n}b^{n}. \tag{16}$$

The value of $\langle n\rangle$, obtained by differentiating Q, is found to be νb. Differentiating again,

$$\langle n^2\rangle-\langle n\rangle=\nu(\nu-1)b^2,$$

from which $\sigma_n^2=\langle n\rangle a.$

For large values of t, a approaches 1 and the Poisson formula, $\sigma_n^2=\langle n\rangle$, is valid.

However, one is usually not interested in $\langle n\rangle$ or σ_n^2, but in the number of atoms that decay in the time interval from t to $t+\Delta$. To discuss the fluctuations in the number decaying in this interval, one requires the probability that there are n atoms at time t, and m at time $t+\Delta$. Let $P(\nu, n, t)$ be the function previously called $P(n, t)$ and defined by Eq. (16); then the required probability is easily seen to be

$$p(n, m)=P(\nu, n, t)P(n, m, \Delta),$$

which has the generating function

$$Q(x, y, t)=\sum_{n=0}^{\infty}\sum_{m=0}^{\infty}p(n, m)x^n y^m.$$

From Eq. (16)

$$\begin{aligned} Q(x, y, t) &= \sum_{n=0}^{\infty}P(\nu, n, t)x^n(\alpha+\beta y)^n \\ &= [a+bx(\alpha+\beta y)]^{\nu}, \end{aligned}$$

where $\beta=1-\alpha=e^{-\lambda\Delta}$.

The probability that there are just s disintegrations in the interval is

$$p(s)=\sum_{m=0}^{\infty}p(m+s, m),$$

with the generating function

$$\begin{aligned} Q(x, 1/x, t) &= [a+b(\alpha x+\beta)]^{\nu} \\ &= [A+Bx]^{\nu}. \end{aligned}$$

where

$$A=a+b\beta, \quad B=b\alpha=1-A.$$

Consequently,

$$p(s)=\binom{\nu}{s}A^{\nu-s}B^{s},$$

$$\langle s\rangle=\nu B=\langle n\rangle_t-\langle n\rangle_{t+\Delta},$$

$$\langle s^2\rangle=(\langle s\rangle)^2+\langle s\rangle A,$$

$$\sigma_s^2=\langle s\rangle A.$$

In case $B\ll 1$ and $\nu\gg 1$ the generating function approximates

$$Q(x, 1/x, t)=\exp[\langle s\rangle(x-1)]$$

and $$p(s)=(1/s!)\exp[-\langle s\rangle](\langle s\rangle)^s,$$

which is the Poisson formula. These results are not new, but by applying the same methods to chain disintegrations, new results are obtainable.

Chain Disintegrations

Suppose one has three substances A, B, and C, such that A disintegrates with decay constant λ_1 to form B, and B disintegrates with decay constant λ_2 to form C, a stable element. Let $\langle k\rangle$, $\langle m\rangle$, $\langle n\rangle$, be the probable number of each present at time t. Then

$$\begin{aligned} (d/dt)(\langle k\rangle) &= -\lambda_1\langle k\rangle, \\ (d/dt)(m) &= \lambda_1\langle k\rangle-\lambda_2\langle m\rangle, \\ (d/dt)(n) &= \lambda_2\langle m\rangle. \end{aligned} \tag{17}$$

The solution of these equations is well known and is

$$\begin{aligned} \langle k\rangle &= \kappa a(t), \\ \langle m\rangle &= \kappa c(t)+\mu b(t), \\ \langle n\rangle &= \kappa e(t)+\mu d(t)+\nu, \end{aligned}$$

where

$$a=e^{-\lambda(1)t},\quad b=e^{-\lambda(2)t},\quad c=[\lambda_1/(\lambda_2-\lambda_1)](a-b),$$
$$d=1-b,\quad e=1-a-c,$$

and κ, μ, ν are the probable numbers of each present at $t=0$.

To study the fluctuations about the average, one must find the probability that at time t there are k, m, n of the three kinds present. The probabilities satisfy the system of differential equations[7]

$$(d/dt)P(k,m,n)=-k\lambda_1P(k,m,n)$$
$$+(k+1)\lambda_1P(k+1,m-1,n)-m\lambda_2P(k,m,n)$$
$$+(m+1)\lambda_2P(k,m+1,n-1). \quad (18)$$

To solve these equations completely one has to have the values of $P(k,m,n)$ at $t=0$, which are usually not given. However, we shall assume that, at $t=0$, $P(k,m,n)$ has a sharp maximum at $k=\kappa$, $m=\mu$, $n=\nu$. Then the generating function for Eq. (18) is approximately given by the boundary condition

$$Q(x,y,z,0)=x^\kappa y^\mu z^\nu.$$

From Eq. (18) one obtains

$$\partial Q/\partial t=\lambda_1(y-x)(\partial Q/\partial x)+\lambda_2(z-y)(\partial Q/\partial y), \quad (19)$$

with the associated ordinary differential equations

$$d\xi/dt=\lambda_1(\eta-\xi),$$
$$d\eta/dt=\lambda_2(\zeta-\eta),$$
$$d\zeta/dt=0.$$

Integrating directly, one gets (using the same definitions of a, $\cdots$, e as above)

$$\xi=ax+cy+ez,$$
$$\eta=\quad by+dz,$$
$$\zeta=\quad\quad z,$$

from which

$$Q(x,y,z,t)=(ax+cy+ez)^\kappa(by+dz)^\mu z^\nu. \quad (20)$$

From the definition of the generating function, one can get $P(k,m,n)$ by picking out the coefficients of $x^ky^mz^n$ in Eq. (20).

The probability, $P(K,t)$ that there are K atoms of kind A regardless of the number of kind B and C is given by the coefficient of x^K in

$$Q(x,1,1,t)=(ax+c+e)^\kappa,$$

from which

$$P(K,t)=\binom{\kappa}{K}(1-a)^{\kappa-K}a^K. \quad (21)$$

Eq. (21) is in the same form as Eq. (16) and therefore the fluctuations in the number of disintegrations $A\rightarrow B$ will be the same as for the simple radioactive case. This is not true for disintegrations $B\rightarrow C$.

The probability, $P(M,t)$ that there are M atoms of kind B at time t is the coefficient of y^M in

$$Q(1,y,1,t)=(a+cy+e)^\kappa(by+d)^\mu. \quad (22)$$

The $P(M,t)$ cannot be calculated without difficulty except for the case $\mu=0$. However $\langle M\rangle$, $\langle M^2\rangle$, and σ_M are easy to determine by differentiation of Eq. (22). The probability $P(N,t)$ for atoms of kind C can be treated in a similar manner.

To study the fluctuations in the number of disintegrations, let $P(\kappa,\mu,\nu;k,m,n;t)$ be the probability of k, m, n atoms of each kind at time t, given κ, μ, ν at $t=0$. Then one can define the function

$$p(k,m,n;k',m',n')$$
$$=P(\kappa,\mu,\nu;k,m,n;t)P(k,m,n;k',m',n';\Delta)$$

as the probability that in an interval t, $t+\Delta$, the number of atoms of each kind has changed from k, m, n to k', m', n'. The $p(k,m,n;k',m',n')$ are generated by

$$Q(x,y,z;u,v,w)$$
$$=\sum_{k=0}^{\infty}\sum_{m=0}^{\infty}\sum_{n=0}^{\infty}P(\kappa,\mu,\nu;k,m,n)x^ky^mz^n$$
$$\times[\alpha u+\gamma v+\epsilon w]^k[\beta v+\delta w]^m w^n$$
$$=[ax(\alpha u+\gamma v+\epsilon w)+cy(\beta v+\delta w)+ezw]^\kappa$$
$$\times[by(\beta v+\delta w)+dzw]^\mu(zw)^\nu,$$

where a, $\cdots$, e are as before, and

$$\alpha=e^{-\lambda(1)\Delta},\quad \beta=e^{-\lambda(2)\Delta},\quad \gamma=[\lambda_1/(\lambda_2-\lambda_1)](\alpha-\beta),$$
$$\delta=1-\beta,\quad \epsilon=1-\alpha-\gamma.$$

[7] The validity of Eq. (18) may be checked by deriving Eq. (17) from them, using the usual definition of k, m, n in terms of $P(k,m,n)$.

The probability that $k=k'+r$, $n=n'-s$, with k, m, n, m' anything whatever is generated by

$$Q(x, 1, 1/w; 1/x, 1, w)$$
$$=[ax(\alpha u+\gamma v+\epsilon w)+c(\beta+\delta w)+e]^{\kappa} \times[b(\beta+\delta w)+d]^{\mu}$$
$$=\sum_{r=0}^{\infty}\sum_{s=0}^{\infty} p(r, s)x^r w^s \qquad (23)$$

if $p(r, s)$ is the probability of r disintegrations of kind $A\rightarrow B$, and s of kind $B\rightarrow C$.

The probability of r disintegrations of kind $A\rightarrow B$, is

$$p'(r)=\sum_{s=0}^{\infty} p(r, s).$$

From Eq. (23), with $w=1$,

$$\sum_{r=0}^{\infty} x^r p'(r)=[A'+B'x]^{\kappa}, \qquad (24)$$

where

$$A'=a\alpha+c+e, \quad B'=a(1-\alpha), \quad A'+B'=1.$$

This $p'(r)$ is then the coefficient of x^r in the expansion of Eq. (24), in agreement with the remark made above. The mean number and standard deviation, from Eq. (24), turns out to be

$$\langle r\rangle=\kappa a(1-\alpha)=\kappa e^{-\lambda(1)t}(1-e^{-\lambda(1)\Delta}),$$
$$\sigma_r^2=(\langle r\rangle)[1-(\langle r\rangle)/\kappa].$$

The probability of s disintegrations of kind $B\rightarrow C$ is

$$p''(s)=\sum_{r=0}^{\infty} p(r, s).$$

From Eq. (23), with $x=1$,

$$\sum_{s=0}^{\infty} w^s p''(s)=[A''+B''w]^{\kappa}[C''+D''w]^{\mu},$$

where

$$A''=a(1-\epsilon)+c\beta+e, \quad B''=a\epsilon+\delta c, \quad C''=b\beta+d,$$
$$D''=\delta b, \quad A''+B''=C''+D''=1.$$

One obtains easily

$$\langle s\rangle=\kappa(a\epsilon+c\delta)+\mu b\delta,$$
$$\sigma_s^2=\langle s\rangle-\kappa(a\epsilon+c\delta)^2-\mu(b\delta)^2.$$

If the disintegration products are indistinguishable it is of interest to find the fluctuations in the total number of disintegrations. Setting $x=w$ in Eq. (23), one obtains for the probability of s disintegrations of either kind

$$p'''(s)=\sum_{r=0}^{\infty} p(s-r, r),$$

which is the coefficient of x^s in the expansion of

$$\sum_{s=0}^{\infty} x^s p'''(s)=[A'''+C'''x+E'''x^2]^{\kappa}[B'''+D'''x]^{\mu},$$

where

$$A'''=a\alpha+c\beta+e, \quad B'''=b\beta+d, \quad C'''=a\gamma+c\delta,$$
$$D'''=b\delta, \quad E'''=a\epsilon,$$
$$A'''+B'''+C'''=B'''+D'''=1.$$

By differentiation, one obtains

$$\langle s\rangle=\kappa(C'''+2E''')+\mu D''',$$
$$\sigma_s^2=\langle s\rangle+\kappa E'''(C'''+2A''')-\mu D'''^2.$$

These formulae are quite elaborate, analytically, but are not difficult for numerical evaluation.

Branch Disintegrations

Suppose an atom A can disintegrate either with decay constant λ_1 to form B, or with decay constant λ_1' to form C, and that B and C disintegrate with decay constants λ_2 and λ_3 to form D, a stable element. The probable number of atoms of each satisfy the equations

$$(d/dt)(\langle h\rangle)=-(\lambda_1+\lambda_1')\langle h\rangle,$$
$$(d/dt)(\langle k\rangle)=\lambda_1\langle h\rangle-\lambda_2\langle k\rangle,$$
$$(d/dt)(\langle m\rangle)=\lambda_1'\langle h\rangle-\lambda_3\langle m\rangle,$$
$$(d/dt)(\langle n\rangle)=\lambda_2\langle k\rangle+\lambda_3\langle m\rangle,$$

with the solutions

$$\langle h\rangle=a\theta,$$
$$\langle k\rangle=b\theta+e\kappa,$$
$$\langle m\rangle=c\theta+g\mu,$$
$$\langle n\rangle=d\theta+f\kappa+j\mu+\nu,$$

where

$$a=e^{-(\lambda_1+\lambda_1')t}$$

$$b=[\lambda_1/(\lambda_2-\lambda_1-\lambda_1')](a-e),$$

$$c=[\lambda_1'/(\lambda_3-\lambda_1-\lambda_1')](a-g),$$

$$a+b+c+d=e+f=g+j=1,$$

and θ, κ, μ, ν are the probable numbers of each present at $t=0$. Just as in the previous problem, one can define

$$Q(w,x,y,z,t)=\sum_{h=0}^{\infty}\sum_{k=0}^{\infty}\sum_{m=0}^{\infty}\sum_{n=0}^{\infty}w^h x^k y^m z^n P(h,k,m,n)$$

and obtain the equation

$$\partial Q/\partial t=(\partial Q/\partial w)(\lambda_1 x+\lambda_1' y-\lambda_1 w-\lambda_1' w)$$
$$+(\partial Q/\partial x)\lambda_2(z-x)+(\partial Q/\partial y)\lambda_3(z-y),$$

to be solved subject to

$$Q(w,x,y,z,0)=w^\theta x^\kappa y^\mu z^\nu.$$

The associated system of ordinary differential equations is

$$d\psi/dt=\lambda_1\xi+\lambda_1'\eta-(\lambda_1+\lambda_1')\psi,$$

$$d\xi/dt=\lambda_2(\zeta-\xi),$$

$$d\eta/dt=\lambda_3(\zeta-\eta),$$

$$d\zeta/dt=0.$$

The value of Q turns out to be

$$Q(w,x,y,z,t)=(aw+bx+cy+dz)^\theta$$
$$\times(ex+fz)^\kappa(gy+iz)^\mu z^\nu,$$

from which one can calculate the fluctuations in the number of atoms present and in the number of disintegrations as before. There is such a variety of possible calculations that it scarcely seems worth while to make any without having some specific experiment in mind.

Concluding Remarks

It has been the aim of the writer to develop a method for the solution of fluctuation problems that cannot be handled by ordinary methods such as the assumption of a Poisson distribution. The method consists of finding the system of differential equations that are satisfied by the probabilities under consideration, the definition of a generating function for these probabilities and the determination of the generating function from the differential equations. The method has been shown to be effective in the solution of a variety of problems and is so general that there are undoubtedly many others that can be solved by its use.

An important feature of the method is that many useful quantities such as the standard deviation and the mean of the distribution can be found from the generating function in those cases where the distribution itself is difficult to work out.

The writer wishes to express his sincere appreciation to Dr. Carl Eckart for suggesting the problem and for continued interest and advice in the progress of its solution.

The Paths of Ions in the Cyclotron

I. Orbits in the Magnetic Field

L. H. THOMAS
Mendenhall Laboratory of Physics, Ohio State University, Columbus, Ohio

(Received July 11, 1938)

Bethe and Rose maintain in a recent letter and paper that a maximum energy for the beam from a cyclotron is fixed by the incompatibility of the conditions for resonance and focusing when the relativity increase of mass with velocity is taken into account. It is shown below that, while this result holds for a radially symmetrical magnetic field, it is not necessarily true in general; and that for a field varying with polar angle there is an additional focusing effect. If the relative variation of the field with polar angle is of the order of the ratio of the velocity of the ion to the velocity of light, this focusing effect will compensate the defocusing effect of Bethe and Rose. It is shown further that if this variation has period $\pi/2$, a family of stable periodic orbits exists which are nearly concentric circles. The second order effects due to the simultaneous action of the variations with polar angle of the magnetic field and the accelerating electric field will be considered in a second paper.

INTRODUCTION

IN a cyclotron a magnetic field H curves the paths of particles of charge e and mass m so that they describe circuits in time $2\pi/\omega=2\pi m/eH$. An electric field oscillating in this period continually accelerates those particles that are in phase so that they describe, with increasing velocity v, circuits of radius v/ω. Particles are introduced near the central line and withdrawn near the curved surface of a short cylindrical region of radius A with generators parallel to the magnetic field, when they have attained velocity $A\omega$.

Since the curvature of the path of a particle in a magnetic field is accurately proportional inversely to its momentum $m_0v/\{1-v^2/c^2\}^{\frac{1}{2}}\approx m_0v(1+\frac{1}{2}v^2/c^2)$, where m_0 is its rest mass, and c the velocity of light, the time of description of a circuit will increase with increasing velocity, and the particles will get out of phase and never attain great energy unless the magnetic field increases in the same ratio as the momentum. If the magnetic field, which must have zero curl, increases with distance from the axis, the magnetic lines must curve outwards above and below a median plane to which they are all perpendicular, (Fig. 1). An orbit above that plane will therefore be curved away from it as well as around the axis, and the beam will be defocused: this effect, discovered by Bethe and Rose,[1,2] is proportional to the relative change in magnetic field, and so to v^2/c^2.

If the magnetic field varies with polar angle about the central line, the path of a particle must have greatest curvature where the field is greatest, and if the path is a closed orbit it must have greatest radial distance where the field is greatest (X, Fig. 2). Along a portion of the orbit in a region (A) in which the field decreases as the polar angle increases, the magnetic lines must curve backwards from the median plane to which they are all perpendicular, and lie in cylindrical surfaces about the axis. In this region the orbits have decreasing radial distances and an orbit above that plane will therefore be curved towards it as well as around the axis; and the beam will be focused (Fig. 3). The same is true in a region (B) in which the field and radial distance both increase with polar angle. This effect is proportional to the product of the relative changes in radial distance and in magnetic field and so to the square of the relative change in magnetic field with polar angle.

The above argument holds for a variation of the magnetic field with polar angle that does not depend on the distance from the axis: It is shown below in detail that if the variation depends on

[1] H. A. Bethe and M. E. Rose, Phys. Rev. **52**, 1254 (1937).
[2] M. E. Rose, Phys. Rev. **53**, 392 (1938).

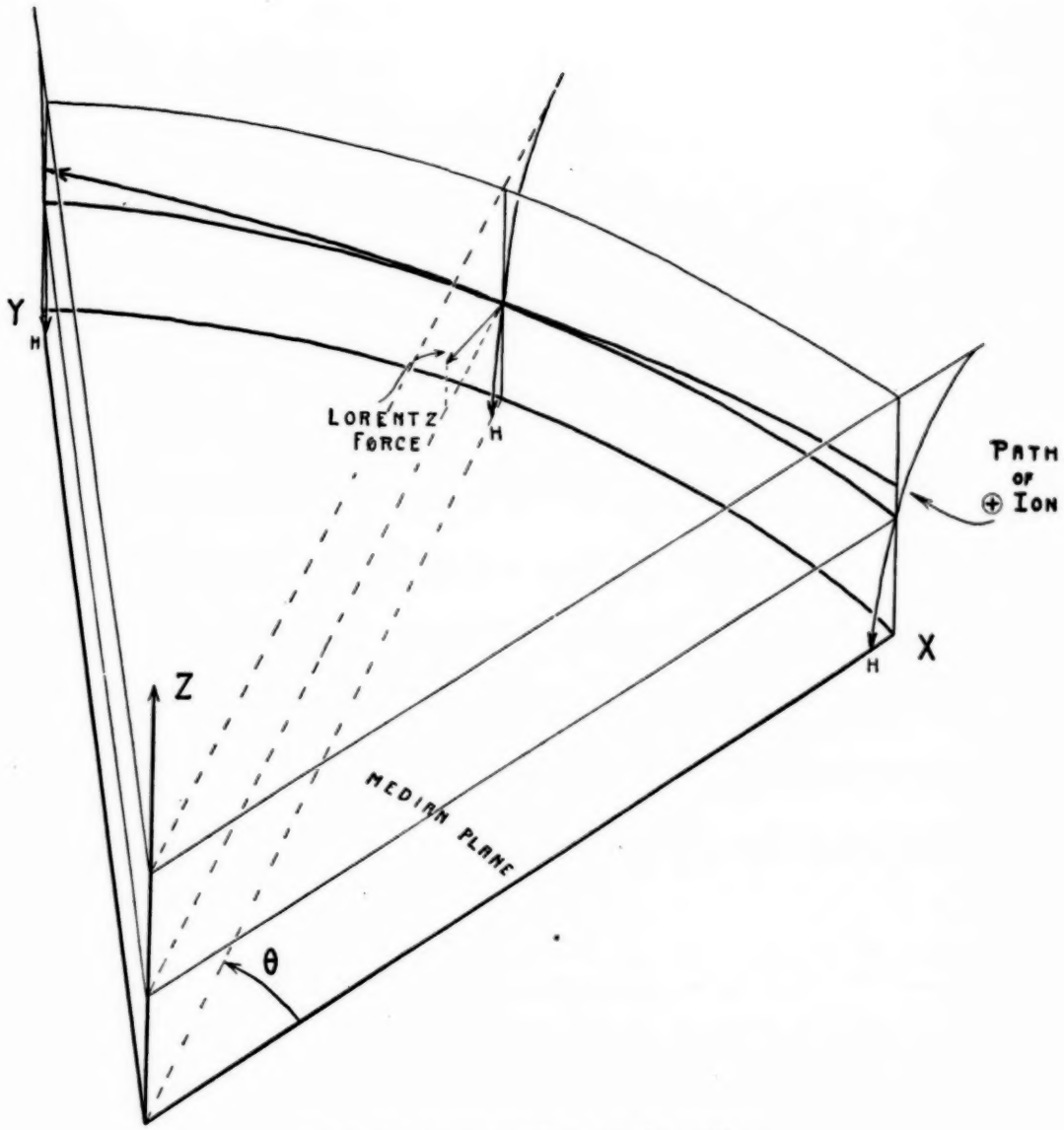

FIG. 1. The defocusing effect of Bethe and Rose.

the distance in such a way as to preserve the time of description of the orbit, the effect is always to focus the beam. A variation of order v/c of the magnetic field with polar angle therefore introduces focusing that will compensate the defocusing effect of Bethe and Rose.

A variation of the magnetic field with position in the median plane will cause a secular change in orbits in that plane regarded as to a first approximation circular. A term in the magnetic field proportional to $\sin\theta$ which we shall suppose is an increase in the y-direction increases the curvature on the side of the circle for which y is positive and decreases it on the side for which y is negative so that the center moves in the positive x-direction (Fig. 4) by an amount per circuit proportional to the product of the radius of the orbit and the change in magnetic field between the two sides.[3] In this case there are no closed orbits.

A term in the magnetic field proportional to $\sin 2\theta$, which we shall suppose is an increase in

[3] I am indebted to a conversation with Professor Bethe for this simple discussion of stability in terms of secular change. See also II §3 below.

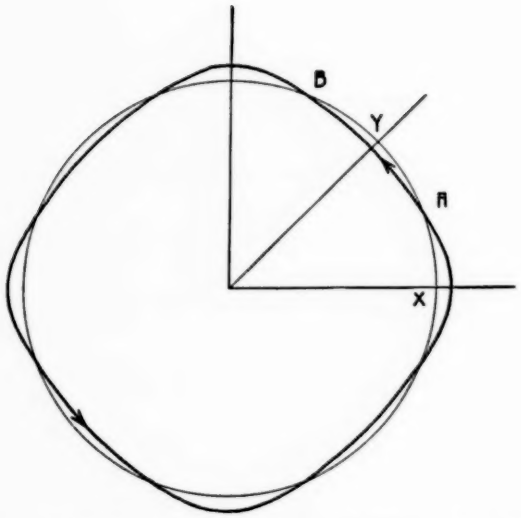

FIG. 2. A periodic orbit in a magnetic field varying with polar angle. (For a positive ion the magnetic field is directed away from the reader.)

both directions for which $x=y$, causes the center to move away from $x=0$ by an amount per circuit proportional to the product of the variation of the magnetic field around the orbit and the distance of the center from $x=0$, as the magnetic field is then greater on the left side by an amount proportional to the product of the ratio of that distance to the radius of the orbit and the variation of the magnetic field around the orbit; and to move towards $y=0$ in a similar way.[3] In this case there is a family of closed orbits but they are unstable.

Thus such terms in the magnetic field will cause particles to approach the outside of the cyclotron along paths of various radii and with various energies; and may, if large enough, so disturb the phase adjustment that the particles will never gain great energy.

It is shown in detail below that a variation of magnetic field proportional to $\cos 4\theta$, or, more generally, any variation periodic with period $\pi/2$ in θ, admits a *stable* family of closed orbits that are approximately circles about the center of the cyclotron.

Thus a variation of the magnetic field with angle, periodic with period $\pi/2$ in θ, approximately proportional to $\cos 4\theta$, where θ may be measured from any initial direction, and of order of magnitude v/c; together with nearly the radial increase of relative amount $\frac{1}{2}v^2/c^2$ of Bethe and Rose; gives stable orbits that are in resonance and not defocused.

1. NOTATION

The equations of motion of a particle of charge e, rest mass m_0, and velocity v, in cylindrical polar coordinates r, θ, z, with the time as independent variable, in magnetic field (H_r, H_θ, H_z), are

$$\begin{aligned}
&\frac{d}{dt}\left(m\frac{dr}{dt}\right)-mr\left(\frac{d\theta}{dt}\right)^2=\frac{e}{c}\left(r\frac{d\theta}{dt}H_z-\frac{dz}{dt}H_\theta\right),\\
&r\frac{d}{dt}\left(m\frac{d\theta}{dt}\right)+2m\frac{dr}{dt}\frac{d\theta}{dt}=\frac{e}{c}\left(\frac{dz}{dt}H_r-\frac{dr}{dt}H_z\right),\\
&\frac{d}{dt}\left(m\frac{dz}{dt}\right)=\frac{e}{c}\left(\frac{dr}{dt}H_\theta-r\frac{d\theta}{dt}H_r\right),
\end{aligned}\tag{1.1}$$

where $mv=m_0v/(1-v^2/c^2)^{\frac{1}{2}}$ is the momentum, (1.2)

$$v^2=\left(\frac{dr}{dt}\right)^2+r^2\left(\frac{d\theta}{dt}\right)^2+\left(\frac{dz}{dt}\right)^2 \tag{1.3}$$

and c is the velocity of light: e is in electrostatic units and the magnetic field in electromagnetic units: and a right-handed screw rotating in the direction of θ increasing travels along the positive z-direction.

The magnetic field must satisfy

$$\begin{aligned}
&\frac{1}{r}\frac{\partial H_z}{\partial\theta}-\frac{\partial H_\theta}{\partial z}=0, \quad \frac{\partial H_\theta}{\partial r}+\frac{1}{r}H_\theta-\frac{1}{r}\frac{\partial H_r}{\partial\theta}=0,\\
&\frac{\partial H_r}{\partial z}-\frac{\partial H_z}{\partial r}=0, \quad \frac{\partial H_r}{\partial r}+\frac{1}{r}H_r+\frac{1}{r}\frac{\partial H_\theta}{\partial\theta}+\frac{\partial H_z}{\partial z}=0.
\end{aligned}\tag{1.4}$$

We shall suppose that in the median plane $z=0$, $H_\theta=0$, $H_r=0$, so that also $\partial H_z/\partial z=0$, and that the field is symmetrical about this plane, so that for small z

$$\begin{aligned}
H_z&=-H+0(z^2),\\
H_r&=-z(\partial H/\partial r)+0(z^3),\\
H_\theta&=-(z/r)(\partial H/\partial\theta)+0(z^3),
\end{aligned}\tag{1.5}$$

where H can be adjusted to be any function of r and θ periodic with period 2π in θ. The negative sign is taken so that if H is a positive constant the orbits in the median plane are circles described in the direction of θ increasing.

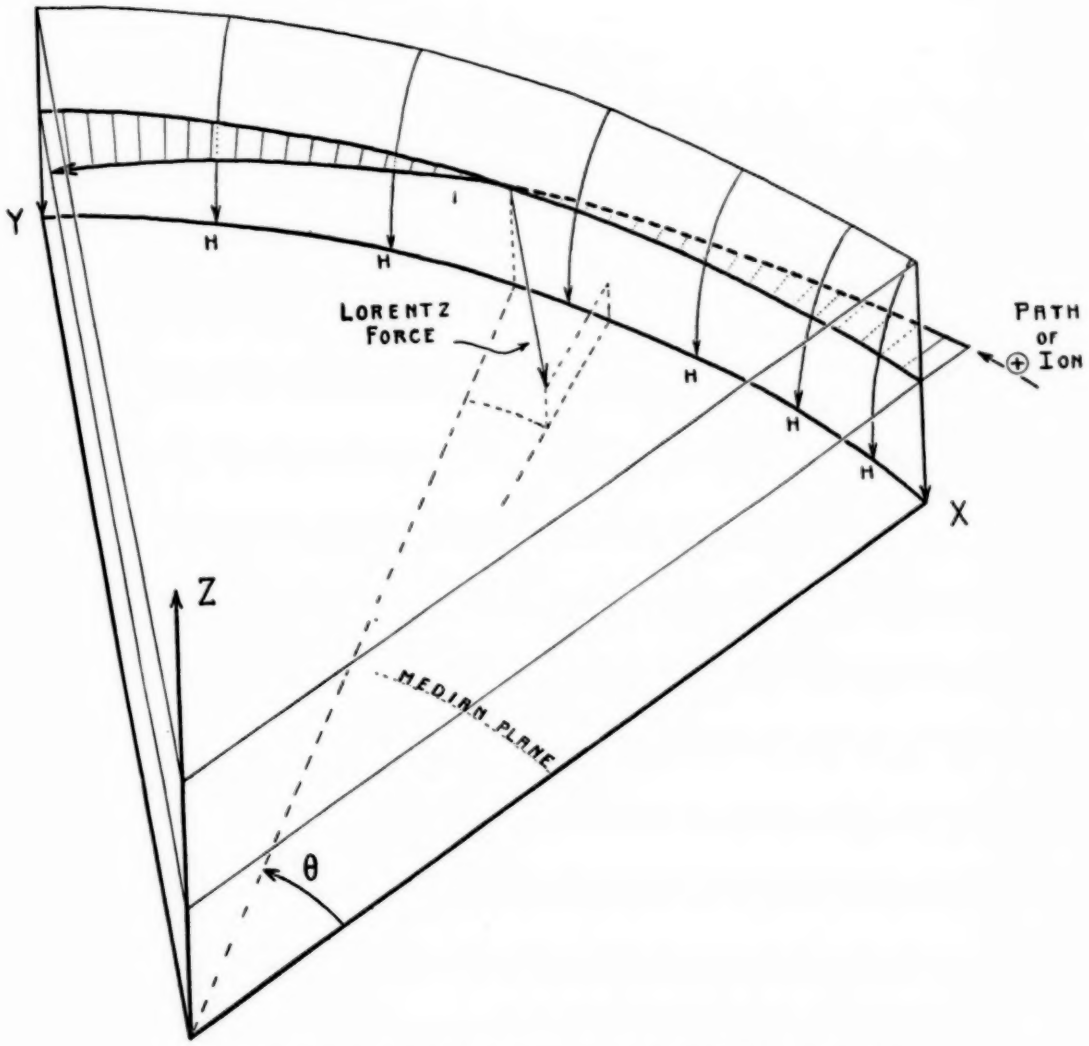

FIG. 3. The focusing effect due to variation of the field with polar angle.

2. THE ORBIT

Eliminating the time, the equation of motion in the plane $z=0$ is

$$\frac{r^2+2(dr/d\theta)^2-r(d^2r/d\theta^2)}{\{r^2+(dr/d\theta)^2\}^{\frac{1}{2}}}=-\frac{1}{v}\frac{eH}{mc}, \qquad (2.1)$$

the time in the orbit being then given by

$$vdt/d\theta=(r^2+(dr/d\theta)^2)^{\frac{1}{2}}. \qquad (2.2)$$

We shall use primes to indicate differentiation with respect to θ. Suppose

$$r=a(1+\epsilon f) \qquad (2.3)$$

where f is a function of a and θ, gives a family of orbits depending on the parameter a, which are

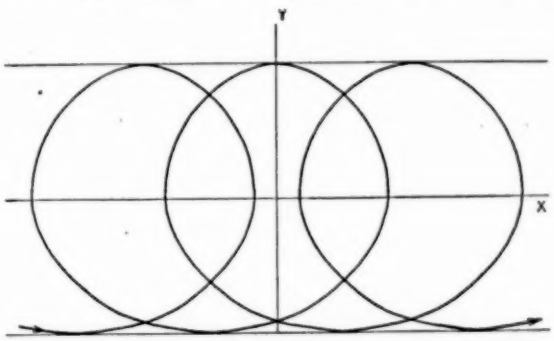

FIG. 4. Instability of a nearly circular orbit due to increase of the field with y. (For a positive ion the magnetic field is directed away from the reader.)

approximately circles about the origin, so that

$$H=\frac{m_0c}{e}\frac{v}{(1-v^2/c^2)^{\frac{1}{2}}}\frac{1}{a}\times\frac{1+\epsilon(2f-f'')+\epsilon^2(f^2+2f'^2-ff'')}{(1+2\epsilon f+\epsilon^2(f^2+f'^2))^{\frac{1}{2}}}, \quad (2.4)$$

$$(dt/d\theta)=(a/v)(1+2\epsilon f+\epsilon^2(f^2+f'^2))^{\frac{1}{2}}. \quad (2.5)$$

We shall suppose that our family of orbits is periodic with period 2π in θ so that f is periodic with period 2π in θ, and that a is so chosen that

$$\langle f\rangle_{Av}\left(=\frac{1}{2\pi}\int_0^{2\pi}fd\theta\right)=0. \quad (2.6)$$

These orbits are exact in the field given by eliminating v and a between (2.3), (2.4), and an arbitrary relation between v and a, which we shall take to be

$$v=a\omega\{1+\epsilon^2g\}, \quad (2.7)$$

where g is a function of a only and ω is a constant.

For small ϵ we have approximately, if v/c is small and of the same order, so that

$$(1-v^2/c^2)^{-\frac{1}{2}}\approx 1+\tfrac{1}{2}a^2\omega^2/c^2,$$

$$H=(m_0c/e)\omega[1-\epsilon(f+f'')+\tfrac{1}{2}(a^2\omega^2/c^2)+\epsilon^2\{g+2ff''+f^2+\tfrac{1}{2}f'^2\}] \quad (2.8)$$

on $r=a(1+\epsilon f)$, or

$$H=(m_0c/e)\omega[1-\epsilon(f+f'')+\tfrac{1}{2}(a^2\omega^2/c^2)+\epsilon^2\{g+2ff''+f^2+\tfrac{1}{2}f'^2+fa(d/da)(f+f'')\}] \quad (2.9)$$

on $r=a$.

Suppose the magnetic field has the form

$$H=(m_0c/e)\omega[1+\epsilon h+\epsilon^2k], \quad (2.10)$$

where h is a function of r and θ periodic in θ with period π and such that

$$\langle h\rangle_{Av}=0 \quad (2.11)$$

and k is a function of r only.

That the radial variation of $\langle H\rangle_{Av}$ is of the second order in (2.10) is not essential; it corresponds to radial variation of v/a being of the second order in (2.7).

The first order equation to be solved is

$$f+f''=-h. \quad (2.12)$$

The solution of this is, when the constants of integration are suitably adjusted, like h, a function f_1 periodic in θ with period π and such that

$$\langle f_1\rangle_{Av}=0, \quad (2.13)$$

and the condition that it has period π determines the constants of integration.

This solution is substituted into the higher order terms in (2.9); the equation averaged over θ determines, dropping the suffix,

$$g=k-\tfrac{1}{2}(a^2\omega^2/\epsilon^2c^2)-2\langle ff''\rangle_{Av}-\langle f^2\rangle_{Av}-\langle\tfrac{1}{2}f'^2\rangle_{Av}-\langle fa(d/da)(f+f'')\rangle_{Av}, \quad (2.14)$$

and its variation with θ gives an equation of the same form as (2.12) and with its right-hand side satisfying the same conditions, to determine f to the second order; and the process can be continued.

Thus we can solve (2.9) or the exact relation to which it approximates for a function f of a and θ, which will be periodic in θ with period π, and a function g of a only, in power series in ϵ.

If, on the other hand, H is only periodic with period 2π in θ, there appears, at some stage in the process, an equation like (2.12), the right-hand side of which contains a term in $\sin\theta$ or $\cos\theta$, so that it has no periodic solution. In this case a periodic solution of (2.9) expansible in powers of ϵ does not exist, though one expansible in powers of $\epsilon^{\frac{1}{2}}$ may exist.

3. Resonance

These orbits will be exactly in resonance if

$$\left(\frac{dt}{d\theta}\right)_{Av}=\left(\frac{1}{2\pi}\int_0^{2\pi}\frac{dt}{d\theta}d\theta\right)=\frac{1}{\omega}, \quad (3.1)$$

where ω is the constant angular velocity for the cyclotron, that is

$$v=a\omega\frac{1}{2\pi}\int_0^{2\pi}\{1+2\epsilon f+\epsilon^2(f^2+f'^2)\}^{\frac{1}{2}}d\theta \quad (3.2)$$

or, approximately, for small ϵ, since $\langle f\rangle_{Av}=0$,

$$v=a\omega(1+\tfrac{1}{2}\epsilon^2\langle f'^2\rangle_{Av}). \quad (3.3)$$

Thus the condition for resonance is (from (2.7))

$$g=\tfrac{1}{2}\langle f'^2\rangle_{Av}. \quad (3.4)$$

4. Focusing

Consider paths in the field given by (2.10) near our family of periodic orbits in the plane $z=0$; on account of the symmetry of the field, the variational equations for motion in the plane and for motion out of it separate; the latter gives the "focusing."

We have

$$\frac{d}{dt}\left(m\frac{dz}{dt}\right)=\frac{e}{c}\left(\frac{dr}{dt}H_\theta-r\frac{d\theta}{dt}H_r\right), \tag{4.1}$$

where H_r and H_θ are given by (1.5) and r, t, are to have their values in terms of θ for the unvaried orbit.

Since the right-hand side is small compared with $m\omega^2 z$, we may integrate over a revolution with z constant and obtain for the change in dz/dt

$$\delta\frac{dz}{dt}=z\frac{e}{mc}\int_0^{2\pi}\left\{r\frac{\partial H}{\partial r}-\frac{1}{r}\frac{dr}{d\theta}\frac{\partial H}{d\theta}\right\}d\theta \tag{4.2}$$

and the condition for focusing is

$$\left\langle r\frac{\partial H}{\partial r}-\frac{1}{r}\frac{dr}{d\theta}\frac{\partial H}{\partial\theta}\right\rangle_{Av}<0. \tag{4.3}$$

Finding $\partial H/\partial r$ and $\partial H/\partial\theta$ on $r=a$ from 2.9 and changing back to $r=a(1+\epsilon f)$, approximately for small ϵ, gives

$$r\frac{\partial H}{\partial r}-\frac{1}{r}\frac{dr}{d\theta}\frac{\partial H}{\partial\theta}=\frac{m_0c}{e}\omega\left[-\epsilon a\frac{d}{da}(f+f'')+\frac{a^2\omega^2}{c^2}\right.$$
$$\left.+\epsilon^2\left\{f'(f'+f''')+a\frac{d}{da}(g+2ff''+f^2+\tfrac{1}{2}f'^2)\right.\right.$$
$$\left.\left.+a\frac{df}{da}a\frac{d}{da}(f+f'')\right\}\right]. \tag{4.4}$$

Thus, averaging, after some integrations by parts, and since $\langle f\rangle_{Av}=0$, the condition for focusing is

$$\frac{a^2\omega^2}{c^2}+\epsilon^2a\frac{d}{da}\{g-\tfrac{1}{2}\langle f'^2\rangle_{Av}\}+\epsilon^2\{\langle -f^2+2f'^2-f''^2\rangle_{Av}$$
$$+\langle(f+a(d/da)f)^2\rangle_{Av}$$
$$-\langle(f'+a(d/da)f')^2\rangle_{Av}\}<0. \tag{4.5}$$

In resonance, by (3.4), the second term of (4.5) vanishes; and we see by expansion of f in a Fourier series, or by the transformations of the calculus of variations, that if f is periodic with period π, and if $\langle f\rangle_{Av}=0$, the third term is always negative, and vanishes only if f vanishes.

Thus a variation of H with θ, periodic with period π in θ, can always be made so large, of order $a\omega/c$, as to compensate the first term in (4.5), and leave a net focusing effect, while resonance is maintained.

In particular, in the magnetic field,

$$H=\frac{m_0c}{e}\omega\left[1+\left(\frac{30}{19}\right)^{\frac{1}{2}}\frac{\omega}{c}r\cos 4(\theta-\beta)+\frac{15}{38}\frac{r^2\omega^2}{c^2}\right], \tag{4.6}$$

where β is any constant, the orbits, which are approximately given by

$$r=a\left\{1+\left(\frac{2}{285}\right)^{\frac{1}{2}}\frac{a\omega}{c}\cos 4(\theta-\beta)\right\} \tag{4.7}$$

are in resonance and are neither focused nor defocused.

5. Stability

The variational equations for motion in the plane $z=0$ separate into equations giving constant displacements of the parameter a and the origin of time, and the equation obtained by varying (2.1) with fixed v and H.

Suppose, then,

$$r=a(1+\epsilon f)+\varphi. \tag{5.1}$$

Substituting this in (2.1), and using the forms (2.7) for v and (2.9) for H, the terms linear in φ give, after some calculation, to terms in ϵ^2.

$$\varphi''-\varphi'[\epsilon f'+\epsilon^2(3f'f''-ff')]$$
$$+\varphi\left[1-\epsilon\left(2f''+a\frac{d}{da}(f+f'')\right)\right.$$
$$+\epsilon^2\left\{3f'^2+2ff''-\left(f-a\frac{df}{da}\right)a\frac{d}{da}(f+f'')\right.$$
$$\left.\left.+a\frac{d}{da}\left(\tfrac{1}{2}\frac{a^2\omega^2}{\epsilon^2c^2}+g+2ff''+f^2+\tfrac{1}{2}f'^2\right)\right\}\right]=0. \tag{5.2}$$

The substitution

$$\varphi=\psi\{1+\tfrac{1}{2}\epsilon f+\epsilon^2((3/4)f'^2-\tfrac{1}{8}f^2)\} \tag{5.3}$$

reduces (5.2) to its normal form

$$\psi''+\psi[1+\epsilon p+\epsilon^2 q]=0, \tag{5.4}$$

where

$$p=-\tfrac{3}{2}f''-a\frac{d}{da}(f+f'') \tag{5.5}$$

$$q=\tfrac{9}{4}f'^2+\tfrac{3}{2}(ff''+f''^2+f'f''')$$
$$-\left(f-a\frac{df}{da}\right)a\frac{d}{da}(f+f'')$$
$$+a\frac{d}{da}\left(\frac{a^2\omega^2}{\epsilon^2c^2}+g+2ff''+f^2+\tfrac{1}{2}f'^2\right). \tag{5.6}$$

The condition that the equation

$$\psi''+\psi[1+\epsilon p]=0 \tag{5.7}$$

should give stable oscillations may be found by variation of parameters. Writing

$$\psi=\alpha\cos\theta+\beta\sin\theta,$$
$$\psi'=-\alpha\sin\theta+\beta\cos\theta,$$

we find

$$\alpha'=\epsilon p\sin\theta\cos\theta\,\alpha+\epsilon p\sin^2\theta\,\beta,$$
$$\beta'=-\epsilon p\cos^2\theta\,\alpha-\epsilon p\sin\theta\cos\theta\,\beta.$$

Averaging over θ, we see that the secular charges in α and β contain terms in $\epsilon^{\pm D\theta}$, where the exponents D are given by

$$D^2=\epsilon^2[\langle p\sin\theta\cos\theta\rangle_{Av}^2-\langle p\sin^2\theta\rangle_{Av}\langle p\cos^2\theta\rangle_{Av}]$$
$$=\tfrac{1}{4}\epsilon^2[\langle p\cos 2\theta\rangle_{Av}^2+\langle p\sin 2\theta\rangle_{Av}^2-\langle p\rangle_{Av}^2]. \tag{5.8}$$

For p given by (5.5), $\langle p\rangle_{Av}=0$, (since $\langle f\rangle_{Av}=0$), so that $D^2>0$ and there is certainly instability, unless $\langle p\cos 2\theta\rangle_{Av}$ and $\langle p\sin 2\theta\rangle_{Av}$ vanish, i.e., unless both $\langle f\cos 2\theta\rangle_{Av}$ and $\langle f\sin 2\theta\rangle_{Av}$ vary as $a^{-\frac{1}{2}}$ (or vanish); in which case the calculation must be carried to the next order in ϵ.

If in Eq. (5.4) we make the change of independent variable

$$\theta_1=\theta+\epsilon\xi, \tag{5.9}$$

where ξ is a function of θ to be chosen, and write

$$\psi_1=\psi(1+\epsilon\xi')^{\frac{1}{2}}, \tag{5.10}$$

so that the transformed equation will be in its normal form, we obtain

$$d^2\psi_1/d\theta_1^2+\psi_1[1+\epsilon(p-\tfrac{1}{2}\xi'''-2\xi')$$
$$+\epsilon^2[q-2p\xi'+3\xi'^2+\tfrac{3}{2}\xi'''\xi'+\tfrac{3}{4}\xi''^2]]=0. \tag{5.11}$$

When $\langle p\rangle_{Av}$, $\langle p\cos 2\theta\rangle_{Av}$, and $\langle p\sin 2\theta\rangle_{Av}$, vanish, we can obtain a periodic function ξ such that

$$\xi'''+4\xi'=2p \tag{5.12}$$

and (5.11) becomes

$$d^2\psi_1/d\theta_1^2+\psi_1(1+\epsilon^2 n)=0, \tag{5.13}$$

where $$n=q-2p\xi'+3\xi'^2+\tfrac{3}{2}\xi'''\xi'+\tfrac{3}{4}\xi''^2 \tag{5.14}$$

and the exponents are given by (cf. (5.7) and (5.8))

$$D^2=(\epsilon^4/4)[\langle n\cos 2\theta\rangle_{Av}^2$$
$$+\langle n\sin 2\theta\rangle_{Av}^2-\langle n\rangle_{Av}^2]. \tag{5.15}$$

The form of (5.8) shows that if the Fourier expansion of f contains terms in $\cos 2\theta$ or $\sin 2\theta$ not varying as $a^{-\frac{1}{2}}$, the orbits will be unstable: and this will follow if H contains such terms not varying as $r^{-\frac{1}{2}}$.

If H is periodic with period $\frac{1}{2}\pi$, the exponent given by (5.8) vanishes: terms in $\cos 2\theta$ or $\sin 2\theta$ cannot arise in any order, so that we conclude from the form of (5.15) that the exponents are either zero to all orders in ϵ, or imaginary in the first order in which they do not vanish; and that the orbit is "stable."

In particular in the magnetic field given by (4.6), (5.15) gives

$$D=\pm\iota\frac{5\times 21}{8\times 19}\frac{a^2\omega^2}{c^2}. \tag{5.16}$$

It should be remarked that the above argument applies only when ϵ is sufficiently small. If we apply it to a field depending only on r,

$$H=\frac{m_0c}{e}\omega(1+\epsilon^2 k), \tag{5.17}$$

so that $f=0$, (5.15) gives

$$D=\pm\iota\frac{\epsilon^2}{2}r\frac{d}{dr}k \tag{5.18}$$

for the variation of α and β,

or

$$D=\pm\iota\left(1+\frac{\epsilon^2}{2}r\frac{d}{dr}k\right) \tag{5.19}$$

for the variation of ψ, agreeing, to terms of order ϵ^2, with the exact result for circular orbits

in a field depending only on r,

$$D^2=-\left(1+\frac{r}{H}\frac{dH}{dr}\right), \qquad (5.20)$$

which gives instability if $|rH|$ decreases as r increases.

6. The Nature of the Orbits

The above results about the orbits in the median plane illustrate the general theory of orbits.[4]

An ion moving in a plane under a magnetic field perpendicular to that plane forms a conservative dynamical system with two degrees of freedom. Using rectangular Cartesian coordinates x, y, and the corresponding momentum components X, Y; and the proper time,

$$s=\int(1-v^2/c^2)^{\frac{1}{2}}dt,$$

as independent variable, the Hamiltonian function takes the form

$$\mathcal{H}=\frac{1}{2m_0}\left\{\left(X-\frac{e}{c}F\right)^2+\left(Y-\frac{e}{c}G\right)^2\right\}, \qquad (6.1)$$

where F and G are functions of x and y, the components in the x and y directions of the magnetic vector potential. In fact, the motion depends only on the magnetic field.

$$H_z=-H=(\partial G/\partial x)-(\partial F/\partial y).$$

In the special case of constant magnetic field $-H_0$, when we take $F=\frac{1}{2}H_0y$, $G=-\frac{1}{2}H_0x$, there are three independent integrals uniform in x, y, X and Y, *viz.*

$$\mathcal{H}=\alpha, \quad X+(e/c)F=\beta, \quad Y+(e/c)G=\gamma.$$

In this case all the orbits are periodic, forming the three-parameter family of all circles.

In the special case of magnetic field depending only on the distance r from a fixed point at a finite distance, which we take to be the origin of coordinates, when we take $F=yK$, $G=-xK$, where K is a function of r only, so that

$$H=2K+r(dK/dr),$$

there are just two independent integrals uniform in x, y, X and Y, *viz.*

$$\mathcal{H}=\alpha, \quad Yx-Xy=\beta.$$

In this case the system is of "soluble type." We see from

$$m_0^2\left(\frac{dr}{ds}\right)^2=\frac{1}{r^2}(Xx+Yy)^2=2\alpha m_0-\left(\frac{e}{c}rK+\frac{\beta}{r}\right)^2$$

that in the "stable" case in which $|rH|$ continually increases as r increases, there is a family of orbits which librate between any two values of r. Together these form a three-parameter family of conditionally periodic orbits, from which a denumerable infinity of two-parameter families of "ordinary" periodic orbits with all four of their exponents zero, can be picked out. The circles with center at the origin form a one-parameter family of "singular" periodic orbits with two exponents zero and the other two real or imaginary as $|rH|$ decreases or increases with r.

In the limiting case of the above in which the fixed point is at infinity, in the x-direction say, H is a function of x only, and we take $F=0$, G a function of x only. There are two independent uniform integrals,

$$\mathcal{H}=\alpha, \quad Y=\beta.$$

From $$m_0^2\left(\frac{dx}{ds}\right)^2=2\alpha m_0-\left(\beta-\frac{e}{c}G\right)^2$$

and $$m_0\frac{dy}{ds}=\beta-\frac{e}{c}G,$$

we see that in the case which might be stable, x being a periodic function of s, y will generally not remain finite. There will then be no conditionally periodic orbits, and no ordinary periodic orbits; the singular periodic orbits, if they exist, must be unstable.

In general the problem is not of soluble type, and there is only one integral uniform in x, y, X and Y, *viz.*

$$\mathcal{H}=\alpha.$$

There are no two-parameter families of ordinary periodic orbits. There may be, and will be if the field is nearly homogeneous and symmetrical about two perpendicular directions, one-parameter families of singular periodic orbits which

[4] Whittaker, *Analytical Dynamics* (Fourth Edition, Cambridge, 1937), Ch. xv.

will in general have two zero and two nonzero exponents. The stability corresponding to imaginary exponents is really only stability to the first order in the variation of the orbit and it remains open whether second and higher order terms would not lead to instability. However, such second order variations do not increase exponentially with the time, but become large only after a time inversely proportional to the initial displacement; and their effects are not expected to be important in the number of revolutions that take place in the cyclotron: Indeed they may be damped by the effects of the accelerating electric field.

7. Conclusion

It is concluded that in a cyclotron the magnetic field of which varies in such a manner as that given by (4.6), the beam of ions may remain in resonance without being defocused or becoming unstable, in spite of the relativity increase of mass with velocity, at least up to velocities at which terms in v^3/c^3 become important.

Modifications of the above results when the simultaneous action of the variations of the magnetic field with polar angle and of the accelerating electric field with polar angle are taken into account will be considered in a second paper. It appears that these effects become continually less and less important as the relative increase of momentum per revolution decreases with increasing energy.

The author wishes to thank Professor M. L. Pool for his encouragement and interest during the writing of this paper.

OCTOBER 15, 1938 PHYSICAL REVIEW VOLUME 54

The Paths of Ions in the Cyclotron

II. Paths in the Combined Electric and Magnetic Fields

L. H. Thomas
Ohio State University, Columbus, Ohio

(Received July 26, 1938)

It has been pointed out in a recent paper that a variation of the magnetic field of a cyclotron with polar angle can produce a focusing effect on the beam, while preserving resonance and stability. In that paper the effects of the magnetic field alone were considered. It is shown below that the effects of variation with polar angle of the accelerating electric field and of the magnetic field can be considered as almost independent; the second order cross terms between them are without practical effect. Thus the results contained in the above paper (I) may simply be superposed on those obtained by other workers.

Introduction

THE argument contained in the former paper[1] is strictly true for orbits in the magnetic field alone; when the effects of the accelerating electric field are taken into account, the closed orbits are replaced by a family of "central paths" which the particles traverse in a phase relationship to the field changing with the radius in a definite way. These central paths can always be found if both magnetic and electric fields are periodic with period π in θ, but will not usually exist if they are only periodic with 2π. If the field is suitably adjusted to resonance, a pencil of the central paths are "spirals" from the center to the outside.

The motion of an ion near a central path separates, on account of the symmetry about the median plane, into motion out of the plane and motion in the plane. The motion out of the plane

[1] L. H. Thomas, Phys. Rev., this issue. (This will be referred to as (I).)

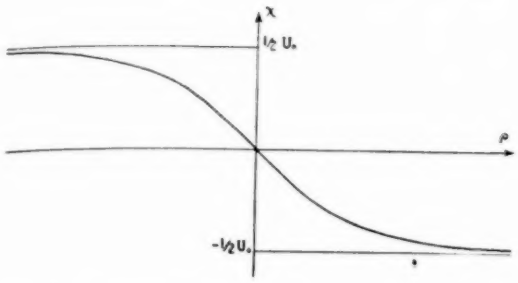

FIG. 1. The potential of the field between the dees.

is regulated by the focusing which contains the terms from the electric field considered by other workers[2,3] as well as the terms from the variation of magnetic field considered above (I).

As regards the motion in the plane, there are four possible displacements, two corresponding to displacements to another path of the family; and two to the displacements of the center of the instantaneous circle considered above (I, introduction).

It is shown below in detail that the effects of the accelerating electric field and of the magnetic field, on resonance, focusing, and stability, can, for practical purposes, be regarded as not interfering with each other.

1. THE ACCELERATING ELECTRIC FIELD

Any electromagnetic field in free space can be resolved into one of electric type with $H_z=0$, for which, in terms of the Hertz function Π,

$$\left.\begin{aligned} E_r &= -\frac{\partial^2\Pi}{\partial r\partial z} \\ E_\theta &= -\frac{1}{r}\frac{\partial^2\Pi}{\partial\theta\partial z} \\ E_z &= \frac{\partial^2\Pi}{\partial r^2}+\frac{1}{r}\frac{\partial\Pi}{\partial r}+\frac{\partial^2\Pi}{\partial\theta^2}=-\frac{\partial^2\Pi}{\partial z^2}+\frac{1}{c^2}\frac{\partial^2\Pi}{\partial t^2} \end{aligned}\right\} \quad \left.\begin{aligned} H_r &= -\frac{1}{rc}\frac{\partial^2\Pi}{\partial\theta\partial t} \\ H_\theta &= \frac{1}{c}\frac{\partial^2\Pi}{\partial r\partial t} \\ H_z &= 0 \end{aligned}\right\} \tag{1.1}$$

and one of the magnetic type in which H and $-E$ have the above forms for E and H.

Only the part of the electric type will be considered; moreover it will be supposed that in the plane $z=0$, $E_z=0$, and that the field is symmetrical about this plane, so that for small z,

$$\left.\begin{aligned} E_r &= -\partial W/\partial r+0(z^2) \\ E_\theta &= -\frac{1}{r}\frac{\partial W}{\partial\theta}+0(z^2) \\ E_z &= z\left(\frac{\partial^2 W}{\partial r^2}+\frac{1}{r}\frac{\partial W}{\partial r}+\frac{1}{r^2}\frac{\partial^2 W}{\partial\theta^2}\right)+0(z^3) \end{aligned}\right\} \quad \left.\begin{aligned} H_r &= -\frac{z}{c}\frac{1}{r}\frac{\partial^2 W}{\partial\theta\partial t}+0(z^3) \\ H_\theta &= +\frac{z}{c}\frac{\partial^2 W}{\partial r\partial t}+0(z^3) \\ H_z &= 0 \end{aligned}\right\}. \tag{1.2}$$

It will appear that the effects of the magnetic part of this field are unimportant; in any case, they affect only the focusing.

Finally we shall suppose the field harmonic in the time with frequency $\omega/2\pi$,

$$W=U\cos\omega t+V\sin\omega t, \tag{1.3}$$

where U and V are functions of r and θ periodic with period 2π in θ and which could, theoretically, be adjusted to be any such functions of r and θ. In practice, $U\cos\theta$, $U\sin\theta$, $V\cos\theta$, and $V\sin\theta$, are periodic with period π in θ. (1.4)

[2] M. E. Rose, Phys. Rev. **53**, 392 (1938).
[3] Wilson, Phys. Rev. **53**, 410 (1938).

For example, for the field between symmetrical straight dees, we could take

$$U=\chi((r\sin\theta)/d),\quad V=0, \tag{1.5}$$

where $\chi(\rho)$ is an odd function of ρ (Fig. 1) asymptotic to $-\frac{1}{2}U_0$ as $\rho\to\infty$, U_0 is the maximum voltage across the dees, and d is of the order of the distance apart of the dees.

Since W will be of the order of 10^5 volts or 300 e.s.u. at most, while the constant magnetic field H will be of order 2×10^4 e.m.u., we shall suppose that the main effects of the accelerating field are small of the first order and subsidiary effects of the second order, and shall write

$$U_0=(m_0a^2\omega^2/e)\epsilon u_0. \tag{1.7}$$

2. Paths in an Electric Field Uniform in Space and Harmonic in Time and a Constant Perpendicular Magnetic Field

If the electric field is

$$E_x=X\cos\omega t,\quad E_y=Y\sin\omega t \tag{2.1}$$

(general for a field uniform in space and harmonic in time, by choice of the origin of time and the directions of rectangular coordinate axes and x and y); if the constant magnetic field is

$$H_z=-H_0; \tag{2.2}$$

and if relativity effects can be neglected; then the equations of motion become:

$$\frac{d^2x}{dt^2}=\frac{e}{m_0}X\cos\omega t-\frac{eH_0}{m_0c}\frac{dy}{dt},\quad \frac{d^2y}{dt^2}=\frac{e}{m_0}Y\sin\omega t+\frac{eH_0}{m_0c}\frac{dx}{dt},\quad d^2z/dt^2=0 \tag{2.3}$$

which have the exact general solution,

$$\left.\begin{aligned} x&=-\left[\frac{e}{m_0\omega^2}\left\{X+\frac{eH_0}{m_0c\omega}Y\right\}\Big/\left\{1-\left(\frac{eH_0}{m_0c\omega}\right)^2\right\}\right]\cos\omega t+A\cos\frac{eH_0}{m_0c}t+B\sin\frac{eH_0}{m_0c}t+C\\ y&=-\left[\frac{e}{m_0\omega^2}\left\{Y+\frac{eH_0}{m_0c\omega}X\right\}\Big/\left\{1-\left(\frac{eH_0}{m_0c\omega}\right)^2\right\}\right]\sin\omega t+A\sin\frac{eH_0}{m_0c}t-B\cos\frac{eH_0}{m_0c}t+D\\ z&=E+Ft \end{aligned}\right\}, \tag{2.4}$$

where A, B, C, D, E, F, are the constants of integration.

If we refer this to coordinates x', y', referring to axes rotating with angular velocity $\frac{1}{2}(\omega+eH_0/m_0c)$ we obtain exactly,

$$x'=\xi,\quad y'=\left[\frac{e}{m_0\omega^2}(X+Y)\Big/\left\{1-\frac{eH_0}{m_0c\omega}\right\}\right]\sin\tfrac{1}{2}\left(\omega-\frac{eH_0}{mc}\right)t+\eta, \tag{2.5}$$

where ξ and η contain terms with fixed coefficients without the factor $\{1-(eH_0/m_0c\omega)\}$ in the denominator, and terms multiplied by (altered) constants of integration.

Thus the motion consists of the superposition of oscillatory motions of amplitudes of the order of the initial velocity divided by eH_0/m_0c, and of $c(X+Y)/\omega H_0$; and a simple harmonic oscillation of amplitude

$$\left[\frac{e}{m_0\omega^2}(X+Y)\Big/\left\{1-\frac{eH_0}{m_0c\omega}\right\}\right]\text{ and frequency }\left(\omega-\frac{eH_0}{m_0c}\right)\Big/4\pi\text{ along the (rotating) }y'\text{-axis.}$$

We see that all ions starting near the origin with small velocity attain a distance from the origin of the order of

$$\frac{c(X+Y)}{\omega H_0}\Big/\left|1-\frac{eH_0}{m_0c\omega}\right|$$

corresponding to a velocity of

$$\frac{c(X+Y)}{H_0}\Big/\left|1-\frac{eH_0}{m_0c\omega}\right|,$$

while their departure from the rotating y'-axis is only of order

$$c(X+Y)/\omega H_0.$$

3. A First Approximation to the Paths

The equations of motion in the plane $z=0$ in the field given by (I(1.5)) and (1.2), can be written with $x=r\cos\theta$, $y=r\sin\theta$, as dependent, and t as independent variable,

$$\left.\begin{aligned}&(d/dt)m(dx/dt)=-e(\partial W/\partial x)-(e/c)H(dy/dt),\\&(d/dt)m(dy/dt)=-e(\partial W/\partial y)+(e/c)H(dx/dt)\\&\text{where}\quad m=m_0\{1-[(dx/dt)^2+(dy/dt)^2]/c^2\}^{-\frac{1}{2}}\end{aligned}\right\}. \tag{3.1}$$

Write

$$\left.\begin{aligned}&x=\xi+a\cos(\sigma t+\alpha),\quad dx/dt=-\sigma a\sin(\sigma t+\alpha),\\&y=\eta+a\sin(\sigma t+\alpha),\quad dy/dt=\sigma a\cos(\sigma t+\alpha)\end{aligned}\right\} \tag{3.2}$$

so that ξ, η, are the coordinates of the center of, a the radius of, and α the phase in, an instantaneous circle, and may vary only slowly. (Note that a and α correspond only approximately to the expressions denoted by these symbols later on in this paper).

The rates of change of a, α, ξ, and η, are given exactly by

$$\left.\begin{aligned}&\frac{da}{dt}=\left(1-\frac{\sigma^2a^2}{c^2}\right)^{\frac{1}{2}}\frac{e}{m_0\sigma}\left[\frac{\partial W}{\partial x}\sin(\sigma t+\alpha)-\frac{\partial W}{\partial y}\cos(\sigma t+\alpha)\right]\\&\frac{d\alpha}{dt}=\left(1-\frac{\sigma^2a^2}{c^2}\right)^{\frac{1}{2}}\frac{e}{m_0a\sigma}\left[\frac{\partial W}{\partial x}\cos(\sigma t+\alpha)+\frac{\partial W}{\partial y}\sin(\sigma t+\alpha)+\frac{a\sigma}{c}\left(H-\frac{m_0c\sigma}{e(1-a^2\sigma^2/c^2)^{\frac{1}{2}}}\right)\right]\\&d\xi/dt=a(d\alpha/dt)\sin(\sigma t+\alpha)-da/dt\cos(\sigma t+\alpha)\\&d\eta/dt=-a(d\alpha/dt)\cos(\sigma t+\alpha)-da/dt\sin(\sigma t+\alpha)\end{aligned}\right\}. \tag{3.3}$$

If we suppose that relativity corrections can be neglected, that the magnetic field is constant, H_0, and that the electric field is that between straight uniform dees given by (1.5), so that $\partial W/\partial x=0$; and choose

$$\sigma=eH_0/m_0c,$$

we have

$$\left.\begin{aligned}&da/dt=-(e/m_0\sigma)(dW/dy)\cos(\sigma t+\alpha)\\&ad\alpha/dt=(e/m_0\sigma)(dW/dy)\sin(\sigma t+\alpha)\\&d\xi/dt=(e/m_0\sigma)(dW/dy)\\&d\eta/dt=0\end{aligned}\right\}. \tag{3.4}$$

Since $$dW/dy=(1/d)\chi'(y/d)\cos\omega t \text{ (from (1.5))},\tag{3.5}$$

the approximation, obtained by averaging over a period, keeping first order terms on the right-hand side, is

$$\left.\begin{aligned}\frac{da}{dt}&=-\frac{1}{\pi}\frac{eU_0}{m_0a\sigma^2}\cos[(\sigma-\omega)t+\alpha], & ad\alpha/dt&=0\\ \frac{d\xi}{dt}&=-\frac{1}{\pi}\frac{\eta}{a}\frac{eU_0}{m_0a\sigma^2}\sin[(\sigma-\omega)t+\alpha], & d\eta/dt&=0\end{aligned}\right\}.\tag{3.6}$$

These equations show, for example, how the center of the instantaneous circle creeps along the dees if its center is off their central line.[4] The creep does not increase exponentially.

If, indeed, instead of dees we have quadrants, so that the electric field is periodic with period $\pi/2$ in θ, the last two of Eq. (3.6) will become

$$\frac{d\xi}{dt}=-\frac{1}{\pi}\frac{\eta}{a}\frac{eU_0}{m_0a\sigma^2}\sin[(\sigma-\omega)t+\alpha],\quad \frac{d\eta}{dt}=-\frac{1}{\pi}\frac{\xi}{a}\frac{eU_0}{m_0a\sigma^2}\sin[(\sigma-\omega)t+\alpha]\tag{3.7}$$

and there is no creep, only a stable oscillation.

The above method can be applied to find higher approximations also even when the electric and magnetic fields are more complicated, and provides the simplest way of obtaining the creep due to variation of the magnetic field periodic with period 2π or π, in θ. The following method, however, seems to be more convenient for our purposes.*

4. The Central Paths

The equations of motion in the plane $z=0$, in the field given by (I(1.5)) and (1.2), can be written, with θ as independent variable, (cf. I(2.1)),

$$\frac{r^2+2\left(\frac{dr}{d\theta}\right)^2-r\frac{d^2r}{d\theta^2}}{\{r^2+(dr/d\theta)^2\}^{\frac{3}{2}}}=-\frac{1}{v}\frac{eH}{mc}+\frac{e\left(r\frac{\partial W}{\partial r}-\frac{dr}{d\theta}\frac{1}{r}\frac{\partial W}{\partial\theta}\right)}{mv^2(r^2+(dr/d\theta)^2)^{\frac{1}{2}}},\tag{4.1}$$

$$v\frac{d}{d\theta}mv=c^2\frac{dm}{d\theta}=-e\left(\frac{dr}{d\theta}\frac{\partial W}{\partial r}+\frac{\partial W}{\partial\theta}\right),\tag{4.2}$$

the time in the orbit being given by

$$vdt/d\theta=(r^2+(dr/d\theta)^2)^{\frac{1}{2}};\tag{4.3}$$

suppose now

$$r=a(1+\epsilon f),\tag{4.4}$$

$$\omega t=\theta-\alpha+\epsilon v,\tag{4.5}$$

where f and v are functions of a, α, and θ, periodic with period 2π in θ, and a and α are such functions of θ that

$$\langle f\rangle_{Av}=0,\tag{4.6}$$

$$\langle v\rangle_{Av}=0,\tag{4.7}$$

---

[4] E. O. Lawrence and D. Cooksey, Phys. Rev. **50**, 1133 (1936).

* *Note added in proof:* The creep in magnetic field $H_0(1+\epsilon r\sin\theta)$ is $d\xi/dt=a^2\sigma\epsilon/2$, that in field $H_0(1+\epsilon r^2\sin 2\theta)$ is $d\xi/dt=a^2\xi\sigma\epsilon$, $d\eta/dt=-a^2\eta\sigma\epsilon$.

while
$$da/d\theta = a\epsilon b, \tag{4.8}$$
$$d\alpha/d\theta = \epsilon^2\delta, \tag{4.9}$$

where b and δ are functions of a and α.

The equations (4.4), (4.5), describe a family of paths depending on the constants of integration of (4.8) and (4.9), which are close spirals about the origin with nearly circular whorls.

By taking the right-hand side of (4.8) of order ϵ while that of (4.9) is of order ϵ^2, we do not imply that the latter is necessarily small compared with the former; but simply that, while we shall be concerned with terms of the second order in the former, we shall consider only terms of the first order in the latter. Since ω has the same value as in 1.3, this assumes approximate resonance.

For small ϵ we have approximately, on $r=a(1+\epsilon f)$, $\omega t=\theta-\alpha+\epsilon v$,

$$\frac{m_0 c}{e}\omega\left[1-\epsilon(f''+v')+\tfrac{1}{2}\frac{a^2\omega^2}{c^2}+\epsilon^2\left\{\delta+f'^2+ff''+v'^2+v'f''-ab\frac{d}{da}(2f'+b+v)\right\}\right]$$
$$=H+\frac{c}{a\omega}\left[\frac{\partial W}{\partial r}-\epsilon\left\{(f-v')\frac{\partial W}{\partial r}+(f'+b)\frac{1}{a}\frac{\partial W}{\partial\theta}\right\}\right] \tag{4.10}$$

and

$$\frac{ma\omega^2}{e}\left[\epsilon(f'-v''+b)+\epsilon^2\left\{ff'+f'f''+3v'v''-2v''f-2v'f'+b\left(2f+f''-2v'+a\frac{df}{da}-2a\frac{dv'}{da}\right)\right\}\right]$$
$$=-\left[\frac{1}{a}\frac{\partial W}{\partial\theta}+\epsilon(f'+b)\frac{\partial W}{\partial r}\right]. \tag{4.11}$$

So long as H and $W\cos\theta$ are periodic with period π in θ, we can solve these equations, subject to (4.4), (4.5), (4.6), and (4.7), for functions f and v, of a, α, and θ, which will also be periodic with period π in θ, and for functions b and δ of a and α only, in power series in ϵ.

To have the right-hand side of (4.9) of order ϵ^2, we must have the mean value (over θ) of the right-hand side of (4.10) of order ϵ^2.

We shall suppose the magnetic field has the form (I (2.10) and (2.11))
$$H=(m_0c/e)\omega[1+\epsilon h+\epsilon^2 k] \tag{4.12}$$

where h is a function of r and θ periodic in θ with period π and such that
$$\langle h\rangle_{Av}=0 \tag{4.13}$$

and k is a function of r only.

We shall suppose further that while the main effect of the accelerating field (given by the term $-\partial W/a\partial\theta$ of (4.11)) is of the first order in ϵ, differentiation of W with respect to r transfers the corresponding term to the next higher order in ϵ to that explicitly indicated. This controls the orders of the terms we retain in a manner convenient for the practical case.

Agreeably with (1.3), and with this understanding, we shall write, on $r=a(1+\epsilon f)$, $\omega t=\theta-\alpha+\epsilon v$,

$$\left.\begin{aligned}\partial W/\partial\theta&=(m_0a^2\omega^2/e)\epsilon\{u\cos\omega t+v\sin\omega t\}\\ \partial W/\partial r&=(m_0a\omega^2/e)\epsilon^2\{l\cos\omega t+m\sin\omega t\}\end{aligned}\right\}, \tag{4.14}$$

where u, v, l, and m are functions of a, α, and θ, the products of which by $\sin\theta$ and $\cos\theta$ are periodic with period π in θ.

The first order equations to be solved are then

$$v'+f''=-h, \tag{4.15}$$

$$b+f'-v''=-\{u\cos(\theta-\alpha)+v\sin(\theta-\alpha)\}, \tag{4.16}$$

so that

$$b=-\langle u\cos(\theta-\alpha)+v\sin(\theta-\alpha)\rangle_{Av}. \tag{4.17}$$

The solutions, with the constants of integration so determined that they are functions of θ periodic with period π, are substituted into the terms of next order in (4.10), and give, on averaging over θ and carrying out some integrations by parts,

$$\delta=k-\frac{1}{2}\frac{a^2\omega^2}{\epsilon^2c^2}+\langle l\cos(\theta-\alpha)+m\sin(\theta-\alpha)\rangle_{Av}+\langle f'^2\rangle_{Av}-\langle v'^2\rangle_{Av}+b^2+ab\frac{db}{da}-\left\langle fa\frac{d}{da}(v'+f'')\right\rangle_{Av}. \tag{4.18}$$

In the special case we have principally in mind we shall take a magnetic field harmonic in θ with period $\pi/2$ so that

$$h=\gamma\cos 4(\theta-\beta) \tag{4.19}$$

and the electric field for straight symmetrical dees given by (1.3), (1.5), and (1.7), so that $v=0$, $m=0$.

As soon as r is large of order $1/\epsilon$ compared with d, the distance apart of the dees, the acceleration takes place in impulses as θ passes 0, π, 2π, $\cdots$, and the solutions of the first order equations are

$$v'=(1/15)\gamma\cos 4(\theta-\beta)-\tfrac{1}{2}u_0\cos\alpha\cos\theta, \tag{4.20}$$

$$f'=-(4/15)\gamma\sin 4(\theta-\beta)-(1/\pi)u_0\cos\alpha+\tfrac{1}{2}u_0\cos\alpha\sin\theta \tag{4.21}$$

for $0<\theta<\pi$, and are periodic with period π, v' diminishing rapidly by $u_0\cos\alpha$ as θ passes 0, π, $\cdots$,

and

$$b=(1/\pi)u_0\cos\alpha. \tag{4.22}$$

Further $\langle l\cos\theta\rangle_{Av}=0$, and

$$\epsilon^2\langle l\sin\theta\rangle_{Av}\frac{m_0a\omega^2}{e}=\frac{d^2}{r^3}\frac{1}{\pi}\int_{-r/d}^{r/d}\rho^2\chi'(\rho)d\rho,$$

and, since χ is of order ϵ, $\langle l\sin\theta\rangle_{Av}$ is to be neglected in (4.18), (this would not be true if the dees were not straight), which becomes

$$\delta=k-\tfrac{1}{2}\frac{a^2\omega^2}{\epsilon^2c^2}+\frac{1}{30}\gamma\left(\gamma+a\frac{d\gamma}{da}\right)-\frac{1}{60\pi}a\frac{d\gamma}{da}u_0\cos\alpha\sin 4\beta+\frac{1}{\pi^2}u_0a\frac{du_0}{da}\cos^2\alpha. \tag{4.23}$$

5. Resonance

The ways in which the mean radius, a, and phase, α vary along a central path are exactly determined by Eqs. (4.8), (4.9), the right-hand sides of which do not contain θ, so that, eliminating θ,

$$da/da=\epsilon\delta/ab, \tag{5.1}$$

The nature of the solutions can be found by dividing an (a, α)-plane into regions by boundaries on which $da/d\theta=0$ and $d\alpha/d\theta=0$.

In the special case given by (4.22), (4.23), $da/d\theta>0$ for $-\pi/2<\alpha<\pi/2$, $da/d\theta<0$ for $\pi/2<\alpha<3\pi/2$; etc.; and $d\alpha/d\theta>0$ if the magnetic field is more than a little larger than $m_0c\omega/e$ (k positive and larger than the remaining terms on the right-hand side of (4.23)); $d\alpha/da<0$ if the field is more than a little less than $m_0c\omega/e$; the exact boundary depends on α.

Since, (1.7), $u_0\propto a^{-2}$, $\cos^2\alpha$ in the last term of (4.23) has a negative coefficient. We shall consider in detail the case in which $\cos\alpha$ in the

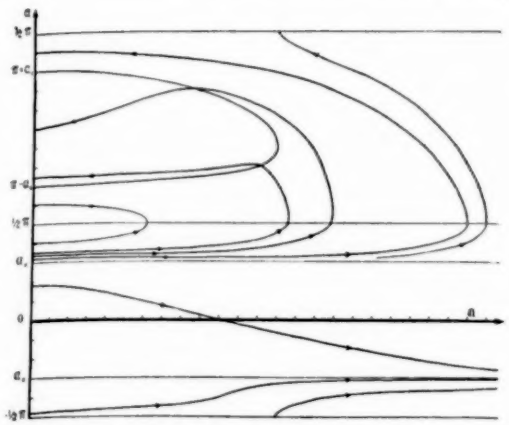

FIG. 2. Variation of α with a in case of very close resonance.

previous term has a negative coefficient; for γ given by (I, (4.6)) so that $\gamma \propto a$, this means

$$\sin 4\beta > 0. \tag{5.2}$$

We shall further suppose the magnetic field adjusted so that the right-hand side of (4.23) is zero for $\alpha = \alpha_0 \leqslant \pi/2$ and less than zero for $\alpha < \alpha_0$. The other value of $\cos\alpha$ which makes the right-hand side of (4.23) zero is then $-(\cos\alpha_0 + j)$ where $j > 0$ and $\propto a^3$, so for small a the corresponding value of α is $\pm(\pi - \alpha_0)$, approaches π for a finite value of a, and then becomes imaginary.

The variation of α with a is then as in the diagram (Fig. 2).

These considerations only hold for a large compared to the distance apart of the dees; for a small compared with that distance, the simple case of §2 should be a good approximation, and we see that near resonance all the ions start out with $\alpha \approx 0$. Thus we should expect α for all the ions following central paths in a field adjusted as above to approach $-\alpha_0$, and the ions to be continually accelerated.

The tolerance for the field to have the above property is given by

$$\delta k < \frac{1}{60\pi} a \frac{d\gamma}{da} u_0 \sin 4\beta - \frac{1}{\pi^2} u_0 a \frac{du_0}{da} \tag{5.3}$$

i.e., in our special case, by (1.7), and I(4.6), if $m_0 c\omega/e = H_0$,

$$\delta H < H_0 \left[\frac{2}{\pi^2} \left(\frac{c}{a\omega} \right)^2 \left(\frac{U_0}{aH_0} \right)^2 + \frac{1}{60\pi} \left(\frac{30}{14} \right)^{\frac{1}{2}} \frac{U_0}{aH_0} \sin 4\beta \right]. \tag{5.4}$$

If the field departs from the value giving resonance by a somewhat larger amount, we may solve (5.1) approximately, obtaining[5]

$$\sin\alpha = (\pi\omega/cU_0) \int_0^A \delta H \, a \, da. \tag{5.5}$$

If, for example, $\delta H = \pm \delta H_0 (0.596 - a/A)$ (as might be obtained by exact adjustment at $a = 0.596A$)[6] the condition that α remains between $-\pi/2$ and $\pi/2$ is

$$\delta H_0 < H_0 \frac{1}{0.0353\pi} \left(\frac{c}{A\omega} \right) \left(\frac{U_0}{AH_0} \right) \tag{5.6}$$

$$\approx 5H_0/n \tag{5.7}$$

if n is the number of times the ion is accelerated.

The expression (5.4) is always small compared to (5.7), and we see that a discussion of the resonance requirement such as that given by Rose will not be affected by the coexistence of dependence on θ of the electric and magnetic fields such as we are considering.

Thus we require for "exact resonance," in our special case

$$\epsilon^2 k = \tfrac{1}{2} \frac{a^2\omega^2}{c^2} - \frac{1}{30} \epsilon^2 \gamma \left(\gamma + a \frac{d\gamma}{da} \right) \tag{5.8}$$

in agreement with (I(4.6)): and the variation of the mean magnetic field from this should not exceed that given by (5.7).

6. FOCUSING

The variational equation for motion out of the plane $z = 0$, from (3.1), as in (I(4.1)), gives

$$\frac{d}{dt} \left(m \frac{dz}{dt} \right) = eE_z + \frac{e}{c} \left(\frac{dr}{dt} H_\theta - r \frac{d\theta}{dt} H_r \right), \tag{6.1}$$

[5] Rose, reference 2, 402, Eq. (59).

[6] This expression is the most favorable linear variation of δH for a fixed difference δH_0 between $a = 0$ and $a = A$, giving a maximum of α on one side equal to its final value on the other. The number 0.596 is the real root of $x^3 + 3x = 2$.

where E_z is given by (1.2), H_r and H_θ are given by I(1.5) and (1.2), and r, t, are to have their values in terms of θ for the unvaried path.

Integrating over a revolution with z constant we obtain

$$\delta\frac{dz}{dt}=z\int_0^{2\pi}\left[\frac{e}{m}\left\{\frac{\partial^2 W}{\partial r^2}+\frac{1}{r}\frac{\partial W}{\partial r}+\frac{1}{r^2}\frac{\partial^2 W}{\partial\theta^2}\right\}\frac{dt}{d\theta}+\frac{e}{mc}\left\{\left(r\frac{\partial H}{\partial r}+\frac{1}{c}\frac{\partial^2 W}{\partial\theta\partial t}\right)-\frac{dr}{d\theta}\left(\frac{1}{r}\frac{\partial H}{\partial\theta}-\frac{1}{c}\frac{\partial^2 W}{\partial r\partial t}\right)\right\}\right]d\theta. \quad (6.2)$$

For small ϵ we have approximately, on $r=a(1+\epsilon f)$, $\omega t=\theta-\alpha+\epsilon v$, using the values (4.12), (4.14), for H and W,

$$\frac{e}{m_0}\left(\frac{\partial^2 W}{\partial r^2}+\frac{1}{r}\frac{\partial W}{\partial r}+\frac{1}{r^2}\frac{\partial^2 W}{\partial\theta^2}\right)\frac{dt}{d\theta}=\epsilon\omega[\{u'\cos\omega t+v'\sin\omega t\}\{1+\epsilon(v'-2f)\}+\epsilon\{l\cos\omega t+m\sin\omega t\}],$$

$$\frac{e}{m_0 c}\left(r\frac{\partial H}{\partial r}-\frac{1}{r}\frac{dr}{d\theta}\frac{\partial H}{\partial\theta}\right)=\omega\left[\epsilon a\frac{dh}{da}+\epsilon^2\left\{a\frac{dk}{da}+af\frac{d}{da}\left(a\frac{dh}{da}\right)-f'h'-fh'\right\}\right], \quad (6.3)$$

the remaining terms being inappreciable.

These values and that of $dt/d\theta$ can now be substituted in (6.2). For the electric field between dees, however, given by (1.5), it is simpler for the first term to note that

$$\frac{e}{m_0}\left(\frac{\partial^2 W}{\partial r^2}+\frac{1}{r}\frac{\partial W}{\partial r}+\frac{1}{r^2}\frac{\partial^2 W}{\partial\theta^2}\right)=\frac{e}{m_0}\frac{1}{d^2}\chi''(\rho)\cos\omega t$$

and to carry out the integration with $\rho=(r/d)\sin\theta$ as variable of integration, since (4.20) and (4.21) are not accurate enough near $\theta=0$, π, etc. and χ'' is only appreciable in those neighborhoods.

In our special case, with (4.19) and (1.5), we obtain,

$$\delta\frac{dz}{dt}=z2\omega\left[\epsilon\sin\alpha u_0-\frac{e^2\cos^2\alpha}{m_0^2a^3\omega^4}\frac{1}{d}\int\chi'^2d\rho+\frac{1}{60}\epsilon^2u_0\left(\left\{\gamma-\left(a\frac{d}{da}\right)^2\gamma\right\}\sin 4\beta\cos\alpha-4\gamma\cos 4\beta\sin\alpha\right)\right.$$
$$\left.+\pi\epsilon^2\left\{a\frac{dk}{da}+\frac{1}{30}\gamma\left(a\frac{d}{da}\right)^2\gamma-\frac{8}{15}\gamma^2\right\}\right]. \quad (6.4)$$

The first term in the parenthesis is the electric focusing due to field change during acceleration.[7]

The second term is the electric focusing due to the ordinary lens effect during acceleration. If we put $\chi(\rho)=-\frac{1}{2}U_0\rho$, $-1<\rho<1$, it becomes $-\frac{1}{2}\epsilon^2u_0^2\cos^2\alpha a/d$; in general it will be

$$-\lambda\tfrac{1}{2}\epsilon^2u_0^2\cos^2\alpha a/d, \quad (6.5)$$

where λ is a number of the order of magnitude of 1.[8] The fourth term gives the magnetic focusing in agreement with the value corresponding to I(4.5) in our special case. The third term is that due to the simultaneous effects of the electric and magnetic fields; for our special case it gives focusing for $-\pi<\alpha<0$, so long as

$$\cos 4\beta<0. \quad (6.6)$$

A small excess of magnetic focusing, however, is sufficient to make the net effect of the last three terms always a focusing effect.

---

[7] Rose, reference 2, p. 394.

[8] Rose, reference 2, p. 395, 407; Wilson, reference 3.

We see that a discussion of focusing based on separate consideration of the electric field such as that given by Rose and by Wilson and of the magnetic field as in (I(4)) will not be appreciably affected by the coexistence of the electric and magnetic fields.

7. Stability

We find the variational equations for motion in the plane $z=0$ by writing

$$r=a(1+\epsilon f)+\varphi, \quad \omega t=\theta-\alpha+\epsilon v+\tau \tag{7.1}$$

in place of (4.4) and (4.5), substituting in (4.1) and (4.2), and taking the terms linear in φ and τ. There results a system of linear differential equations for φ and τ of the fourth order, of which we know two independent solutions, obtained by varying the constants of integration of (4.8) and (4.9), and representing displacements to neighboring central orbits. We use these two known solutions to reduce the fourth order system to a second order system which represents the departure from the central orbits. This second order system reduces to a normal form (cf. I(5.4)) to terms of the second order in ϵ

$$\psi''+\psi[1+\epsilon p+\epsilon^2 q]=0, \tag{7.2}$$

where p is an expression linear in f, v, h, u, v, and their derivatives, and q is quadratic in these and linear in k, l, m.

To the first order in ϵ (cf. I(5.8)) the stability depends on $\langle p\cos 2\theta\rangle_{Av}$, $\langle p\sin 2\theta\rangle_{Av}$, and $\langle p\rangle_{Av}$. For a magnetic field given by (4.12) and (4.14), as in I, the contributions to these expressions all vanish. As we shall see immediately the contributions due to the accelerating electric field do not vanish. As a increases the ratio of the contributions from the magnetic field to those from the electric field increases. Thus, for small a only the terms from the electric field in p need be taken into account; for large a only the terms from the magnetic field in q; the terms from the electric field, and the cross product terms, in q, can always be neglected, whatever a.

The terms from the electric field in p can be obtained most directly from (3.2); the terms from the magnetic field in p and q were given before (I(5.5), (5.6)), so that, with (4.12), (4.14), (I(5.6), (2.14))

$$p=u\sin(\theta-\alpha)-v\cos(\theta-\alpha)-\frac{3}{2}f''-a\frac{d}{da}(f+f''),$$

$$q=\frac{9}{4}f'^2+\frac{3}{2}(ff''+f''^2+f'f''') \tag{7.3}$$

$$-\left(f-a\frac{df}{da}\right)a\frac{d}{da}(f+f'')+a\frac{d}{da}\left(2ff''+f^2+\tfrac{1}{2}f'+k\right.$$

$$\left.-\langle 2ff''\rangle_{Av}-\langle f^2\rangle_{Av}-\langle\tfrac{1}{2}f'\rangle_{Av}{}^2-\left\langle fa\frac{d}{da}(f+f'')\right\rangle_{Av}\right),$$

where $f+f''=-h$, only the terms arising from the magnetic field being included in f.

To the first order in ϵ the discussion in §3 applies. For a general accelerating field, keeping in phase, there is a stable oscillation. For a field between dees, $\langle p\cos^2\theta\rangle_{Av}\approx\langle p\rangle_{Av}$, $\langle p\sin 2\theta\rangle_{Av}\approx 0$, and the exponents, given by (I(5.8))

$$D^2=\tfrac{1}{4}\epsilon^2[\langle p\cos 2\theta^2\rangle_{Av}+\langle p\sin 2\theta^2\rangle_{Av}-\langle p^2\rangle_{Av}]$$

are zero. This case differs from that considered in (I(5)), under the above magnetic field alone, in that the terms in D^2 merely cancel, and are not zero separately; and there is still motion to the first order in ϵ; in fact the creep of the center of the orbit parallel to the central line of the dees is at a rate proportional to the distance of the center from that line (§3).

For small a this is the varied motion; for large a the terms of the second order in ϵ considered in (I(5)), only are effective, giving a stable oscillation. A complete investigation would consider the transitional case; this we omit, remarking that since the ratio of the effective terms in the magnetic field to those in the electric field is proportional to γ^2/u_0 (cf. (6.4)), i.e., to a^4, the transitional case is relevant only for a small range of a.

8. The Nature of the Paths: Conclusion

For a magnetic field constant in time, symmetrical about a median plane and in that plane perpendicular to it and periodic with period π about an axis perpendicular to that plane, and for an electric field harmonic in time, symmetrical about the median plane and in that

plane parallel to it and periodic with period π about the axis, there is a two-parameter family of central paths. If the electric field is generally suitable and the magnetic field ((4.12), (4.19)) is within a certain tolerance (5.7) of that giving exact resonance (5.8), a pencil of these paths are spirals from the center to the outside (a one-parameter family actually pass through the center). Other paths near the central paths oscillate about the central paths if these are focused for motion out of the median plane and stable for motion in it.

Three regions may be distinguished. (*A*) Near the center, where the ions start. All the ions will be swept up into a beam (§2). The conditions for focusing require a more exact treatment than that given here (cf. Wilson, reference 3). The desirable condition is that at points in phase the electric field near the median plane should have a component towards that plane on the average. Stability is here not of great importance; especially if the electric field were given by quadrants instead of dees (3.7). With dees the particles should leave the central region on concentric circles whose centers depart from the central line of the dees by so small an amount that the creep along the dees that accumulates through the whole motion (3.6) does not become important.

(*B*) The transition from electric to magnetic control of focusing and stability. In the earlier part the magnetic field should be, if anything, slightly less than the exact resonance value, so that the ions lag behind the field, and the first order electric term (Rose, reference 2) focuses the beam ((4.5), (6.4), $\alpha<0$). The electric field from quadrants will give stability (3.7), from dees a slow creep (3.6). In the latter part the magnetic field should have no more than very small terms varying as $\cos\theta$, $\sin\theta$, giving steady creeps of the instantaneous circles, or $\cos 2\theta$, $\sin 2\theta$, which give creeps proportional to the departure from the center (§ 3 note). Terms in $\cos 4\theta$ and $\sin 4\theta$ are desirable as (6.4) they give focusing without instability. Indeed (I(4.5)) any small variation of the magnetic field with θ periodic in period $\pi/2$ gives focusing without instability.

(*C*) Where relativistic effects become important. We see that up to terms in v^3/c^3, no difficulty is to be anticipated. As a variation of magnetic field with angle of order v/c has to be introduced to maintain focusing and resonance. It would be necessary to carry the calculation (I, 2, 3, 4, 5) to higher order in ϵ to predict the effect of still higher terms.

It is concluded that the effective limit to the velocities attainable will be fixed by the possibility of adjusting the magnetic field sufficiently exactly for resonance. It is suggested that the adjustment would be easier and the energy of the resulting beam more uniform if the whole instrument has symmetry about its axis with period $\pi/2$; or at least if the dees were replaced by quadrants.

Vibrational-Rotational Radiation Transitions in Water Molecules In Nonpolar Solvents

J. W. ELLIS AND E. L. KINSEY
University of California, Los Angeles, California

(Received August 9, 1938)

The $1.875\mu(\sigma+\delta)$ and $1.379\mu(\sigma+\pi)$ absorption bands of H_2O molecules in CCl_4 and CS_2 solutions and the $1.985\mu(\sigma+\pi)$ band of D_2O in CCl_4 are presented. They are interpreted as indicating free rotation of water vapor-like molecules in solution. The dominant feature of each band is an enhanced Q-branch. We are unable to decide to what extent this enhancement is caused by a possible departure from the usual rotational distribution characteristic of vapors and to what extent by possible alterations in transition probabilities.

WE have previously shown[1] spectroscopically that there is free rotation of water vapor-like molecules when water is dissolved in carbon disulfide. This was demonstrated through a partial development in solution of rotational structure in the $1.379\mu(\sigma+\pi)$ and the $1.875\mu(\sigma+\delta)$ vibration-rotation bands. We found that there is a considerable alteration of relative intensities with respect to vapor band structure among the partially resolved rotational components, but we were not able to determine whether the branch whose intensity is enormously increased is a Q-branch or a P-branch. We have evidence indicating that it is a Q-branch.

This evidence was obtained in part by repeating our investigation with carbon tetrachloride as a solvent. This solvent was not tried before, because, as pointed out in our previous paper, data obtained from the *International Critical Tables* and elsewhere give the solubility of water in CS_2 as ten times greater than in CCl_4. This information is questionable, for the absorption bands obtained with saturated CCl_4 are more intense than with CS_2. If it is correct, then the transition probabilities for the bands differ greatly with the two solvents.

In this paper we are presenting the percentage transmission plots of the 1.379μ and 1.875μ bands of H_2O from vapor and from CS_2 and CCl_4 solution records, all determined under similar conditions of resolution in the recording spectrograph. The liquid water plots, which differ greatly from those of vapor and solution, are this time omitted. Also we are including the graph of the $1.985\mu(\sigma+\pi)$ band of D_2O, corresponding to the 1.379μ band of H_2O. The $(\sigma+\delta)$ band of D_2O is not obtainable with our spectrograph. A brief report[2] on H_2O in CCl_4 has already been made.

In Fig. 1 are plotted the 1.875μ vapor band and the corresponding bands of CS_2 and CCl_4 solutions. The slit width is indicated by the width of the line marked S. In a previous paper[1] we pointed out that Mecke's[3] partial analysis indicates that the central, most intense part of the vapor band is contributed to largely by Q-type transitions and hence we may refer to it as a Q-branch. And, although there is some overlapping of P, Q and R lines, the long and short wave-length portions of the band are essentially P- and R-branches. In the solution bands it appears fairly definite now that the Q-branch is greatly intensified and shifted to longer wave-length positions, the CS_2 shift being the greater. We are led to this conclusion primarily by the fact that, although in CS_2 the solution minima coincide in wave-length with certain vapor minima, in CCl_4 such a complete correlation does not occur. This interpretation finds further support in a comparison of the displacements of the water bands with those produced in other polar molecules by the same solvents. In Fig. 2 some of these displacements from the vapor positions are shown for comparison. Upward- and downward-pointing arrows indicate displacements in CCl_4 and CS_2 solution, respectively. In all instances the shifts are to longer wave-lengths, and wherever both solvents have been used the CS_2 displacement is the greater. The figure also shows

[1] Kinsey and Ellis, Phys. Rev. **51**, 1074 (1937).

[2] Ellis and Kinsey, Phys. Rev. **53**, 672 (1938).

[3] Mecke, Zeits. f. Physik **81**, 313 (1933).

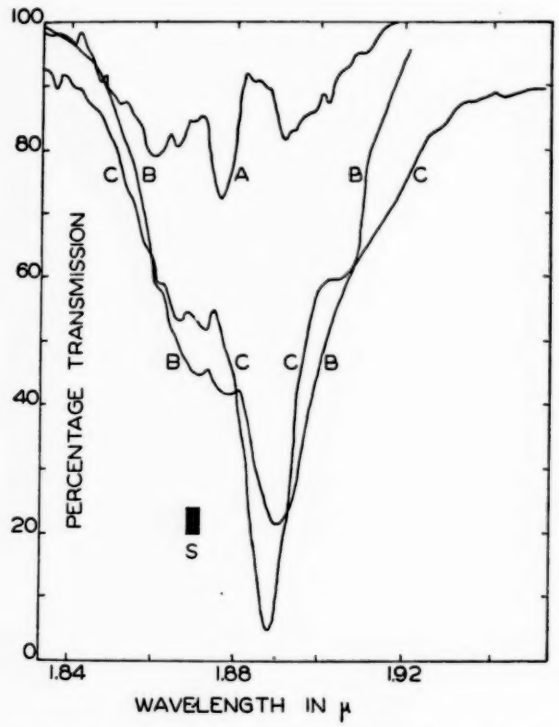

FIG. 1. The $1.875\mu(\sigma+\delta)$ H_2O band. *A*: Vapor. *B*: CS_2 solution. *C*: CCl_4 solution.

that in general frequencies which may be characterized as "OH frequencies" show greater shifts than "CH frequencies." Also the higher frequencies show greater displacements than the lower frequencies of the same type. The length of the horizontal double-headed arrow indicates the half-slit width in wave numbers, 5 cm^{-1}, corresponding to 0.2 mm on the record plate. A shift of this amount can be observed easily by the superposition of two transparent records.

In the solution bands of Fig. 1, structure is developed on both the high and low frequency sides of what we may now call the *Q*-branch. It is impossible, however, to correlate the structure satisfactorily with details of the vapor bands. This is not surprising because the *P*, *Q* and *R* lines overlap some and the resolution of the instrument is not complete. The failure definitely to establish a long wave shoulder in the CS_2 solution, corresponding to the one in CCl_4, can probably be explained by the presence there of a solvent band of nearly 100 percent absorption.

All of the solution bands of Figs. 1 and 3 were obtained with a 96 cm cell. The solution bands represent differential absorptions between saturated and unsaturated solutions. The unsaturated solutions were Eastman "highest purity" CCl_4 showing considerable residual water and Eimer and Amend CS_2 showing a trace of water after distillation over phosphorus pentoxide. The saturated solutions were obtained by shaking the specimens mechanically for several hours and allowing them to remain for several days before using.

In Fig. 3 are plotted the 1.379μ vapor band and the corresponding solution bands. From the similarity of appearances between this band and the 1.875μ one we again identify the strong component in the solution bands as a *Q*-branch. Although Mecke has recorded no *Q* line identifications, Dennison's[4] analysis of a perpendicular-type band indicates a central grouping of *Q* lines. The development of a short wave portion of the solution bands and the nondevelopment of the long wave portion is consistent with the great discrepancy in intensities in the two sides of the vapor band. As pointed out previously,[1] the absorption maximum at 1.468μ is to be interpreted

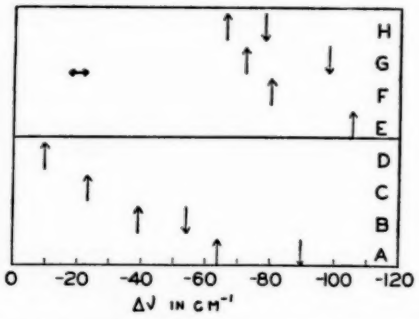

FIG. 2. Wave number displacements from vapor positions. *A–D*: CH bands. *E–H*: OH bands. *A*: Chloroform, 1.145μ. *B*: Chloroform, 1.680μ. *C*: Ethyl alcohol, 1.730μ. *D*: Formic acid, 1.727μ. *E*: Formic acid, 1.435μ. *F*: Ethyl alcohol, 1.395μ. *G*: Water vapor, 1.379μ. *H*: Water vapor, 1.875μ.

not as a portion of the 1.379μ band but as a separate band $(\sigma+2\delta)$.

Figure 4 shows the $1.985\mu(\sigma+\pi)$ band of D_2O in CCl_4. An excess of 99.9 percent D_2O was shaken for $1\frac{1}{2}$ hours with 1 liter of CCl_4. The CCl_4 had been distilled over calcium chloride but still showed the presence of a considerable amount of H_2O. That there was no appreciable reaction

[4] Dennison, Rev. Mod. Phys. **3**, 280 (1931).

between the H_2O and D_2O to form HDO during the 3 hours required for mixing and obtaining the record was revealed by the intensity of the original H_2O band, which remained constant, and the absence of new strong bands. The D_2O band of Fig. 4 shows the general characteristics of the H_2O band of Fig. 3.

Although the full interpretation and significance of the intensity changes shown in Figs. 1, 3 and 4 must await the application of instruments of greater resolving power, we nevertheless think it is safe to state that in solution there is an enormous enhancement of Q lines over P and R lines. An application[1] of a calculation by

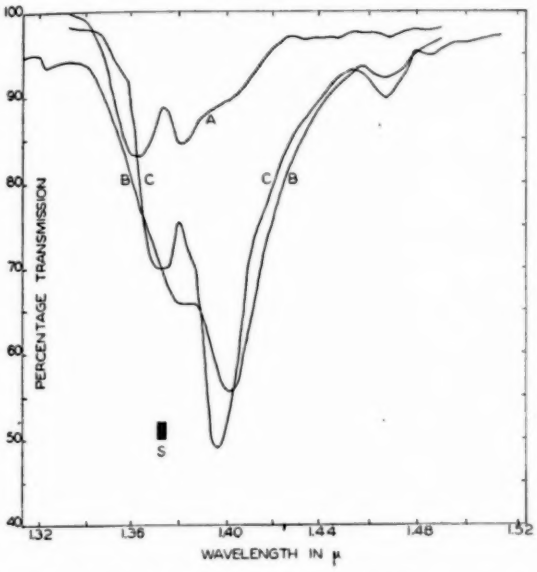

FIG. 3. The $1.379\mu(\sigma+\pi)$ H_2O band. A: Vapor. B: CS_2 solution. C: CCl_4 solution.

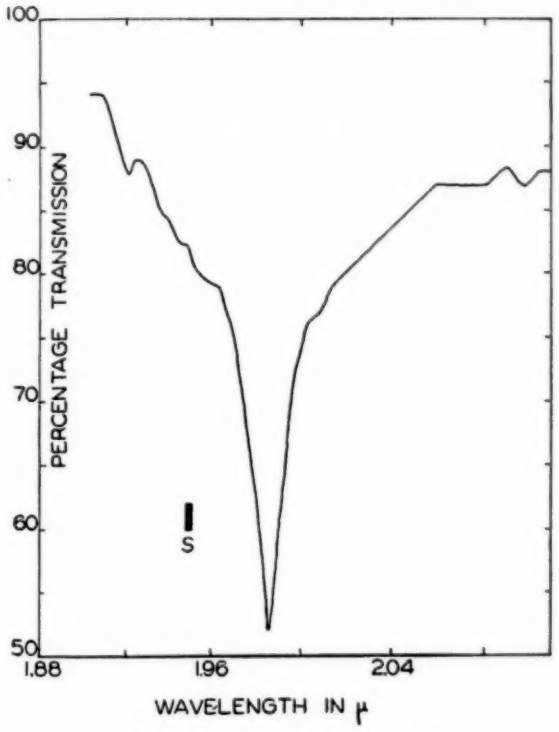

FIG. 4. The $1.985\mu(\sigma+\pi)$ band of D_2O in CCl_4.

Debye[5] to the problem of water in nonpolar solvents leads us to assume that most of the water molecules in CCl_4 and CS_2 solutions are free to rotate. We are, however, unable to decide to what extent the intensity enhancement of the Q-branch is caused by a possible departure from the usual rotational distribution characteristic of vapors and to what extent by possible alterations in transition probabilities.

[5] Debye, Physik. Zeits. **35**, 100, 193 (1935).

The Zeeman Effect in the Spectrum of Neon*

J. B. GREEN AND J. A. PEOPLES, JR.†
Mendenhall Laboratory of Physics, Ohio State University, Columbus, Ohio

(Received August 18, 1938)

Measurements on about two hundred and fifty lines of the spectrum of neon in fields of 27,000–32,000 gauss have now been completed. The neon discharge was excited by means of an electrodeless high frequency discharge (about 40 megacycles) at right angles to the magnetic field and to the line of sight. The lines, extending from about λλ3100–9000A include transitions involving all of the levels of the $2p^5 4p$, the $2p^5 3d$, $2p^5 4d$ configurations, and parts of others. A large number of "forbidden" lines also appear.

Sampson's calculations for the parameters of the $2p^5 3d$ configuration and Shortley's for the parameters of the $2p^5 4d$ configuration have been used to calculate the g-values. The agreement between theoretical and experimentally determined values is excellent.

THE earliest important work on the Zeeman effect of neon gave complete data for the $2p^5 3s$ and $2p^5 3p$ configurations. This was the classical work of Back[1] who, by means of it, was the first to establish the g-sum rule. Later work by Murakawa and Iwana[2] gave a little more data on the $2p^5 3d$, $2p^5 4d$ and $2p^5 5s$ configurations. Jacquinot[3] gave complete results for the $2p^5 5s$, $2p^5 6s$, and $2p^5 7s$ configurations. The purpose of the present paper is to give complete data for the $2p^5 4p$, $2p^5 3d$, and $2p^5 4d$ configurations, and to compare the g-values determined from the Zeeman patterns with the values calculated by means of the quantum mechanics. In some cases, the "observed" g-values were determined from distorted patterns showing beginning Paschen-Back effect. The discussion of these patterns must be left to a later paper.

The source of the neon discharge was a capillary tube of Geissler form with external electrodes. The capillary was really thin-walled Pyrex tubing about 2.5 mm internal diameter. Copper foil wrapped tightly on the bulbs of the tube served as external electrodes. It is necessary for the foil to make smooth contact with the tube over a fairly large area in order to prevent the development of hot spots. A rather heavy blast of compressed air plays on both sides of the capillary and on the bottom bulb.

The tube is placed with capillary between the poles of the magnet and parallel to the slit of the grating spectrograph, and the discharge is excited

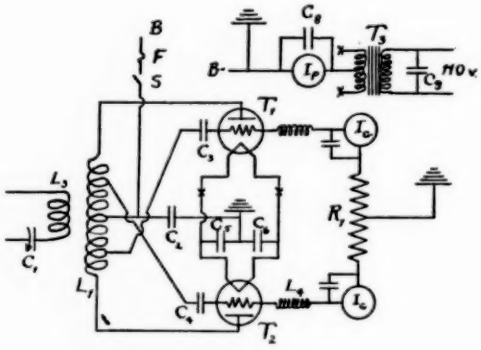

FIG. 1. Circuit diagram.

T_1 and T_2 are two Taylor T-200 high frequency oscillator tubes with 200 watts each plate dissipation.
L_1 is the tank coil wound of ¼" copper tubing; diameter about 3", turns spaced about ¼". The coil is supported on porcelain stand-off insulators.
L_2, the pick-up coil is constructed like L_1 but is 1½" diameter, so that it can be placed inside L_1. It is also supported on stand-off insulators.
L_3 and L_4 are high frequency choke coils consisting of about 50 turns of No. 24 copper wire wound 12 turns per inch on ½" Pyrex tubing.
C_1 the lead-tuning condenser is a radio receiving condenser with a maximum capacity of 0.00025 mf.
C_3 and C_4 are grid-excitation condensers; capacity 0.0001 mf., rated at 12,500 volts.
C_2 0.002 mf.
C_5 and C_6 0.002 mf. High frequency by pass condensers.
C_7 and C_8 0.01 mf.
C_9 0.10 mf.
R_1 10,000 ohm grid leak, 200 watts
I_g 0–150 milliampere grid-current meter
I_p 0–500 milliampere plate-current meter
T_3 Thordarson 10-volt filament transformers
F ½ ampere high-voltage fuse
S plate-current switch placed on the wall and operated by means of a long stick.

* Since reporting on the above material at the April, 1938 meeting of the American Physical Society, an article by Lörinczi has appeared in the Zeits. f. Physik **109**, 175 (1938) with calculations of parameters for the $np^5\,md$ configurations of the rare gases, together with calculations of the g-factors for these configurations. These are then compared with Murakawa and Iwana's[2] values for the case of neon, and a few isolated values in the case of argon. In both cases we differ markedly from Lörinczi's observations and calculations. Lörinczi is evidently unaware of the results of Sampson[8] and Shortley,[9] which give much better agreement than his with observed energy levels.

† Now instructor in physics, Lehigh University.

[1] Back, Ann. d. Physik **76**, 317 (1925).

[2] Murakawa and Iwana, Tokyo Inst. Phys. Chem. Res. **13**, 283 (1930).

[3] Jacquinot, Comptes rendus **202**, 1578 (1936).

TABLE I. *Zeeman effect for lines in the spectrum of neon.*

λ	Classification	J values	Pattern	g_a	g_b	λ	Classification	J values	Pattern	g_a	g_b
8771.64	$3p_2 - 3s_1'$	1, 1	(–), 0.749, 1.338†	1.338	0.749	5719.532	$3p_8 - 4s_1''''$	2, 2	P.B.	1.229*	1.115
8681.93	$3p_7 - 3d_2$	1, 1	(–), 0.680, 0.866†	0.680	0.866	5719.236	$3p_6 - 4s_1'''$	2, 3		0.669*	0.783
8679.50	$3p_3 - 3s_1'$	0, 1	(0), 0.755	0/0	0.755	5656.656	$3p_7 - 4s_1''''$	1, 2	P.B.		1.237
8655.52	$3p_4 - 3s_1''''$	2, 2	P.B.	0.669*	0.783	5656.330	$3p_7 - 4s_1''$	1, 2			
8654.38	$3p_4 - 3s_1'''$	2, 3			1.131	5652.571	$3p_7 - 4s_1'$	1, 1	(0.137)#, 0.742#	0.674	0.812
8647.04	$3p_4 - 3s_1''$	2, 2	(0.099), 1.280	1.301	1.259	5563.047	$3p_8 - 4s_1''''$	2, 2	P.B.	1.137*	1.116
8634.668	$3p_7 - 3d_1''$	1, 2	P.B.	0.669*	0.945	5562.765	$3p_8 - 4s_1'''$	2, 3			
a	$3p_7 - 3d_1'$	1, 3			1.247	5562.441	$3p_8 - 4s_1''$	2, 2			
8591.266	$3p_5 - 3s_1''''$	1, 2‡	(*0*), (0.185), *0.658*, 0.848, 1.006	1.006	0.775	5412.655	$3p_2 - 5d_3$	1, 2	(0), 1.297#	1.340*	1.311
						5383.257	$3p_3 - 5d_3$	0, 1	(0), 1.360	0/0	1.360
a	$3p_8 - 3d_4'$	2, 4	P.B.	1.137*		5374.976	$3p_3 - 5d_2$	0, 1	(0), 0.791	0/0	0.791
8495.36	$3p_8 - 3d_4$	2, 3			1.037	5343.295	$3p_{10} - 4d_6$	1, 0	(0), 1.986	1.986	0/0
8463.42	$3p_8 - 3d_2$	2, 1	(*0*), (0.276), —, 1.154, *1.425*	1.154	0.855	5341.099	$3p_{10} - 4d_5$	1, 1	(0.594), 1.394, 1.983	1.984	1.393
						5330.791	$3p_{10} - 4d_3$	1, 2	(*0*), (—), *0.845*, 1.320, 1.985	1.987	1.318
8418.447	$3p_8 - 3d_1''$	2, 2	P.B.	1.137*	0.947						
8417.24	$3p_8 - 3d_1'$	2, 3				5326.407	$3p_{10} - 4d_2$	1, 1	(1.176), 0.810, 1.987	1.987	0.810
8377.630	$3p_9 - 3d_4'$	3, 4	P.B.	1.329*	1.249	5208.865	$3p_6 - 5d_3$	2, 2	(0), 1.267#	1.229*	1.305
8376.45	$3p_9 - 3d_4$	3, 3		1.329*	1.034	5193.118	$3p_2 - 5s_1''$	1, 2	(0), 1.221#	1.340*	1.261
8365.82	$3p_9 - 3d_3$	3, 2	(0), 1.323	1.329*	1.337	5191.327	$3p_2 - 5s_1'$	1, 1	(0.516), 0.809, 1.329	1.330	0.810
8301.56	$3p_9 - 3d_1''$	3, 2	P.B.	1.329*	0.951	5158.894	$3p_2 - 5s_1'$	0, 1	(0), 0.805	0/0	0.805
8300.338	$3p_9 - 3d_1'$	3, 3			1.247	5156.662	$3p_7 - 5d_2$	1, 2	(0), (—), –, –, 1.942	0.669*	1.305
8267.14	$3p_6 - 3s_1''''$	2, 2	P.B.	1.229*	0.804	5154.423	$3p_7 - 5d_2$	1, 1	(0), 0.726#	0.669*	0.783
8266.092	$3p_6 - 3s_1'''$	2, 3			1.128	5117.011	$3p_{10} - 4s_1''$	1, 2	P.B.	1.984*	1.221
8259.392	$3p_6 - 3s_1''$	2, 2	(0), 1.248#	1.229*	1.267	5116.495	$3p_{10} - 4s_1''''$	1, 2			
8136.423	$3p_7 - 3s_1''''$	1, 2	P.B.	0.669*	0.776	5113.665	$3p_{10} - 4s_1'$	1, 1	(1.193), 0.796, 1.982	1.986	0.792
a	$3p_7 - 3s_1'''$	1, 3			1.119	5080.376	$3p_8 - 5d_4$	2, 3	P.B.	1.137*	1.093
8128.95	$3p_7 - 3s_1''$	1, 2	(*0*), (0.570), —, 1.243, *1.817*	0.669	1.243	*a*	$3p_8 - 5d_4'$	2, 4		1.137*	1.20(?)
						5035.989	$3p_9 - 5d_3$	3, 2	(0), 1.356#	1.329*	1.309
8118.554	$3p_7 - 3s_1'$	1, 1	—, 0.715†	0.669*	0.761	5011.005	$3p_3 - 6d_2$	0, 1	(0), 0.800	0/0	0.800
7944.18	$3p_8 - 3s_1''''$	2, 2	P.B.			4823.174	$3p_3 - 6s_1'$	0, 1	0, 0.857	0/0	0.857
7943.193	$3p_8 - 3s_1'''$	2, 3		1.137*	1.123	4818.789	$3p_7 - 6d_2$	1, 1	(0), 0.718#	0.669*	0.767
7544.08	$3p_{10} - 3d_6$	1, 0	(0), 1.996	1.996	0/0	4817.644	$3p_7 - 6d_1''$	1, 2	(0), 1.122#	0.669*	0.971
7535.78	$3p_{10} - 3d_5$	1, 1	(0.595), (1.399), 1.999	1.998	1.400	4710.058	$3p_{10} - 5d_4$	1, 0	(0), 2.004	2.004	0/0
7488.85	$3p_{10} - 3d_3$	1, 0	(*0*), (–), *0.724*, 1.351, 1.985	1.985	1.354	4708.857	$3p_{10} - 5d_5$	1, 1	(0.604), 1.381, 1.979	1.980	1.380
						4704.394	$3p_{10} - 5d_3$	1, 2	(0), (–), —, 1.317, —		1.312
7472.425	$3p_{10} - 3d_2$	1, 1	(1.127), 0.857, 1.995	1.987	0.858	4425.416	$3p_{10} - 6d_6$	1, 0	P.B.	1.984*	0/0
7112.2	$3p_1 - 4d_2$	0, 1	(0), 0.814	0/0	.814	4424.809	$3p_{10} - 6d_5$	1, 1			1.389
7059.113	$3p_{10} - 3s_1''$	1, 2	(*0*), (0.753), *0.500*, 1.242, 1.985	1.987	1.240	4422.518	$3p_{10} - 6d_3$	1, 2	(–), *0.620*, 1.264†, —	1.984*	1.331
						3754.206	$3s_2 - 4p_{10}$	1, 1	(–), —, 1.930		1.930
7051.288	$3p_{10} - 3s_1'$	1, 1	(1.241), 0.750, 1.987	1.988	0.749	3701.222	$3s_2 - 4p_8$	1, 2	(0), 1.159#	1.034*	1.117
6738.058	$3p_1 - 4s_1'$	0, 1	(0), 0.803	0/0	0.803	3685.728	$3s_2 - 4p_7$	1, 1	(0), 1.004#	1.034*	0.974
6276.039	$3p_2 - 4d_6$	1, 0	(0), 1.340	1.340	0/0	3682.232	$3s_2 - 4p_6$	1, 2	(*0*), (0.325), 1.031, 1.362, *1.690*	1.036	1.363
6258.796	$3p_2 - 4d_5$	1, 2	(0), 1.315#	1.340*	1.332						
6225.742	$3p_3 - 4d_5$	0, 1	(0), 1.397	0/0	1.397	3633.657	$3s_2 - 4p_5$	1, 0	(0), 1.030	1.030	0/0
6205.787	$3p_3 - 4d_2$	0, 1	(0), 0.812	0/0	0.812	3609.170	$3s_3 - 4p_{10}$	0, 1	(0), 1.921	0/0	1.921
6189.076	$3p_4 - 4d_3$	2, 2	(0), 1.310#	1.301*	1.319	3600.161	$3s_2 - 4p_5$	1, 1	(0.346), 0.680, 1.030	1.029	0.681
6175.291	$3p_4 - 4d_1''$	2, 2	(0), 1.123#	1.301*	0.945	3593.631	$3s_2 - 4p_2$	1, 1	P.B.	1.035*	1.412
6174.888	$3p_4 - 4d_1'$	2, 3	(0), 0.940#	1.301*	1.120	3593.519	$3s_2 - 4p_4$	1, 2			
5987.933	$3p_5 - 4d_3$	2, 2	(0), 1.279#	1.229*	1.325	3520.467	$3s_2 - 4p_1$	1, 0	(0), 1.031	1.031	0/0
5966.171	$3p_4 - 4s_1''''$	1, 2	P.B.	1.340*	1.221	3515.186	$3s_4 - 4p_8$	1, 2	(*0*), (363), *0.752*, 1.123, 1.460	1.479	1.113
5965.438	$3p_2 - 4s_1''$	1, 2									
5961.626	$3p_2 - 4s_1'$	1, 1	(0.518), 0.809, 1.331	1.330	0.808	3510.714	$3s_5 - 4p_{10}$	2, 1	(*0*), (0.430), *1.075*, 1.500, 1.924	1.502	1.929
5934.458	$3p_7 - 4d_6$	1, 0	(0), 0.682	0.682	0/0						
5918.914	$3p_3 - 4s_1'$	0, 1	(0), 0.805	0/0	0.805	3501.211	$3s_4 - 4p_7$	1, 1	(0.495), 0.978, 1.467	1.465	0.975
5913.642	$3p_7 - 4d_2$	1, 1	(0.152), 0.742#	0.669*	0.819	3498.059	$3s_4 - 4p_6$	1, 2	(0), 1.307#	1.464*	1.359
5906.440	$3p_7 - 4d_1''$	1, 2	P.B.	0.669*	0.991	3472.568	$3s_5 - 4p_9$	2, 3	(0), 1.144#	1.503*	1.324
a	$3p_7 - 4d_1'$	1, 3			1.248	3466.575	$3s_3 - 3p_5$	0, 1	(0), 0.682	0/0	0.682
5902.792	$3p_4 - 4s_1''''$	2, 2	P.B.	1.301*	1.117	3464.334	$3s_5 - 4p_8$	2, 2	(0.386), (–), 0.742, *1.112*, *1.493*, 1.867	1.497	1.108
5902.475	$3p_4 - 4s_1'''$	2, 3									
5902.097	$3p_4 - 4s_1''$	2, 2				3460.523	$3s_3 - 4p_2$	0, 1	(0), 1.382‡	0/0	1.407
5868.417	$3p_5 - 4s_1'$	1, 1	(0.194)#, 0.895#	0.999*	0.795	*a*	$3s_3 - 4p_4$	0, 2			
5820.91	$3p_8 - 4d_4'$	2, 4	P.B.	1.137*	1.252	3454.193	$3s_4 - 4p_3$	1, 0	(0), 1.450	1.450	0/0
5820.176	$3p_8 - 4d_4$	2, 3				3450.761	$3s_5 - 4p_7$	2, 1	(*0*), (0.508), 0.970, 1.474, *1.999*	1.488	0.977
5811.417	$3p_8 - 4d_2$	2, 1	(*0*), (0.304), —, 1.146, *1.457*	1.143	0.829						
						3447.701	$3s_5 - 4p_6$	2, 2	(0), 1.424#	1.503*	1.345
5764.432	$3p_9 - 4d_4'$	3, 4	P.B.	1.329*	1.247	3423.910	$3s_4 - 4p_5$	1, 1	(–), 0.682, 1.448†	1.448	0.682
5764.063	$3p_9 - 4d_4$	3, 3			1.040	3418.002	$3s_4 - 4p_2$	1, 1	P.B.	1.465*	
5760.585	$3p_9 - 4d_3$	3, 2	(0), 1.345#	1.329*	1.313	3417.901	$3s_4 - 4p_4$	1, 2			1.197
5748.650	$3p_9 - 4d_1'$	3, 3	P.B.			3369.905	$3s_5 - 4p_2$	2, 1	P.B.	1.503*	
5748.286	$3p_9 - 4d_1''$	3, 2		1.329*	0.978	3369.806	$3s_5 - 4p_4$	2, 2			1.171

* Back's measurement; assumed in calculation of other *g*-factor.
‡ Examples of almost symmetrical patterns whose separations are badly disturbed by beginning P.B. effect.
† Measured in perpendicular polarization.
# Unresolved.
a Ordinarily "forbidden" transition.

by a high frequency oscillator, the diagram of which is shown in Fig. 1.

The plate current is supplied from a 2000 volt d.c. generator. The whole oscillator is enclosed in a grounded copper wire screen. By using different tank coils, it is possible to vary the frequency from about 25 to 50 megacycles. The leads from the pick-up coil to the discharge tube were cut to approximately ¼ the wave-length emitted by the oscillator. Additional adjustment afforded by the lead-tuning condenser allowed ample power to be delivered to the tube. Eastman spectroscopic plates were used and developed in Edwal 12.

The discharge is started in the following way. The tube and ballast chamber and charcoal trap are completely pumped out and a small quantity

TABLE II. *Comparison of observed and calculated g-values.*

LEVEL	J	$2p^5 4p$ $g_{OBS.}$	$g_{CALC.}$
$4p_2$	1	1.409	1.412
$4p_5$	1	0.682	0.695
$4p_7$	1	0.974	0.963
$4p_{10}$	1	1.929	1.930
	Σg	4.994	5.000
$4p_4$	2	1.184	1.190
$4p_6$	2	1.360	1.363
$4p_8$	2	1.112	1.114
	Σg	3.656	3.667
$4p_9$	3	1.328	1.333

of neon is introduced from the reservoir. The plate-current switch is closed, and then a Tesla coil-type leak-tester starts a discharge which is usually limited to the neighborhood of the electrodes. The tuning condenser is then adjusted until the plate current is a maximum. Neon is then admitted, a small quantity at a time until the discharge suddenly breaks through the capillary. The pressure of the neon is then increased slightly until a very bright discharge is produced. The best operating pressure seems to depend somewhat on the size of the capillary bore, larger bores seeming to give more favorable results. The pressure of the neon in most cases was about 7 mm Hg and the plate current varied between 200 and 400 ma.

The usual exposure lasted about 48 hours, and in general required practically no attention. Both polarized and unpolarized exposures were made. While the perpendicular runs were in general satisfactory, the parallel showed very serious lack of purity, undoubtedly caused by the breakdown of the usual selection rules caused by the presence of the strong electric fields.

The sodium lines were used as standards when they appeared on the plates; otherwise Back's measurements of λλ5852 and 6074 of Ne were used.

About 250 lines were measured. The results are given in Table I. Wave-lengths and classification are as given by Paschen.[4] Only those 150 lines involving $2p^5 4p$ and $2p^5 md$ have been recorded. The other 100 lines are transitions involving the $2p^5 ms$ configurations, and give results in substantial agreement with Jacquinot.[3]

Parameters for the $2p^5 4p$ configuration have been calculated by means of least-squares methods by Bartberger,[5] and the g-values calculated with their aid. This was done by determining the transformation coefficients from the LS-matrix. It was necessary to use this method rather than the one suggested by Marvin[6] in order to determine the phases of the coefficients for the calculation of the Paschen-Back effect. Table II gives a summary of the results. $4p_2$ and $4p_4$ are very close together and all of the lines involving them show beginning Paschen-Back effect. Extensive calculations were needed to reduce the observed patterns and determine their g-factors. The observed g-values are, wherever possible, averages taken from resolved patterns, except in the case of $4p_9$, where it was determined by the method of Shenstone and Blair.[7]

The agreement between theory and experiment is extremely satisfactory. Our usual allowance for experimental error is about 0.5 percent. Most of the observed values are within this limit compared with the calculated values. Even more surprising is the agreement of the g-sums. Where

TABLE III. *Average g-values and g-sums for the $2p^5 3d$ and $2p^5 4d$ configurations.*

LEVEL	J	$2p^5 3d$ m = 3 $g_{OBS.}$	$g_{CALC.}$	$2p^5 4d$ m = 4 $g_{OBS.}$	$g_{CALC.}$
ms_1'	1	0.752	0.752	0.797	0.797
md_2	1	0.860	0.851	0.812	0.812
md_5	1	1.396	1.397	1.396	1.391
	Σg	3.008	3.000	3.005	3.000
ms_1''	2	1.242	1.232	1.230	1.241
ms_1''''	2	0.781	0.783	0.783	0.791
md_1''	2	0.948	0.952	0.990	0.978
md_3	2	1.356	1.366	1.322	1.323
	Σg	4.327	4.333	4.326	4.333
ms_1'''	3	1.125	1.133	1.116	1.120
md_1'	3	1.249	1.247	1.248	1.247
md_4	3	1.034	1.036	1.040	1.049
	Σg	3.408	3.416	3.404	3.416
md_4'	4	1.249	1.250	1.251	1.250

[4] Paschen, Ann. d. Physik **60**, 405 (1919).

[5] Bartberger, Phys. Rev. **48**, 682 (1935).

[6] Marvin, Phys. Rev. **44**, 818 (1933).

[7] Shenstone and Blair, Phil. Mag. **8**, 765 (1929).

we might reasonably expect a discrepancy of as much as 2 percent, the g-sums are even closer than the individual values.

Average g-values and g-sums for the $2p^5 3d$ and $2p^5 4d$ configurations are listed in Table III. The parameters for the $2p^5 3d$ configuration have been obtained by Sampson[8] and for the $2p^5 4d$ by Shortley;[9] the latter neglected interaction between the upper and lower levels of the configuration. The agreement for the $2p^5 3d$ configuration is almost perfect; for the $2p^5 4d$ configuration almost as good.

The $2p^5 md$ configurations are involved in transitions which yield complicated patterns that are difficult to interpret due to incipient Paschen-Back effect. This type of interaction takes place between $d_6(j=0)$ and d_5, between d_4 and d_4', between d_1' and d_1'', and among the levels s_1'', s_1''', and s_1''''. The g-values of these levels as given in Table III have been determined by first calculating the Paschen-Back pattern to be expected from the calculated g-value for the level in combination with Back's value for the lower level, and then adjusting the assumed g-value to fit the measured pattern.

[8] Sampson, Phys. Rev. **52**, 1157 (1937).
[9] Shortley, Phys. Rev. **44**, 666 (1933).

TABLE IV. *Some g-values for the $2p^5 5d$ configuration.*

LEVEL	J	$g_{\text{OBS.}}$	LEVEL	Σg	2.983
$5s_1'$	1	0.809	$5s_1''$	2	1.251
$5d_2$	1	0.791	$5d_3$	2	1.298
$5d_5$	1	1.383	$5d_4$	3	1.093

Table IV gives a few additional g-values. Since complete configurations were not observed, it was not thought worth while to calculate the g-values from known parameters, which in any case do not seem to be accurate enough to yield good agreement for the positions of the levels.

The conclusions that may be drawn from the foregoing results are fairly obvious. Wherever it is possible to determine parameters for a configuration that will yield calculated positions for the levels in agreement with the observed positions, then related parameters, like the g-values, will also be in good agreement. Thus, the parameters determined for the $2p^5 3p$ configuration[9] give very poor agreement with observed levels, and the calculated g-values are correspondingly poor, while for the $2p^5 3d$ configuration[8] the largest discrepancy in position is 0.9 cm^{-1} and the agreement in g-values is practically perfect. The same sort of situation should hold with respect to intensities.

OCTOBER 15, 1938 PHYSICAL REVIEW VOLUME 54

Application of Clay's New Value of the Jaffé-Zanstra Coefficient for Air to High Pressure Ion Current Measurements

JAMES W. BROXON AND GEORGE T. MERIDETH
University of Colorado, Boulder, Colorado

(Received September 1, 1938)

Clay has found the coefficient $1.24(10)^{-4}$, employed by Zanstra in his treatment of high pressure ionization data for air by Jaffé's columnar theory, should actually be applied to nitrogen, and the coefficient 10^{-5} substituted in the case of air. We have used the new coefficient in a repetition of the analysis of our experimental data. The straight lines predicted by the theory are obtained in the collecting field range, 1769–4520 volts/cm, in most cases, and the curvatures of the Jaffé-Zanstra curves are lessened in the remaining cases. The curves obtained by plotting the theoretical "saturation" current values against the specific gravity of the air do not display the definite breaks indicated before.

IN a recent paper[1] which will hereafter be referred to as paper 1, we presented the results of the application of the equation

$$1/i = 1/I + (q/I)\, f(x) \qquad \text{(A)}$$

formulated by Zanstra[2] from the Jaffé theory, to

[1] J. W. Broxon and G. T. Merideth, Phys. Rev. **54**, 9 (1938).
[2] H. Zanstra, Physica **2**, 817 (1935).

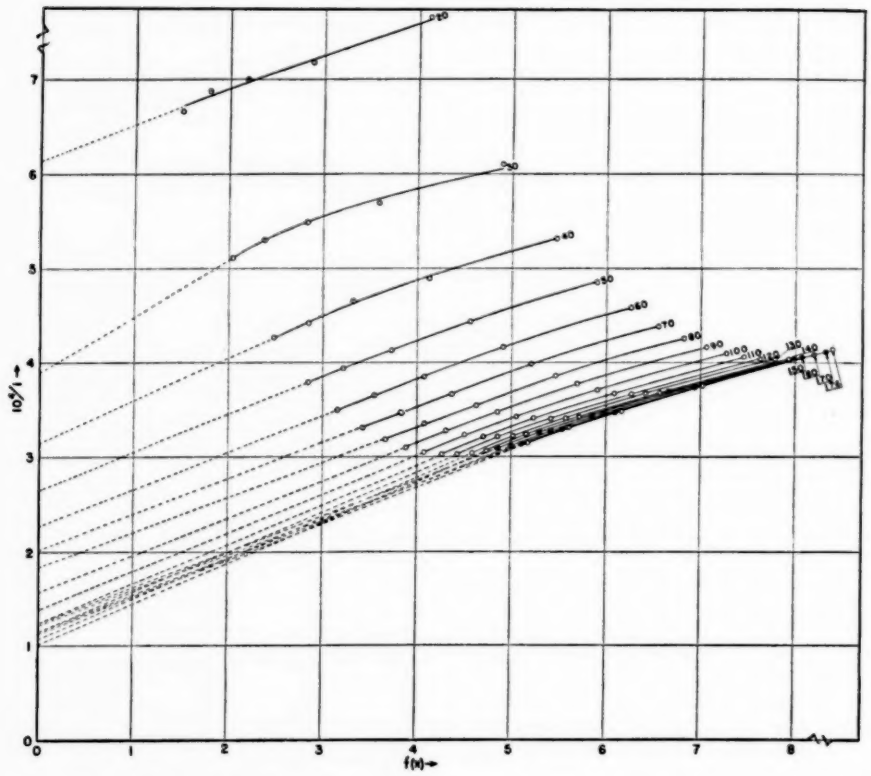

FIG. 1A. Jaffé-Zanstra function curves corresponding to our measurements with central-source. Air at 28°C. Central source of gamma-radiation. Numbers at upper ends of curves represent specific gravity relative to air at N. T. P.

our high pressure ion current measurements[3] in air. The terminology was discussed in detail in paper 1. In particular, Zanstra found upon examination of ion current measurements by Erikson,[4] that for air $x=1.24(10)^{-4}(E/p)^2$, where E is the collecting field intensity in volts/cm, p is the pressure in atmospheres, and x is the argument of the function presented for a wide range in graphical form by Zanstra. This relation was tested by Clay[5] and Clay and van Tijn[6] with their measurements of ion currents in air, and equation (A) was thereby verified.

In order to provide for comparison of data corresponding to other than room temperatures, we substituted for p the specific gravity of the air, σ, relative to air at N.T.P., but used the same coefficient. On this basis we found the reciprocals of our measured currents plotted against $f(x)$ did not yield quite straight lines at very high field intensities, as predicted, but curves slightly concave toward the $f(x)$ axis. These curves are shown in Figs. 1 and 2 of paper 1.

Immediately upon receipt of paper 1, Professor Clay wrote us they had found recently that air compressed by themselves did not yield straight Jaffé-Zanstra curves such as they had obtained formerly with air supplied by a commercial concern. Upon investigation they found that nitrogen yielded straight curves with use of the coefficient $1.24(10)^{-4}$ specified above, whereas for increasing fractions of oxygen, decreasing values of the coefficient were required to provide straight curves, until with 12 percent to 29 percent oxygen, the coefficient value 10^{-5} must be employed. (Professor Clay informs us these findings have appeared in the August 1 issue of *Physica* which we have not yet received.) It appears, then, that their earlier measurements were actually made with nitrogen rather than air. The situation relative to Professor Erikson's data is not clear.

[3] J. W. Broxon and G. T. Merideth, Phys. Rev. **54**, 1 (1938).
[4] H. A. Erikson, Phys. Rev. **27**, 473 (1908).
[5] J. Clay, Physica **2**, 811 (1935).
[6] J. Clay and M. A. van Tijn, Physica **2**, 825 (1935).

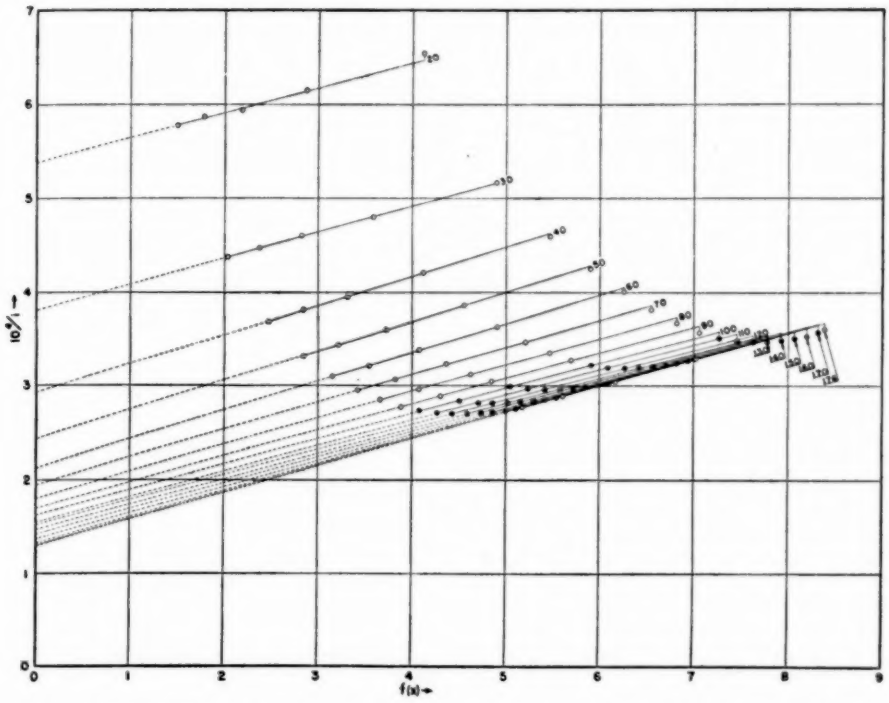

FIG. 2A. Jaffé-Zanstra function curves corresponding to our measurements with ring-source. Air at 27°C. Ring-source of gamma-radiation beneath chamber. Numbers at upper ends of curves represent specific gravity relative to air at N. T. P.

In view of this situation Professor Clay suggested that we repeat the analysis of our data, using the value 10^{-5} instead of $1.24(10)^{-4}$. This we have done. The results are presented in Figs. 1A and 2A corresponding to Figs. 1 and 2, respectively, of paper 1. The curvatures are definitely reduced by the use of the new coefficient. In Fig. 1A, corresponding to the central source of gamma-radiation the points corresponding to the four highest field intensities, 1769, 2727, 3617 and 4520 volts/cm, may be regarded as lying on a straight line for the range of specific gravities, 50 to 80. At both lower and higher densities, however, there seems even in this high range of field intensities to be a lessened curvature in the same sense as before. In Fig. 2A, corresponding to the ring-source of gamma-radiation the points corresponding to the designated four highest field intensities lie remarkably close to straight lines for all densities. In view of this situation only straight lines determined by the four highest intensity values were drawn. Vertical lines connect these to the points corresponding to the fifth field intensity, 888 volts/cm.

As in paper 1, "saturation" currents were determined by extrapolations formed by drawing tangents to the curves at the termini corresponding to highest field intensity. In the case of the straight lines of Fig. 2A, "least-squares" calculations were employed as an aid in the determination of the intercepts in view of the long extrapolations, although this may not appear justified on account of the arbitrariness of construction of the original current curves drawn from the experimental data.[3] The "saturation" currents obtained from the reciprocals of the intercept values are plotted against the specific gravity in Figs. 3A and 4A which correspond, respectively, to Figs. 3 and 4 of paper 1. Again, the curves representing experimental currents at the highest field intensities are included for comparison.

For both gamma-radiation sources, considerably higher "saturation" current values are yielded by the new than by the old coefficient. The new "saturation" current curves resemble the earlier ones in that if extrapolated at their low density ends they would appear to intercept the current-axis above the origin, and they both

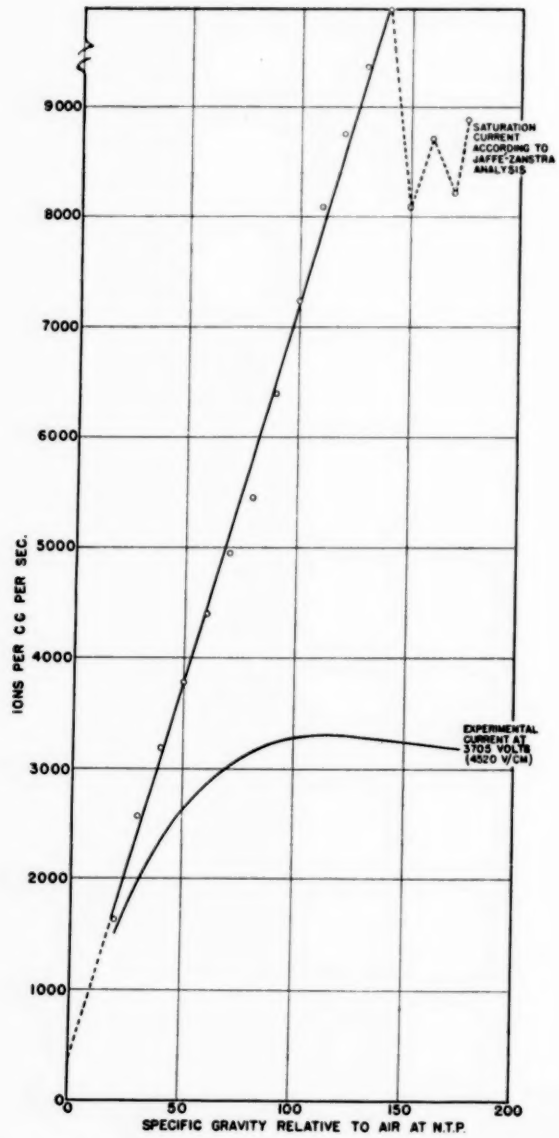
IONS PER C C PER SEC.
SATURATION CURRENT ACCORDING TO JAFFE-ZANSTRA ANALYSIS
EXPERIMENTAL CURRENT AT 3705 VOLTS (4520 V/CM)
SPECIFIC GRAVITY RELATIVE TO AIR AT N.T.P.

FIG. 3A. "Saturation" current curve corresponding to our observations with central-source, together with experimental curve obtained with strongest collecting field.

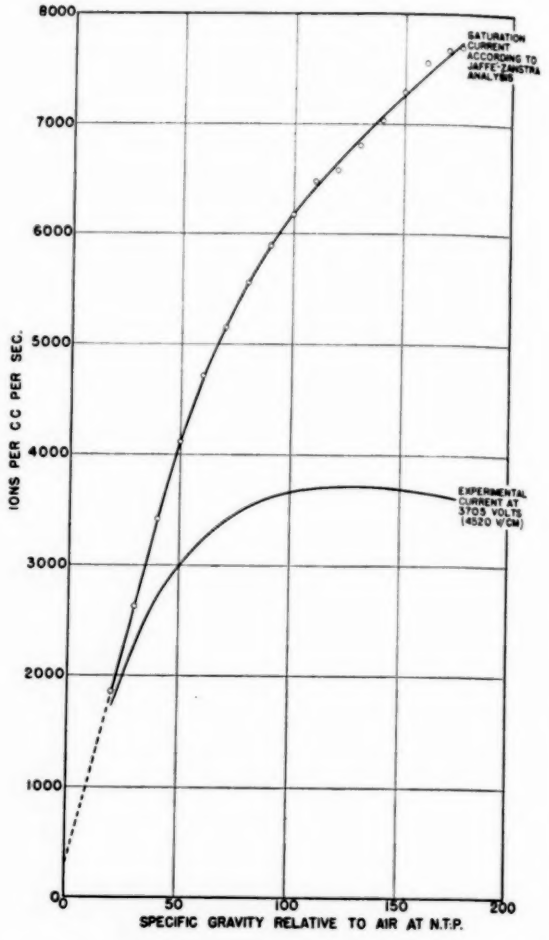
IONS PER C C PER SEC.
SATURATION CURRENT ACCORDING TO JAFFE-ZANSTRA ANALYSIS
EXPERIMENTAL CURRENT AT 3705 VOLTS (4520 V/CM)
SPECIFIC GRAVITY RELATIVE TO AIR AT N.T.P.

FIG. 4A. "Saturation" current curve corresponding to our observations with ring-source, together with experimental curve obtained with strongest collecting field.

lie above the highest experimental current curves. However, the straight line segments with definite breaks do not appear to be indicated. In the case of the central-source, Fig. 3A, a straight line appears best to represent the relation between "saturation" current and density for all densities to $\sigma = 140$ (or 156 atmospheres). Above this the variation is rather irregular as at the higher densities in paper 1. This may be related to the large extrapolations. The ring-source values, Fig. 4A, appear to indicate a smooth curve throughout the density range. In this connection it should be noted that a smooth curve might well be substituted for the broken line curve of Fig. 4 of paper 1.

The "saturation" currents corresponding to negative and positive ion currents (see Fig. 6 of paper 1) have been determined with the use of the new coefficient. At 120 atmospheres the "saturation" currents may be regarded as practically identical for both signs, but at the other two pressures there seems no better agreement than before.

The Production of Collimated Beams of Monochromatic Neutrons in the Temperature Range 300°–10°K

LUIS W. ALVAREZ
Radiation Laboratory, Department of Physics, University of California, Berkeley, California
(Received August 20, 1938)

An electrical velocity selector is described, which allows the production and use of highly collimated beams of pure thermal neutrons. The mean temperature of the neutrons may be varied from 300°K to an undetermined lower limit, probably less than 10°K, without the use of refrigerants. The temperature width of the neutron "line" is also adjustable. Fast neutron effects are completely eliminated. Qualitative verification of the $1/v$ law for Boron has been extended to 30°K. The intensity of neutrons available from the cyclotron allows counting rates of 1000 per minute to be obtained at 30°K, with a source-detector distance of 4 meters, and an angular spread of 1°.

INTRODUCTION

IN 1934, Fermi and his collaborators[1] found that neutrons could be slowed to thermal velocities, by collisions with protons in various hydrogenous materials. This discovery has proved to be one of the most fruitful in recent years. Bohr[2] proposed his "liquid drop" model of the nucleus to explain the resonance capture of slow neutrons in the range from 0–100 volts. Schwinger and Teller[3] have shown that a determination of the scattering cross sections of ortho- and para-hydrogen for slow neutrons can yield much information about the spin dependence and range of nuclear forces. Bloch's[4] suggestion that slow neutron beams could be polarized by passing through magnetized plates of iron has opened several valuable fields of investigation. For example, it should make possible the determination of the magnetic moment of the neutron,[5] and also give information on fundamental problems of magnetism. Interesting questions relating to the nature of the chemical bonds of hydrogen in organic molecules may also be attacked for the first time by the application of slow neutron technique.

It is indeed remarkable that so much good work has been done in this field, when one remembers that in all these experiments, the slow neutron effects were superposed on a background due to fast neutrons. It can be shown on quite simple grounds that it is impossible to obtain a pure slow neutron beam by absorption methods. The absorption coefficients of fast neutrons are less than or equal to those of slow neutrons, so the latter can exist only in partial equilibrium with their fast parents. Chalmers[6] found that it was possible to lead slow neutrons around corners through a tunnel in a block of paraffin. Since the scattering coefficient of slow neutrons on paraffin is much greater than that for fast neutrons, the emergent beam was relatively more rich in thermal neutrons than the original beam. But since the reflection coefficient of thermal neutrons on paraffin is only 0.83, it may easily be seen that this method cannot be very successful in yielding a slow neutron beam free from faster ones. The method which has been used in most thermal neutron work thus far consists in taking a series of measurements with and without cadmium sheets interposed in the neutron beam. The difference between the two sets of data is due to the thermal neutrons. It has thus been impossible to perform slow neutron scattering or absorption experiments with "good geometry," because if one restricts the solid angle of slow neutrons by cadmium slits, the ratio of fast neutron to slow neutron effects becomes too high.

For many purposes, it is desirable to work with neutrons having energies corresponding to temperatures of less than 300°K. The attempts to cool neutrons[7] have been rather disappointing, for although liquid hydrogen is available in

[1] Amaldi, D'Agostino, Fermi, Pontecorvo, Rasetti, and Segrè, Proc. Roy. Soc. **149**, 522 (1935).
[2] Bohr, Nature **137**, 344 (1936).
[3] Schwinger and Teller, Phys. Rev. **51**, 775 (1937).
[4] Bloch, Phys. Rev. **50**, 259 (1936).
[5] Frisch, von Halban and Koch, Phys. Rev. **53**, 719 (1938).
[6] Chalmers, Brit. J. Radiology, **8**, 163 (1935).
[7] Libby and Long, Phys. Rev. **52**, 592 (1937).

several laboratories, it has been found impossible to obtain neutrons with a temperature of much less than 60°K. The explanation is probably that at temperatures lower than the Debye temperature of paraffin, the neutrons interact elastically only with the lattice, and therefore rebound with most of their incident energy. They cannot lose energy by inelastic collisions, as they have insufficient energy to excite the lowest rotational state of the cold paraffin molecules.

A method[8] has recently been developed, which allows the production of intense, highly collimated beams of pure, monochromatized thermal neutrons from 300° to an undetermined lower limit (probably <10°K). The energy of the neutrons may be changed at will without the use of refrigerants, and the background is determined only by the natural background of the detector—fast neutron effects are completely eliminated.

Theory of the Method

Soon after the discovery of slow neutrons, several of the members of the Radiation Laboratory staff suggested that it would be possible to measure the velocity of the neutrons by "keying" the radiofrequency oscillators which drive the cyclotron, i.e., turning them off suddenly, and then observing on an oscillograph, the interval of time elapsing before the slow neutrons were detected near the control panel, a distance of about 15 meters. The idea was abandoned when the results of the rotating wheel method of velocity measurement were announced.[9] But the fact that slow neutrons take an appreciable time to travel distances of the order of meters is the basic principle of the method to be described.

In this method, the deuteron beam from the cyclotron is modulated at 120 cycles per second, so that fast neutrons are generated in a beryllium target about half of the time. A BF_3-filled ionization chamber is placed 8 meters from the Be target, and the linear amplifier to which it is connected is arranged to be sensitive only when the cyclotron is off. Since fast neutrons have a mean life of less than 10^{-5} second, it is impossible for them to be detected with this arrangement. But since it takes a thermal neutron 1/240 second to travel 8 meters, the amplifier will record those neutrons which were slowed to thermal velocities by a paraffin block near the Be target. The mean life of a slow neutron in paraffin is about 10^{-4} sec., which is small compared to the 4×10^{-3} sec. it takes to reach the counter. The BF_3 chamber and the paraffin block are placed at opposite ends of a cadmium-lined tube, so that no neutrons except those which travel in a straight line between the two may be counted. This latter feature assures that the beam is highly collimated. One might at first think that the tube is responsible for the collimation, but the beam would be just as well collimated if the cadmium tube had a diameter ten times as great; it merely serves to isolate a volume in which no slow neutrons may be produced or reflected.

While it is obvious that this method does not actually produce a pure thermal neutron beam, the effect on the recording instruments is exactly the same as though it did. On the operational viewpoint, therefore, one is justified in asserting that the beam is composed solely of thermal neutrons.

A feature of the method which increases its usefulness considerably is that the velocity of the recorded neutrons can be changed merely by altering either the modulation frequency or the source-detector distance. There are always neutrons of low energy present in a piece of neutron-irradiated paraffin, and it is possible to use the modulated beam method as a Maxwellian demon to sort out these slow ones. If the distribution of neutron velocities in paraffin is of Maxwellian form, the number of recorded neutrons will fall off about linearly with distance as one moves the counter toward the source, and the temperature will fall with the square of the distance. The Maxwell distribution is given by the relation[10]

$$N_{dv}=(4N/\alpha^3\pi^{\frac{1}{2}})(v^2\exp -v^2/\alpha^2)dv \qquad (1)$$

or for velocities less than the most probable, α,

$$N_{dv}\approx v^2dv. \qquad (2)$$

The distribution of velocities in a molecular beam is well known to have an additional velocity dependence due to the increased probability of

[8] Alvarez, Phys. Rev. **54**, 235 (1938).
[9] Rasetti, Segrè, Fink, Dunning, Pegram, and Mitchell, Phys. Rev. **49**, 104, 777 (1936).
[10] Loeb, *Kinetic Theory of Gases* (McGraw-Hill, 1927), p. 78.

fast molecules hitting the exit slit. The same argument will apply to neutron beams, so

$$N_{dv} \approx v^3 dv. \tag{3}$$

If one uses the same modulation scheme with the chamber at different distances, d, from the source, the velocity spread of counted neutrons will be a constant percentage of the velocity, so dv will be proportional to v. Then neglecting the exponential term

$$N \sim v^4. \tag{4}$$

As one moves the detector toward the source, v decreases linearly with d (for constant frequency). But the solid angle subtended by the detector at the source increases as $1/v^2$, and the detection efficiency of a (thin) BF_3 chamber increases as $1/v$. The effects of the exponential term in (1) and the deep boron chamber are small, and of opposite sign, so

$$N \sim v \sim d. \tag{5}$$

While there are several reasons why the number of very slow neutrons will be less than that required by the Maxwell law, it is evident that if the method is successful for 300°K neutrons, there is a good possibility that beams of considerably colder neutrons may be realized.

Beam Modulation

Initial rough calculations of the intensity available indicated that it would be desirable to work 2 meters from the source, which would require a modulation frequency of 500 per second. A 500-cycle generator was available in the laboratory, and the first attempts to modulate the beam were made with it. A special transformer was constructed, the secondary of which could be placed in the grid circuit of the final stage of the power amplifier which energizes the cyclotron dees. A few trials showed that considerably more power at 500 cycles would be needed, than was available from the 1 kw motor generator set. Attempts were next made at modulating the emission voltage on the cyclotron filament. A special filament assembly was made which had a closer grid spacing at ground potential. It was found possible with this arrangement to cut off the beam completely by raising the filament to a few hundred volts positive with respect to the grounded shield. (With the usual type of filament mounting, the R.F. fields are able to pull out enough electrons to give a measurable beam even when the filament is highly positive.) Two modulation circuits were tried with this arrangement, but the time constants could not be lowered sufficiently to allow modulation at a frequency of 500 cycles. The timing was done by a commutator driven by a d.c. motor, and the operation was satisfactory up to about 50 cycles per second. The cause of the large time constant was never cleared up, but it might have been due to the ionization of deuterium atoms by the relatively slow deuterons near the center of the cyclotron. This does not seem probable, but no high resistances or large capacities could be found in the circuit which would explain the oscillographic record of the beam obtained in this manner.

The method finally adopted was simple plate modulation of the last two stages of the power amplifier. When the cyclotron is in normal operation, the plate voltage for the amplifier is supplied by a three-phase, full wave rectifier, through an a.c. filtering choke. The output of such a rectifier system is essentially d.c. For modulation purposes, the three high-voltage transformers normally used are replaced by one single phase transformer of higher kva rating. The circuit is shown in Fig. 1. The change from one supply to the other can be made very rapidly, by throwing the appropriate switches. The modulation frequency with this arrangement is 120 cycles per second. If the plate leads to two of the rectifier tubes are broken, the beam is modulated at 60 cycles.

One might first suspect that the 120-cycle modulation would not be usable, since there is always voltage on the oscillator plates. The simple theory of the cyclotron shows that it is possible to obtain a beam with any voltage on the dees—the lower the voltage, the more times the ions have to circulate around to reach their final energy. But with the inhomogeneity of magnetic field needed for focusing purposes, it is necessary for the dee voltage to be greater than some sharply defined value, which in the case of the Berkeley cyclotron is about half of the maximum value. (For lower voltages, the ions get

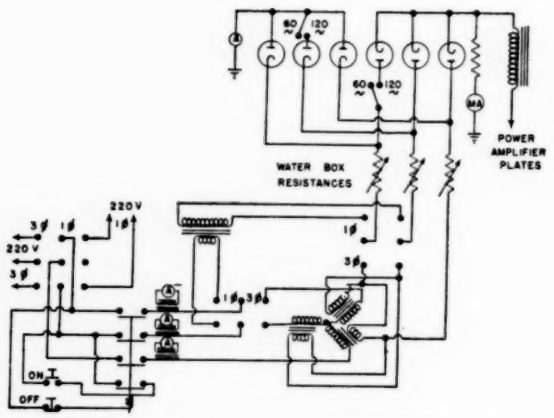

FIG. 1. Circuit for modulating neutron beam.

out of phase, and spiral back to the center with decreasing energy.) The result of this threshold is that there is an interval of time each cycle during which no beam reaches the edge of the cyclotron, and which is therefore devoid of neutrons. Oscillograph records of the beam current show that deuterons strike the target during about 50–60 percent of each cycle. At 60 cycles, the beam is on for 25–30 percent of the time.

AMPLIFIER MODULATION

The problem of modulating the amplifier sensitivity was easily solved when the beam modulation was controlled by a commutator. It was only necessary to short the output terminals of the amplifier with the same commutator. But the commutator could not be synchronized at 120 cycles, so the circuit shown in Fig. 2 was tried; it has proved to be entirely satisfactory. The essential feature of the scheme is the Rossi coincidence circuit, which has proved so useful in cosmic-ray researches. If the plates of two pentodes are connected in parallel through a resistance to a voltage supply, the potential of the plate will be insensitive to large changes in the grid voltage of either tube. If the potential of one grid is made negative enough to cut off all plate current through that tube, the current through the other will double, and therefore the *IR* drop across the resistance will be unaltered. But if both grids cut off at once, the *IR* drop will fall to zero, and the potential of the plate will rise to that of the *B* supply.

The pulses from a linear amplifier are fed through the 6C5, which inverts them to the negative sign required by the Rossi stage, sharpens them by distortion amplification, and eliminates the background noise level by the application of a high negative bias. The output of this tube is coupled to the grid circuit of one of the Rossi pentodes. The grid of the other pentode is maintained at a high positive value (about 300 volts), by means of a standard power pack, and a high resistance is placed in series with the grid to prevent large grid currents from flowing. The potential of the grid is then swung below the cut-off value once each cycle by the application of a high negative voltage from an unfiltered rectifier outfit in series with the steady positive supply. Pulses pass through this modulating stage only when the grid potential of the upper tube is below about −10 volts. The length of the sensitive time is easily altered by means of the potentiometer in the unfiltered supply. The bias voltages are made high so that little time is expended in passing from the conducting to the nonconducting state in the upper tube. The primary voltage for the unfiltered power pack is supplied from the secondary of a Selsyn transformer. The phase of the sensitive time of the amplifier may thus be altered through 360° merely by turning a knob on the control panel. The other controls on the panel are the potentiometer mentioned above, another potentiometer in the grid circuit of the 6C5, and a switch in the unfiltered power supply which makes it possible to change from 120 to 60 cycle modulation. The

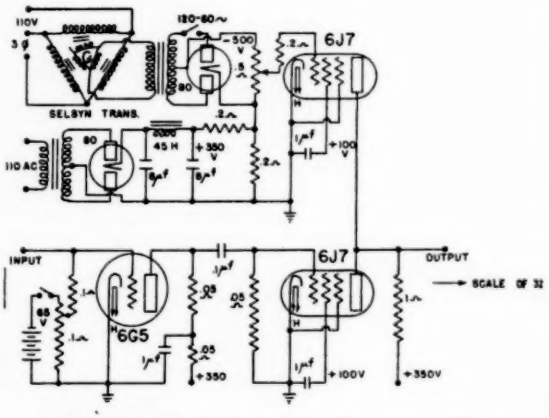

FIG. 2. Modulating unit for linear amplifier.

second potentiometer controls the size of pulses from the linear amplifier which will be recorded on the scale counter. As the bias is reduced, smaller kicks are effective, until finally the background noise gets through. The bias is increased to a point where microphonics due to persons walking in the room will no longer trip the counter. It was found necessary to place R.F. filters in each of the five power lines entering the modulation unit. If a Selsyn transformer were not available, there are several simple phase shifting networks which might be used in its place.

Ionization Chamber

The first tests on the method were made with a standard shallow ionization chamber of the Wynn-Williams type, fitted with a LiF lining. The intensity was just sufficient to show that the fast neutron background was indeed negligible. A BF_3 chamber of the type described by Schultz[11] was next tried, but the pulses from it were too long compared with the modulation time; if the voltage were increased, sparking occurred. It is quite certain that a chamber of this type could be made to work satisfactorily, and a modification of this one is at present under construction. A parallel plate BF_3 chamber was next constructed, and it has been used in most of the tests to be described below. The brass plates were $6\times18\times0.5$ cm, and were mounted on hard rubber insulators, 1 cm apart. In addition to the usual grounded guard ring, there was a high voltage guard ring half way down the insulator supporting the high voltage plate. With 800 volts across the chamber and a BF_3 pressure of 38 cm of Hg, the pulses were quite narrow and smooth. The defining slit of the chamber consisted of the two brass plates, so the beam as it entered the counter had a cross section of $1\text{ cm}\times6$ cm.

Geometrical Features

The arrangement of the cyclotron room is shown in Fig. 3. The magnet is surrounded by water tanks 3 feet in thickness. The 6-inch pipe which passes through one of the tanks was arranged to allow fast neutrons from the ordinarily used target holder to pass into a pressure cloud chamber outside the water shield. The center of the paraffin block is about 6 inches from the old target position, so the cadmium tube is mounted diagonally through the large pipe, as shown in the figure. The BF_3 chamber is surrounded by cadmium and placed in a hole in the large paraffin block. This latter feature cuts down the number of fast neutron pulses in the off cycle of the counter, but it is probably not essential for the proper operation of the apparatus. Most of the data have been obtained with the chamber near the wall of the room, but some measurements have been made with it just outside the water tanks. Absorbers have always been placed half way between the source and detector, and the same applies for the Cd sheet used in determining the background count. The angular divergence of the beam is about 1°.

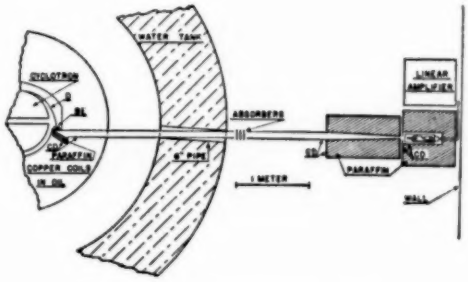

Fig. 3. Plan of cyclotron room.

Adjustment of the Apparatus

After the ionization chamber has been aligned on the axis of the cadmium tube, and the linear amplifier has been allowed to warm up, the modulation units must be "timed" with respect to each other. This adjustment is a very simple one; it is accomplished with the aid of a cathode-ray oscilloscope. Most of the work has been done at 120 cycles, so the timing procedure at this frequency will be described. As may be seen from the plan of the cyclotron room, it is impossible to place the chamber 8 meters from the paraffin source, as required for room temperature neutrons. If the chamber is placed near the wall, the neutrons should have a temperature of about 90°K.

[11] Schultz, Phys. Rev. **53**, 622 (1938).

The oscilloscope sweep circuit is set for 120 cycles, and the synchronizing control is turned full on, to assure that the phase of the sweep will remain constant in time. It is necessary on the RCA outfit we have used, to employ an external source of 120 cycle a.c. for the synchronizing. If one uses the 60 cycle a.c. for this purpose, the two sweeps per cycle do not coincide on the screen, and it is therefore impossible to set the timing accurately.

The linear amplifier is connected directly to the oscilloscope, and the cyclotron is turned on. Pulses are then seen over most of the length of the sweep. But if a piece of cadmium is interposed in the beam, the number of pulses is diminished. and all of them occur in one-half of the cycle, The phase of the cyclotron modulation is then determined, and marks are made on the screen for future reference. The output of the amplifier modulation unit is then connected to the oscillograph plates, and the gain of the oscillograph amplifier is turned up. Under these conditions, the sensitive time of the linear amplifier modulation appears as a sharply defined trough in the normally straight sweep. It is a simple matter to vary the width of this trough, and to shift its center, by means of the controls mentioned above. It is only necessary to locate the trough completely in that part of the cycle during which no fast neutron pulses were observed. The marks on the screen allow this adjustment to be made with certainty. Now the modulation unit may be connected between the linear amplifier and the scale counter, and the apparatus is ready for use. A simple test will demonstrate that the fast neutron background is negligible. With the apparatus adjusted as described, the author has obtained counting rates of 300 and 1 per minute, with no absorber and a cadmium absorber, respectively. This background is the natural background of the chamber, and is less than 0.3 percent of the slow neutron count. With the paraffin source block removed, and no cadmium absorber in the beam, the background count of 1 per minute is also observed. This is perhaps the most striking demonstration of the method—although the cyclotron is surrounded by many tons of water, the removal of one pound of paraffin stops the beam completely.

Experimental Results

The data given above show that the collimation and purity of the thermal neutron beam is as good as one could possibly hope from the simple theory of the method. But as yet nothing has been proved about the homogeneity of the neutron energies. An obvious way to test this point is to measure the boron absorption coefficient for these neutrons. There are good theoretical reasons for believing that the absorption coefficient is inversely proportional to the neutron velocity over a large velocity range. The "$1/v$ law" has been checked in a small region on either side of 300°K, by the rotating wheel method,[9] and has been confirmed to about 100°K with neutrons cooled in paraffin by liquid air.[7] On the high velocity side, the law has been verified to some tens of volts, at which point the absorption coefficient becomes small with respect to the constant scattering coefficient. This verification[12] consists in establishing the energies of resonance neutrons by the boron absorption method, and finding that they agree with the values obtained from the spatial distribution of resonance neutrons in water surrounding a Rn-Be source. So there is every reason at present to believe that the absorption coefficient of slow neutrons in boron varies as $1/v$.

It is unfortunate that boron is one of the most difficult elements to prepare in the thin layers required for absorption of very slow neutrons. Pyrex plates are the most convenient form of thin homogeneous boron absorbers, but even then it is necessary to grind or etch them to the smallest size needed. Since the absorption coefficient of 300°K neutrons differs considerably in the reports of various workers, it seemed worth while to calibrate the Pyrex plates used in this work directly with room-temperature neutrons, with the same geometry as employed for the slower ones. The standard neutrons were obtained by operating the cyclotron on d.c., and removing the upper pentode in Fig. 2 from its socket. With this arrangement, the counting rates with and without cadmium absorbers were about 4000 and 1000 per minute, respectively. This high counting rate made the large background relatively unimportant, as the probable errors of the points

[12] Amaldi and Fermi, Phys. Rev. **50**, 899 (1936).

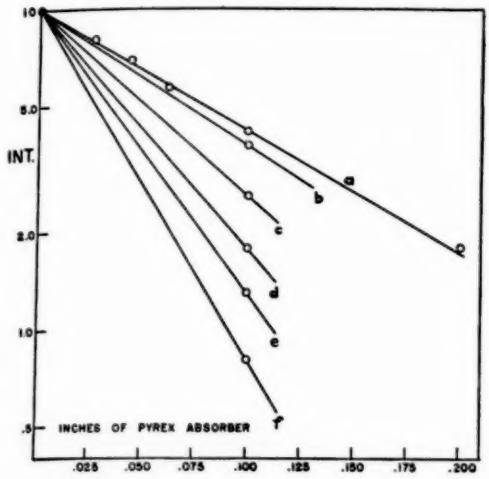

FIG. 4. Variation in boron absorption with timing scheme.

could be made very small in short periods of counting. The absorption curve of the 300°K neutrons is shown in Fig. 4(a).

With the modulation scheme as described under the section on adjustments, the absorption curve was again determined. From the simple theory, one would expect the absorption coefficient to be approximately twice that for room-temperature neutrons. Actually, the difference is quite small (Fig. 4(b)). But the reason for this discrepancy is quite obvious if one examines the modulation scheme, shown in Fig. 5(b). The time from the center of the beam pulse to the center of the amplifier sensitivity is that required by a 90° neutron to travel from the source to the detector. But a 300° neutron needs only half that time to travel the same distance. Consequently, all room-temperature neutrons which are formed in the latter half of the beam pulse will be recorded in the first half of the amplifier sensitive time. Since the number of these faster ones is so much greater than the number of 90° neutrons, most of the recorded counts will be due to the former. In order to obtain a low temperature beam, it is therefore necessary to have the amplifier insensitive for an appreciable fraction of each cycle after the deuteron beam has been turned off.

The result of shifting the amplifier sensitivity toward the end of the cycle (Fig. 5(c) and 5(d)) is to lower the effective neutron temperature, as shown in Fig. 4, (c) and (d). It may be seen that the neutron temperature with the latter timing arrangement is about what one would predict from the $1/v$ law. The apparatus in this adjustment is not as stable as one would desire—the counting rate with no absorber in the beam varies considerably more than one would expect from statistical considerations. The reason for this instability was found when the amplifier modulation "trough" was observed on the oscilloscope screen. The length of the sensitive time was found to vary erratically by about 20 percent. This instability is due to small changes in the opposing voltages on the grid of the modulating pentode. The effect is, of course, most pronounced when the amplifier sensitive time is short, but it could easily be cured if a peaking transformer were placed in the primary of the unfiltered power pack. Perhaps the most satisfactory solution would be to have the pulsating negative voltage on the pentode grid supplied by a relaxation oscillator, synchronized in the same manner as the sweep circuit of an oscillograph. With this arrangement, the modulating voltage wave would cut the horizontal axis at a steep angle, for all timing adjustments.

The detecting chamber was next moved to the outside edge of the water tank, where the temperature should have been about 20°, or the absorption coefficient in boron about four times that at room temperature. Fig. 4(e) shows that the temperature is somewhat lower than with the same adjustment near the wall of the room. The half thicknesses for absorption in boron as shown in Fig. 4 indicate temperatures greater than the average value for the beam, particularly for the steepest curves. This is due to the fact that these lower curves are drawn through only two experimentally determined points, 0 and 0.1″ of Pyrex. Since the spread in neutron energies must be about ±30 percent, the actual curves are due to the superposition of several exponentials. Therefore, the curves must be convex toward the origin, and start down with a greater slope than is indicated by the chord actually drawn.

Sixty-cycle modulation was next tried, and it proved to be the most satisfactory arrangement. The chamber was returned to the wall, and the timing was set as shown in Fig. 5(f). The long interval between the beam pulse and the amplifier sensitive time completely eliminates the possibility of counting room-temperature neu-

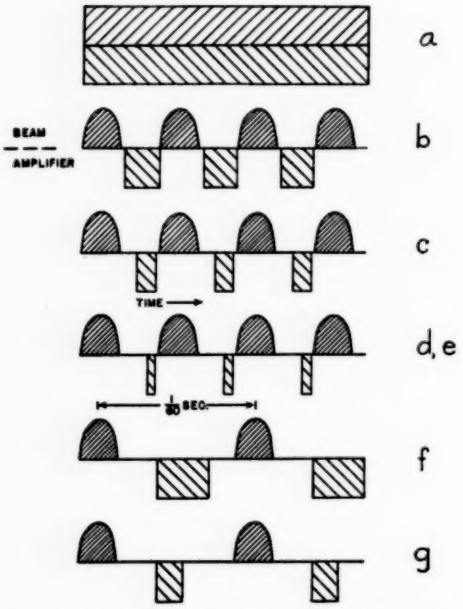

FIG. 5. Phase relations in modulation circuits.

trons. The absorption curve with this timing is shown in Fig. 4(f). The temperature given by the straight line is about 30°, but it is certain that considerably lower temperature neutrons contributed an important part to the counting rate at zero absorber thickness. The velocity of the neutrons obtained from the time interval and distance is consistent with the velocity deduced from the $1/v$ law. The timing was next changed to that shown in Fig. 4(g). As would be expected, the counting rate fell but little from that recorded with the previous timing. This shows that the number of neutrons in the second half of the amplifier sensitive period was small compared to that in the first half. But the background was cut in half, so the second timing scheme is to be preferred. The counting rate with this latter arrangement was 30 per minute, with a background of 1.2 per minute.

In the hope of obtaining more intensity, a cold piece of paraffin was used to slow the neutrons. The paraffin was reinforced with two concentric helical copper tubes, which helped to keep it from falling apart when cooled, and also speeded the attainment of thermal equilibrium at liquid-air temperature. Since no large soft glass Dewar flasks were available, the paraffin was placed in a large Pyrex Dewar filled with liquid air, for several hours. It was then substituted for the usual paraffin block, and the resulting counting rate was quickly measured. The initial rate was 75 per minute, but it fell slowly back to 30 per minute as the paraffin warmed up. So it does not seem at the present time to be worth while bothering with cooled sources. It is much easier to increase the intensity by improving the detecting chamber.

The chamber under construction at the present time will be operated at 4 atmospheres pressure of BF_3. This increase will give a factor of from 4–8 times in intensity, depending on the energy of the neutrons. The chamber will be of cylindrical form, with a diameter of about 10 cm, so the intensity will be increased several-fold due to the greater solid angle available. The new chamber should therefore allow data to be collected at counting rates in excess of 1000 per minute, for temperatures of the order of 30°K.

POSSIBILITIES AND LIMITATIONS OF THE METHOD

Up to the present time, the only measurements made with the apparatus have been on the absorption and scattering of ultraslow neutrons in boron, paraffin and iron. It seemed more important at first to explore the characteristics of the method, and to learn something of its reliability, etc. Considerable trouble was at first experienced in obtaining reproducible data. Some of the trouble was traced to faulty design of the modulation circuit. But with the arrangement shown in Fig. 2, it is possible to turn on in the morning and take reproducible data all day without touching any controls. The linearity of the counting circuits has been checked by taking absorption curves in iron at various beam intensities. The absorption coefficient is independent of the intensity. Counting intervals are usually 1 microampere hour, as measured on an integrating beam meter connected to the beryllium target. With 60-cycle modulation, the average deuteron currents are 5–10 microamperes, so the counting periods are about 8 minutes long. The steady currents obtainable with d.c. operation are 50–60 microamperes at 8 Mv. The number of counts per μ an hr. as measured on the integrator is not quite independent of the deuteron current, which is probably due to a slight nonlinearity of the

integrator. But the beam is so steady under these conditions of light load that the integrator gives a reliable indication of the total number of slow neutrons produced in a given time interval.

Sixty-cycle modulation seems to be much more satisfactory than 120, so it will probably be used exclusively in the future. It is very convenient that the laboratory power is supplied at this frequency, although 120 cycles would quadruple the available solid angle for any temperature, and allow the method to be used in smaller rooms. The reason for preferring 60-cycle to 120 in actual practice is, of course, that the former is obtained by half-wave rectification, allowing more freedom in timing. It is planned for the future to mount the paraffin block in which the counter rests, on a truck, so that temperature changes can be made without the realigning now necessary. The truck will run on rails, which will pass several meters beyond the wall, on a platform to be constructed outside the building.

There does not seem to be any convenient way to take advantage of the larger solid angle offered by faster modulation. With the large pressure Van de Graaff machines which are now under construction, it would be quite convenient to modulate the source at about 200 cycles per sec. If one tried to use much higher frequencies, he would experience trouble in sharpening the amplifier pulses. Even if this factor did not enter, the mean life of slow neutrons in paraffin would soon become comparable with the time of transit, and the homogeneity of the beam would suffer on that account. With the distances used in the present work at 60-cycle modulation, considerable intensity is lost by neutron absorption in nitrogen. It will probably be worth while to place evacuated tubes between the source and detector, in the future. Since the tubes are already in place, it will merely be necessary to close the ends and connect them to a vacuum pump.

One source of trouble which was anticipated, but which fortunately did not materialize, was the possible formation of Li^8 in the reaction $B^{11}+n\rightarrow Li^8+He^4$. Li^8 has a half-life of 0.8 sec. after which it disintegrates into an electron and two alpha-particles. If this reaction were more probable, fast neutrons could be recorded by alpha-particles expelled during the sensitive time of the amplifier, from Li^8 nuclei formed while the beam was on several cycles earlier. This reaction, if observable, may set the lower limit of attainable neutron temperatures.

One would, of course, hope that it would be possible to investigate the resonance neutrons with a velocity selector such as this. With the modulation limits discussed above, the distance from source to detector becomes prohibitively large, and therefore the intensities are too low. If the pulse breadth could be narrowed sufficiently, the source-modulated Van de Graaff machine could be used for this purpose. The trouble due to the mean life of thermal neutrons in paraffin is nonexistent in this case, as resonance neutrons are formed from fast ones in times of the order of 10^{-7} second, and are converted into thermal neutrons in about the same length of time.

The apparatus is then seen to be most useful in the range from 300° down. The lower limit is unpredictable, and depends largely on the neutron intensities available in future cyclotrons. It will be surprising if the new pressure chamber does not permit measurements to be made as low as 10°K. Theoretically there is no lower limit; single scattering can give rise to neutrons with zero velocity.

The author is indebted to Dr. S. N. Van Voorhis and Professor E. O. Lawrence for valuable discussions of the problems involved in this report. He also wishes to thank Professor O. S. Duffendack for assistance in taking data. The work has been aided by grants to the laboratory from the Chemical Foundation and the Research Corporation. The assistance of the W.P.A. is also gratefully acknowledged.

"Transverse" Acoustic Waves in Rigid Tubes

HENRY E. HARTIG AND CARL E. SWANSON
Institute of Technology, University of Minnesota, Minneapolis, Minnesota

(Received September 2, 1938)

Recently considerable work has been done, both theoretical and experimental on the transmission of electromagnetic waves through dielectric wave guides and hollow metal tubes. An analogous phenomenon is the propagation of transverse acoustic waves in gaseous media confined by rigid cylindrical tubes. Apparatus and methods are described for the production of some of the lower ordered acoustic waves and measurements are made with a tube of circular section filled with air. Measured values of wave-length, threshold frequency, and pressure distribution for some of the possible harmonic wave types are found to be in excellent agreement with theoretical values. Absorption measurements by the standing wave method in which transverse waves are used are suggested.

THE problem of transverse aerial vibrations within a rigid cylindrical tube received attention many years before the analogous problem of electromagnetic oscillations in hollow metal tubes and dielectric columns. The latter phenomenon which has recently been the subject of great interest was investigated mathematically by Lord Rayleigh[1] in 1897. The reality of the predicted waves was experimentally verified by Zahn[2] in 1916. Improvements in the means for producing ultra-high frequency radio waves and very likely the possibility of practical use for the tubular radio wave guides has renewed interest in the phenomenon. For a bibliography of the previous principal work in the field an article by Schelkunoff[3] may be consulted.

It is only natural that the revived interest in the electromagnetic problem should call attention to the older and similar acoustic problem. Indeed it was a consideration of the remarkable properties of the dielectric wave guides which led the writers to investigate what seemed like an analogous phenomenon manifesting itself as a nuisance in an experimental tube intended for the measurement of acoustic impedance by the standing plane wave method. It was observed that, above a certain impressed frequency, difficulty in obtaining uniformly spaced nodes and antinodes in the tube was experienced. This was recognized by its behavior as an effect chargeable to transverse particle velocity. This same difficulty had also been reported by Davis and Evans,[4] who using a pipe having a diameter of 15 cm found undesirable "radial vibrations" to set in above 1290 cycles per second. So far as the writers are aware, however, no systematic experimental investigation of the transmission of transverse acoustic waves had been made. Recent workers in the field of electromagnetic tubular guides have invoked acoustic analogies to aid in making familiar some of the properties of the radio waves, but apparently went no further in their thinking than plane acoustic waves propagated through tubes or radiated from horns. An exception, however, must be noted in the remarks by Leon Brillouin[5] at the close of a very recent paper entitled "The Theoretical Study of Dielectric Cables" in which a more far reaching comparison is drawn.

Lord Rayleigh,[6] probably before 1875, made a systematic theoretical study of the normal modes of aerial vibration within a cylindrical tube, and credits Duhamel[7] with a still earlier investigation limited, however, to the symmetrical vibrations within a cylindrical boundary. Accordingly the theoretical beginnings of the phenomenon before us date back nearly 90 years.

Experimental methods, however, lagged far to the rear. Thus Rayleigh is constrained to quote the results[8] of very limited observations, but careful and excellent ones, on the period of waves produced on water in cylindrical vessels in sup-

[1] Lord Rayleigh, Phil. Mag. **43**, 125–132 (1897).
[2] H. Zahn, Ann. d. Physik **49**, 907–933 (1916).
[3] Schelkunoff, Proc. I. R. E. **25**, 1491 (1937).
[4] A. H. Davis and E. J. Evans, Proc. Roy. Soc. **127**, 89 (1930).
[5] Electrical Communication, April 1938, No. 4, Vol. 16.
[6] Lord Rayleigh, *Theory of Sound*, Vol. II, p. 297.
[7] Duhamel, Liouville J. Math. **14**, 69 (1849).
[8] F. Guthrie, Phil. Mag. **50**, 290–302 (1875).

port of the general correctness of his computation of normal vibration periods. Such has been the advance, however, in acoustic measurement and the production of sustained and controlled waves that what was not possible in 1875 may now be done readily.

It is perhaps not necessary to emphasize that a knowledge of the behavior of transverse acoustic waves is of advantage in the illumination of ideas concerning the analogous electromagnetic phenomenon, particularly in questions relating to the stability of certain types of waves when the assumed theoretical conditions are departed from, as for example the actual ellipticity of a tube supposed circular, the effect of bends, etc. In the acoustic case means are available for measuring continuously the relative phase conditions in various parts of the wave and consequently wave-type identifications can be made more readily than in the case of ultra-high frequency radio waves where as yet this cannot be done. Moreover, the acoustic experimental technique is relatively simple and lends itself to intuitive guidance and to the experimental solution of problems not readily obtainable by mathematical methods.

Transverse Acoustic Waves, Theoretical

Suppose a smooth tube has an inner radius R and extends indefinitely in the z direction. It will be assumed that there is no energy dissipation in the tube. Then in cylindrical coordinates the wave equation for excess pressure is

$$\frac{1}{r}\frac{\partial}{\partial r}\left(r\frac{\partial P}{\partial r}\right)+\frac{1}{r^2}\frac{\partial^2 P}{\partial \theta^2}+\frac{\partial^2 P}{\partial z^2}=\frac{1}{c^2}\frac{\partial^2 P}{\partial t^2}. \qquad (1)$$

Let us first determine the frequencies of the internal normal transverse oscillations, which are defined as those which do not depend on z. With this restriction the solution of Eq. (1) is

Table I. *Lower roots of $J_n'(kr)=0$; m is the number of internal circular nodes.*

	$n=0$	$n=1$	$n=2$	$n=3$
$m=0$	3.832	1.841	3.054	4.201
$m=1$	7.015	5.332	6.705	8.015
$m=2$	10.174	8.536	9.965	11.344
$m=3$	13.324	11.706		

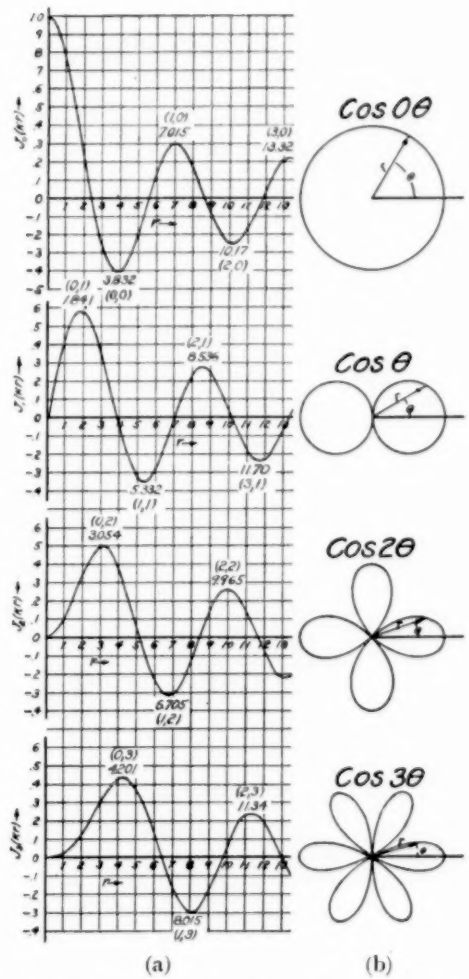

Fig. 1. Rectangular graphs of Bessell's J_n functions each associated with the polar graph of the appropriate circular function, from which the pressure variation at a tube section may be visualized.

the sum of terms of the type

$$J_n(kr)[A\cos n\theta+B\sin n\theta]\sin kct,$$

where $J_n(kr)$ is the Bessell's function of the first kind and n is zero or a positive integer. Since the particle velocity at $r=R$ is zero, $\partial P/\partial r=0$ and accordingly[9] $J_n'(kr)=0$. The lower roots of this equation are shown in Table I, taken from the *Theory of Sound*,[6] p. 298, and the positions of the roots are indicated on the graphs of the appropriate functions in Fig. 1(a). In Fig. 1(b) are shown, associated with the proper $J_n(kr)$ function, the polar graphs of $\cos n\theta$.

[9] This is the same boundary condition that holds in the case of electromagnetic waves of the so-called H type.

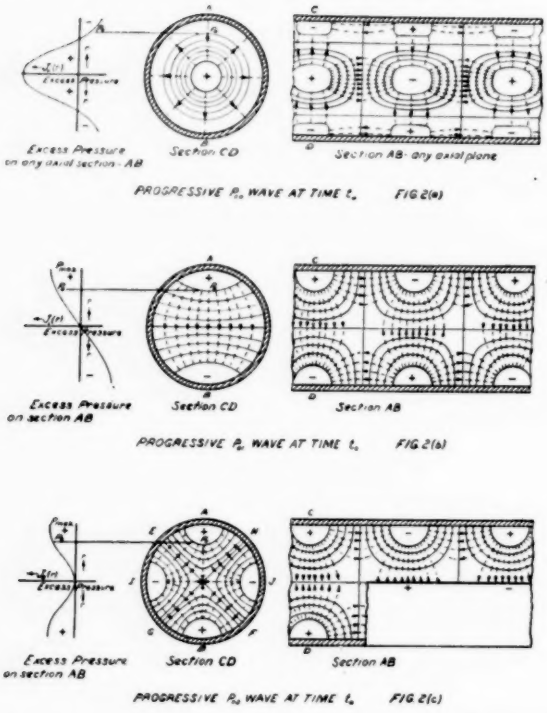
Excess Pressure on any axial section: AB
Section CD
Section AB: any axial plane
PROGRESSIVE P_{11} WAVE AT TIME t_0 FIG 2(a)
Excess Pressure on section AB
Section CD
Section AB
PROGRESSIVE P_{01} WAVE AT TIME t_0 FIG 2(b)
Excess Pressure on section AB
Section CD
Section AB
PROGRESSIVE P_{02} WAVE AT TIME t_0 FIG 2(c)

FIG. 2. Approximate configuration of stream lines and surfaces of equal excess pressure. Dotted lines represent stream lines with arrows to indicate the direction of instantaneous particle velocity. Solid lines represent sectional traces of equal pressure surfaces.

The tabular numbers will be denoted by $(kR)_{mn}$. If $(kR)_{mn}/R$ is denoted by k_{mn} and f_{mn} is defined as the frequency of normal oscillation of the type mn, and c is the velocity of plane sound transmission for the medium within the tube, then $k_{mn}=2\pi f_{mn}/c$. For any particular tube radius and sound velocity,

$$f_{mn}=(kR)_{mn}c/2\pi R. \tag{2}$$

If one turns to Eq. (1) and removes the restriction that the excess pressure is independent of z, the general solution may be expressed as the real part of a series of terms of the type

$$J_n(k_{mn}r)[A\cos n\theta+B\sin n\theta]\times\exp[i(\omega t\pm k\psi_{mn}z)], \tag{3}$$

where A and B are arbitrary constants having in general different values for each value of m and n, $\psi_{mn}=[1-(f_{mn}/f)^2]^{\frac{1}{2}}$, $\omega=2\pi f$, and $k=\omega/c=2\pi/\lambda$. Now suppose that by means of external harmonic forces a pressure distribution is maintained in the steady state on the tube section at $z=0$ corresponding to that of the mn normal mode of transverse oscillations, then for a proper choice of signs it is seen that (1) when the frequency of the impressed force is constant and less than f_{mn}, the phase angle of the propagated acoustic wave is independent of z and its amplitude tends toward zero as $z\to\infty$, but (2) if the impressed frequency is greater than f_{mn}, then the amplitude of the wave is propagated with undiminished magnitude as $z\to\infty$ while the phase angle decreases linearly. Consequently only in the latter case are progressive waves possible.

An appropriate particular solution of Eq. (1) for the investigation of progressive waves propagated in the positive z direction is,

$$P_{mn}=J_n(k_{mn}r)[A\cos n\theta\sin(\omega t-2\pi z\psi_{mn}/\lambda)+B\sin n\theta\cos(\omega t-2\pi z\psi_{mn}/\lambda)]. \tag{4}$$

The wave-length of the mn wave relative to that of the plane wave is

$$\lambda_{mn}/\lambda=\psi_{mn},\quad f>f_{mn}. \tag{5}$$

In Eq. (4) when $n=0$ a particularly simple wave type results in which circular symmetry exists and the particle velocity is in axial planes.

$$P_{m0}=J_0(k_{m0}r)A\sin(\omega t-2\pi z\psi_{m0}/\lambda). \tag{6}$$

The resulting pressure distribution and stream lines are shown in Fig. 2(a) for the case $m=0$.

It will be observed Fig. 1(a) that $J_0(kr)$ satisfies the boundary condition $J_0'(kr)=0$ for one additional value not shown in Table I, namely $kr=0$, which however does not imply transverse oscillations but rather represents the ordinary plane wave. If we denote the corresponding critical frequency by $f_{-1,0}$ it will be seen that Eq. (2) predicts the correct result namely that plane waves of all frequencies may be transmitted through tubes.

For every admissible value of n different from zero two independent components of excess pressure are predicted by Eq. (4). If for the sake of concreteness $m=0$, $n=1$,

$$P_{01}=J_1(k_{01}r)[A\cos\theta\sin(\omega t-2\pi z\psi_{01}/\lambda)+B\sin\theta\cos(\omega t-2\pi z\psi_{01}/\lambda)], \tag{7}$$

where A and B are arbitrary. The pressure distribution and stream lines for the case $B=0$, and appropriate choices of z and t, are shown in Fig. 2(b). The wave may be said to have a kind of linear polarization since each particle

moves in a line. It possesses a diametral nodal plane section AB on which the normal particle velocity is zero, and an antinodal plane at right angles on which the excess pressure is zero. These nodal planes are not present in the general (0,1) wave, for the second component is in space and time phase quadrature and the resultant wave is in general elliptically polarized and all particles except those on the tube axis and the circumference vibrate in elliptical paths. The wave can be line polarized by introducing a rigid diametral plane in the tube coinciding in position with the nodal plane of one of the components which accordingly is unaffected, the other component suffering reflection.

Obviously similar relations hold for the higher n-ordered transverse waves, one term of Eq. (4) producing a wave linearly polarized, let us say, by sectors, the second component being space shifted $\pi/2n$ radians and in time quadrature combines to give a resultant elliptical polarization. At this point it may be noted that in the experimental investigation of transverse waves it is of great advantage to be able to measure phase relationships. For example if $A=B$ in Eq. (4), then the pressure amplitude and particle velocity amplitude remain constant as θ is varied. Consequently there is nothing to distinguish a wave of one n-order from another except phase and radial variations.

In Fig. 2(c) are shown the lines of equal pressure and of flow for one component of the (0, 2) wave. Obviously the complete delineation of one of the higher ordered (mn) waves is a matter of considerable labor and difficulty.

Apparatus

The experimental tube, Fig. 3, was constructed of thin galvanized iron, the circularity of the cross section being maintained by closely fitted external wooden rings. The tube was inclosed in a compartment filled with sand to prevent the elastic response of the tube walls to acoustic excitation. The tube was mounted on a pair of heavy wooden rails which extended so as to form a guide for a sliding carriage, the latter carrying a heavy, shielded brass chamber within which was mounted in felt a telephone watch-case receiver which served as a sound pressure microphone. Through the end of the brass chamber extended a sound probe consisting of a nest of brass tubes, the outer one $\frac{1}{2}$ inch in diameter, the inner one, which served as the actual sound probe, had an opening $\frac{3}{16}$ inch in diameter. Spiral servings of wool yarn were applied between the tubes so as to reduce the lateral sound transmission. The outer tube was fitted loosely so that it could be turned with respect to the inner tubes and was provided with a circular dial marked in degrees at one end, and with a nozzle into which off-set probe tubes of different off-set radii could be inserted. The nozzle end was supported by a collar fitted with slideable wire loops adjusted to the inside of the main tube. It was possible by these means to explore the excess pressure continuously along a cylinder having the radius of the particular off-set probe tube selected and coaxial with the galvanized main tube. To measure pressures continuously along a diameter a special horizontal support was cemented to the inside of the galvanized tube, and a straight probe drawn across the top of the support to definite positions by a music wire cable.

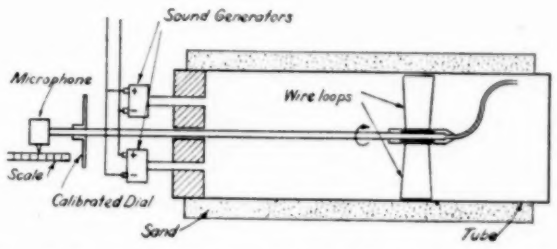

Fig. 3. Sectional diagram of experimental acoustic tube arranged to generate one component of the (0,1) wave.

It was of no consequence that the sound probe and microphone varied in sensitivity with frequency as comparisons were made only with pressures at the same frequency. A check of the apparatus made by stopping the end of the sound probe verified that the voltages developed by the

Table II. *Frequencies of (m, n) modes of vibration for a rigid tube of circular section filled with air, c = 35,000 cm/sec, diameter 14.92 cm.*

	$n=0$	$n=1$	$n=2$	$n=3$
$m=0$	2,860	1,374	2,279	3,135
$m=1$	5,235	3,979	5,004	5,981
$m=2$	7,575	6,370	7,437	8,466
$m=3$	9,943	8,736		

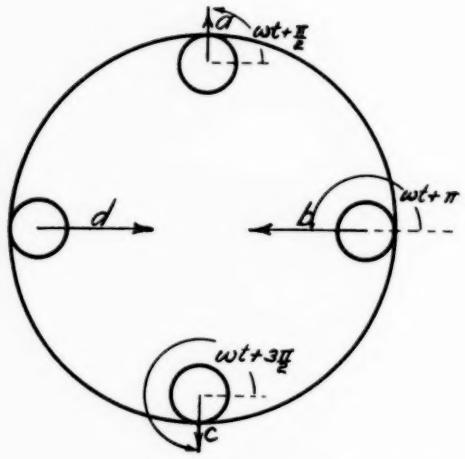

FIG. 4. Section of tube showing location and time phase relation of loudspeakers for producing the (0,1) wave.

microphone were due solely to sound entering at the probe. The output of the microphone was amplified by a vacuum-tube amplifier having 90 decibels gain and then filtered with an adjustable inductance-capacity circuit to eliminate extraneous harmonics. A 3-inch cathode-ray oscilloscope was used for measuring the relative pressure amplitudes, it having been previously established that vertical oscilloscope deflection varied linearly with excess pressure at the end of the sound probe. The horizontal deflecting plates of the oscilloscope were connected through a phase shifting device to the same vacuum-tube oscillator which supplied power to the loudspeakers producing the sound pressures in the main tube. Thus relative phase and amplitude measurements could be made simultaneously. With one exception to be noted later, Western Electric 555 type loudspeaker units were employed as sound generators and the power source was a battery operated 6010B Western Electric oscillator having an excellent sinusoidal wave form, careful frequency calibration, and a very low frequency drift.

PROCEDURE AND EXPERIMENTAL RESULTS

In the investigation of transverse waves in a given tube filled with a particular medium, it is convenient to have a table of the lower frequencies below which a given type of vibration is not expected. Table II presents this information computed by Eq. (2) for the experimental tube with a diameter of 14.92 cm. Air is the medium and the velocity of sound propagation is taken to be 35,000 cm per second. It will be observed that when $m=0$, $n=1$ the lowest critical frequency for transverse waves is predicted. Consequently the (0,1) wave type is particularly easy to elicit without at the same time producing disturbing transverse waves of other types. It is necessary only to avoid the production of plane waves in the tube in the approximate frequency interval 1370–2270 in order to have substantially a pure wave form of the (0,1) type. While, strictly speaking, a pressure distribution on the plane $z=0$ as given by Eq. (7) is theoretically indicated, a sufficiently good approximation is obtained by providing relatively concentrated harmonically varying forces as shown in Fig. 4. This may be done by means of loudspeakers arranged as shown in Fig. 3. Any effect due to a departure from the required pressure distribution is rapidly damped out as is the case for plane waves.

The pressures indicated with arbitrary magnitudes and suitable time phase by the arrows in Fig. 4 obviously are such as to inhibit the generation of plane waves. For experimental simplicity a single pair of balanced pressures (*bd*) was employed. The balancing was performed at a frequency just under the critical (0,1) frequency by adjusting the input voltage of one loudspeaker and it was verified that sound pressures in the tube at points distant, say 150 centimeters, from the loudspeakers could be reduced to negligible amplitudes. Now as the frequency was increased and passed $f=1360$,

TABLE III. *Calculated and measured values of wave-length in cm for the (0,1) wave.*

FREQUENCY	WAVE-LENGTH, (0,1) TYPE CALCULATED	MEASURED	DIFFERENCE	PERCENT ERROR
1400	130.0	130.8	0.8	0.6
1420	97.51	95.5	−2.0	−2.1
1440	81.11	77.0	−4.1	−5.0
1460	70.91	69.3	−1.7	−2.4
1500	58.13	58.00	−0.13	−0.2
1600	42.68	42.64	−0.04	−0.1
1700	34.96	35.07	0.11	0.3
1800	30.10	29.95	−0.15	−0.5
1900	26.67	26.76	0.09	0.3
2000	24.08	23.93	−0.15	−0.6
2200	20.37	20.33	−0.04	−0.2
2400	17.79	17.82	0.03	0.2
3000	13.12	13.14	0.02	0.15

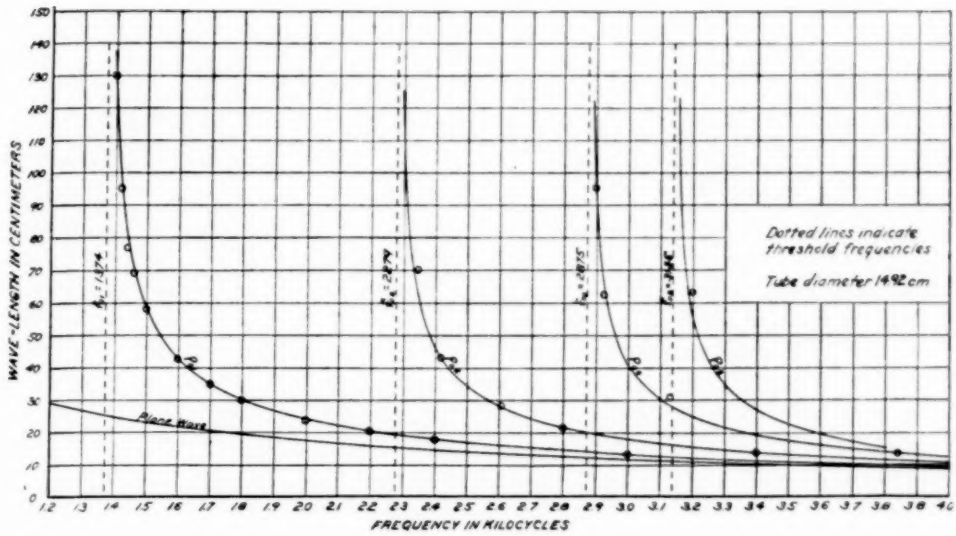

FIG. 5. Variation of wave-length as a function of frequency, for the plane wave and for the (0,0), (0,1), (0,2) and (0,3) type of waves. Curves are theoretical, points are measured values.

the measured excess pressures increased with extreme rapidity and reached such large amplitudes that any residual plane wave component was entirely negligible. Indeed even with a single speaker the (0,1) wave predominated. In spite of the sharpness of the onset of the transverse wave, however, the critical frequency $f_{0,1}$ could be located more accurately through the measurement of the wave-lengths of standing waves. These were produced through reflection by stopping one end of the pipe with a plane-faced cast-iron plug. The longitudinal location of successive minima could then be made for the higher frequencies with considerable accuracy as shown by the degree of equality between successive half-wave-length steps. Data obtained in this way are shown in Table III. It is clear that although the measurements above 2200 cycles were subject to interference from waves of the (0,0) and (0,2) type, the mode of excitation employed was sufficiently unfavorable to substantially suppress the latter. The computed wave-lengths in Table III were obtained by the use of Eqs. (2) and (5) with $R=7.46$ cm and $c=35{,}000$ the latter determined from plane wave measurements in the tube made under the same temperature conditions. The value of $f_{0,1}$ thus obtained was 1374 cycles per second. These wave-length data are also shown in Fig. 5 as the centers of the small circles. The solid lines are the graph of Eq. (5), for the wave type under consideration and others, in which the appropriate computed values of $f_{m,n}$ are inserted.

Measurements were also made of the variation of excess pressure in a progressive wave consisting of one (0,1) component, measured at a tube cross section and along the circumference of a circle with center at the tube axis. At one end of the tube a disk of $1\frac{1}{4}$ inch Celotex covered with loose felt provided an almost perfect absorber of the (0,1) wave at a frequency of 1500 cycles per second. The data obtained by use of a probe having a radius of 6.5 cm are shown by the small circles, Fig. 6. The two solid line circles shown within the tube section are the corresponding theoretical curves. It was observed that the pressures recorded as circles in Fig. 6 were in identical time phase, and that points (not shown) corresponding to the lower circle were in phase opposition. It may be remarked, however, that when an attempt was made to produce one component only of the (0,1) wave the quadrature component was also sometimes faintly excited. On investigation it was found that a very slight ellipticity of the tube, the axis being oblique to the axis drawn through the two loudspeaker inlets, Fig. 3, was sufficient to produce this result. By means of simultaneous observations of phase and amplitude the quadrature component could be definitely identified. Measurement of

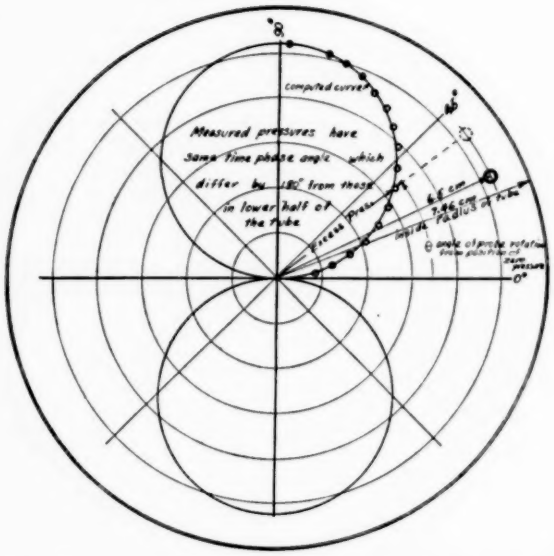

FIG. 6. Excess pressure variation for the (0,1) type of progressive wave measured on the circumference of a 6.5 cm circle coaxial with the tube axis. The curve is the polar graph of sin θ, the points are measured values of relative excess pressure. Frequency 1500 cycles per second.

the maximum amplitudes of the two components and substitution in Eq. (7) yielded values for the resultant which were in excellent agreement with measured resultant values for corresponding values of θ.

The pressure measurements made on the (0,1) wave component were completed by a set in which a straight probe was carried along a tube diameter by a mechanism previously described. The diameter selected was one which passed through the points of maximum peripheral pressure. The frequency was 1500 cycles and the wave progressive. The experimental data obtained are shown by the circles in Fig. 7, the solid line showing the theoretical variation as a function of r, Eq. (7), in which the numerical average of the extreme measured pressure amplitudes was taken as the maximum amplitude of the $J_1(k_{01}r)$ function. In view of the difficulty in directing the motion of the probe accurately along a diameter and through the tube axis with the inflexible means used, the results obtained are quite satisfactory. The departure from the theoretical curve of the actual pressures near the extremities of the diameter may perhaps be attributed to the influence of the probe on the pressure at these points.

To produce other types of transverse waves, special excitation arrangements were, of course, necessary and interference from transverse waves having a lower f_{mn} frequency was expected. In setting up longitudinal standing waves, however, advantage may be taken of the possibility of increasing the amplitude of the desired wave type through tuning by adjusting the length of the air column. By this means it was found possible to excite the (0,0), (0,2) and (0,3) modes with sufficient freedom from interference to obtain the wave-length data shown in Fig. 5, the relative abundance of the points shown near each theoretical curve being a rough measure of the ease of obtaining them. For the (0,2) wave, two speakers with inlets at a and b, Fig. 4, and driven in time phase opposition proved to be sufficiently close to the theoretical pressure distribution to produce a strong (0,2) wave, not however without an admixture of the (0,1) wave type. The latter was satisfactorily minimized by longitudinal tuning. The wave-length data obtained are shown in Table IV as well as graphically in Fig. 5.

On investigating excess pressure in circles coaxial with the tube, it was found that the second (0,2) quadrature component was also present, and as a result the pressure varied with θ approximately as cos 2θ as shown in Fig. 1(b)

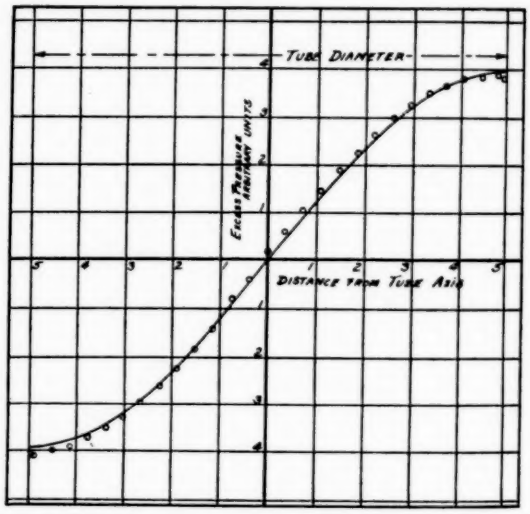

FIG. 7. Excess pressure variation along a diameter of maximum pressure for the (0,1) type of progressive wave, frequency 1500 cycles per second. The curve represents the graph of the Bessell function $J_1(x)$ from $x=0$ to $x=1.84$. Points are measured values of excess pressure.

except that the pressure amplitude at the minimum points was different from zero, leading and lagging respectively in time phase the pressures at points just ahead and behind by one quadrant.

To elicit the (0,3) wave type it would seem from the cos 3θ graph, Fig. 1(b), that at least six loudspeakers equally spaced around the periphery of the tube and alternately driven in time phase opposition would be required. However it was found that a single pair arranged for the generation of the (0,1) wave produced a strong (0,3) wave when the frequency was above the computed threshold value namely 3135 cycles per second. Furthermore, by selecting a frequency and a tube length most favorable for the (0,3) wave and least favorable for the (0,1) wave type, a relatively pure wave form of the (0,3) type was produced. The wave-length at a single frequency was measured and was in satisfactory agreement with the theoretical curve, Fig. 5. It was also verified that the (0,3) wave was still present at a frequency of 3150 cycles, and was definitely absent at 3100 cycles, thus roughly defining the threshold frequency.

When the end of the tube, remote from the generating end, Fig. 3, was left open, radiation to the outside atmosphere naturally occurred, and the general nature of the wave, whether it had one or more diametral antinodes, could be determined directly by listening with one ear covered. The relative amount of the radiation was large and on investigating the standing wave pattern within the tube it was concluded that under some conditions the open end provided a fairly good approximation to an ideal absorber. As in the case of electromagnetic transverse wave guides the analogous conception of an average acoustic impedance of the tube to transverse waves may be introduced.

TABLE IV. *Calculated and measured values of wave-length in cm for the (0,2) wave.*

FREQUENCY	WAVE-LENGTH, (0,2) TYPE CALCULATED	MEASURED	DIFFERENCE	PERCENT ERROR
2345	62.5	70.2	7.7	12.0
2420	43.2	43.3	0.1	0.3
2607	27.7	28.3	0.4	1.4
2800	21.5	21.2	−0.3	−1.4
3000	17.95	17.9	−0.05	−0.3
3400	13.87	13.88	0.01	0.1

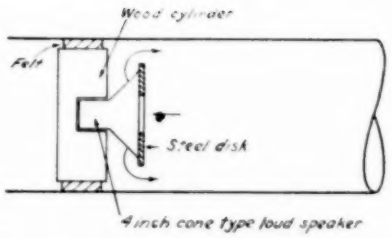

FIG. 8. Sectional diagram showing an arrangement for generating the (0,0) wave.

Discussion of the (0,0) wave type has been deferred until now because this wave is unique and requires a special driving apparatus, (Fig. 8), to produce it. Only waves of the (m,0) type, Fig. 1(b), possess circular symmetry and consequently they alone consist of one component only. Moreover, only waves of this type have excess pressures at the tube axis different from zero. The fact that the pressure for the (0,0) wave is maximum on the tube axis while the contributions of all other waves (except the plane wave) are zero is a circumstance of considerable convenience in making wave-length measurements. Such measurements were made by using the sound generator described and by plugging the loudspeaker holes in the cast iron cylinder, Fig. 3, which thus served as a reflector. It should be observed that in this case the sound probe was included in the portion of the tube in which the measured standing waves were formed, one effect of which is to reduce the effective tube diameter. When this was allowed for, as well as a change in the velocity of the plane sound wave transmission due to temperature conditions prevailing, the normal frequency of the (0,0) transverse mode was computed to be 2875 cycles per second, a small departure from the value in Table II. The experimental wave-length data obtained are shown in Fig. 5 and are in satisfactory agreement with the corresponding theoretical values. The principal irregularity was due to the presence of plane waves which were minimized by longitudinal resonance tuning. On investigating the wave at other points than on the tube axis, however, it was found that a strong (0,1) wave was also present. Indeed the latter component was very difficult to eliminate, such devices as longitudinal diametral barriers being relatively ineffective, probably due to

slight residual dissymmetries in the generator, barrier and tube.

Attenuation

The effects of energy dissipation in the tube were observed only in the standing wave-length measurements. Successive minima caused by the interference of the incident and the reflected wave steadily became larger with the distance from the reflecting surface. Measurements made on the (0,1) wave type indicated that the effect of attenuation can be satisfactorily allowed for by means of an exponential attenuation factor. While, of course, attenuation is a fact of major importance in the practical consideration of the long distance transmission of electromagnetic waves through hollow tubes, the principal features of the theoretical dissipationless transverse wave phenomena in short tubes appear to be very similar to those in which small energy losses by dissipation are present.

Discussion

Obviously other than circular cylindrical sections may be used for determining and transmitting transverse acoustic waves. Indeed various cross sections have already been studied[5] for the analogous electromagnetic waves. The normal modes of oscillation for rectangular sections were examined theoretically by Lord Rayleigh[6] many years ago. Also it may be remarked that many features of aerial vibrations within cylinders are similar to the vibration characteristic of plates, which have been extensively investigated experimentally as well as theoretically.

One practical use for acoustic transverse wave transmission has already been suggested by Brillouin,[5] who pointed out that with suitable terminal devices for exciting and detecting a single transverse wave type, a high-pass filter could be constructed. Such a filter could be made to have an extremely sharp cut-off frequency and the amount of attenuation provided in the stop-band could be increased to any desired amount simply by increasing the length of the tube. Acoustic filters of the Stewart[10] type, while they may be designed as high-pass filters are in reality intrinsically band-pass filters so that transmission is not uniform in the so-called pass band.

In determining acoustic absorption coefficients of various commercial materials, the reverberation chamber method is largely used although the results obtained thereby by different laboratories are discordant. The standing plane wave method, on the other hand, gives reproducible coefficients but they are in general lower than those obtained by the reverberation chamber method. It is objected that wave incidence is entirely normal and consequently the conditions of the measurement do not agree with the actual conditions of use. It is to be expected, and some evidence is at hand, that if standing transverse waves are used, higher absorption coefficients will be obtained than for the corresponding plane wave measurement. This matter is now being examined.

In conclusion a caution may be expressed against the use in experimental apparatus of large ducts and pipes intended for plane wave measurements, but which in reality are excellently adapted to the transmission of transverse waves, thereby largely vitiating the results.

---

[10] W. P. Mason, Bell Sys. Tech. J. **6**, 258 (1927).

Calculation of Coulomb Wave Functions for High Energies

L. E. Hoisington and G. Breit
University of Wisconsin, Madison, Wisconsin

(Received August 17, 1938)

For high energies and moderate radii Coulomb functions are conveniently calculated by evaluating certain integrals numerically.

THE power-series method[1] of calculating Coulomb wave functions is cumbersome if the radius and energy are large on account of slow convergence of the series. A way of eliminating some of the labor has been given by Wheeler,[2] who developed the phase-amplitude method using a transformation recommended for numerical work by Milne.[3] The phase-amplitude method is especially suitable for the treatment of scattering of alpha-particles by helium. Another simple method suitable for the treatment of the scattering of protons by protons is described in this note. The Coulomb functions are expressed in terms of definite integrals which can be conveniently evaluated by numerical integration. The arrangement of the calculation is such as to have $\sin\rho$, $\cos\rho$ as the first order approximations for $L=0$. Here ρ is $2\pi r/\Lambda$, Λ is the wave-length at a large distance, Lh is the angular momentum. The regular and irregular solutions are linear combinations of $\sin\rho$ and $\cos\rho$ multiplied by slowly varying factors expressible by means of definite integrals. For high energies one of the factors is small while the other is nearly unity. The difference between the actual function and the first approximation can be estimated sufficiently accurately by using a relatively rough numerical evaluation of the integrals.

The differential equation to be solved is

$$\frac{d^2Y_L}{d\rho^2}+\left(1-\frac{2\eta}{\rho}-\frac{L(L+1)}{\rho^2}\right)Y_L=0.$$

Here η is the collision parameter $ZZ'e^2/\hbar v$ where Z, Z' are the atomic numbers of the colliding nuclei and v is the relative velocity. The equation is solved by[4]

$$Y_L=F_L+iG_L=\frac{ie^{-i\rho}}{(2L+1)!C_L\rho^L}\int_0^\infty t^{-i\eta+L}\times(t+2i\rho)^{i\eta+L}e^{-t}dt. \quad (1)$$

Here F_L, G_L are respectively the regular and irregular functions having asymptotic forms for large ρ given in reference 1. In order that (1) be a solution of the differential equation it is essential that

$$e^{-t}t^{L-i\eta+1}(t+2i\rho)^{L+i\eta-1}$$

be zero for $t=0$. This is true for all real η. Negative energies correspond to imaginary η. For these Y_L is not a solution. Negative energies of relative motion are not needed, however, in the discussion of collision problems. The number C_L occurring in Eq. (1) is independent of ρ and is given by

$$C_L=[L^2+\eta^2]^{\frac{1}{2}}[(L-1)^2+\eta^2]^{\frac{1}{2}}\cdots[1+\eta^2]^{\frac{1}{2}}\times(2\pi\eta)^{\frac{1}{2}}(e^{2\pi\eta}-1)^{-\frac{1}{2}}2^L/(2L+1).$$

For $L=0$ one obtains from Eq. (1)

$$\begin{aligned}F_0&=(I_0\sin\rho+II_0\cos\rho)/C_0,\\ G_0&=(I_0\cos\rho-II_0\sin\rho)/C_0,\end{aligned} \quad (2)$$

where

$$I_0=\int_0^\infty e^{-t-\alpha}\cos\beta\,dt;\quad II_0=-\int_0^\infty e^{-t-\alpha}\sin\beta\,dt, \quad (3)$$

$$\alpha=\eta\tan^{-1}\frac{2\rho}{t},\quad \beta=\eta\ln\left(1+\frac{4\rho^2}{t^2}\right)^{\frac{1}{2}}. \quad (3.1)$$

[1] F. L. Yost, J. A. Wheeler and G. Breit, Phys. Rev. **49**, 174 (1935); the notation of this reference is used in present note; J. Terr. Mag. At. Elec. **40**, 443 (1935). E. R. Wicher, J. Terr. Mag. At. Elec. **41**, 389 (1936).
[2] J. A. Wheeler, Phys. Rev. **52**, 1123 (1937).
[3] W. E. Milne, Phys. Rev. **35**, 864 (1930).
[4] E. T. Whittaker and G. N. Watson, *Modern Analysis* (Third Edition, Cambridge University Press, 1920), p. 340.

TABLE I. *Comparison of calculations by series with calculations by Eqs. (2) and (4).**

PROTON ENERGY	RADIUS	NO. OF INTEGRATION INTERVALS USED		F_0	G_0	A	F_0'
2.6 Mev ($\eta=0.09805$)	$r=0.5e^2/mc^2$ ($\rho=0.24915$)	18 Intervals $t=0.0001$ to $t=6$	By integral	0.2135	1.070	1.096	0.865
			By series	0.2152	1.073	1.094	0.866
			Difference	0.8%	0.3%	0.2%	0.1%
2.6 Mev ($\eta=0.09805$)	$r=3e^2/mc^2$ ($\rho=1.4919$)	18 Intervals $t=0.0001$ to $t=6$	By integral	0.999	0.2505	1.062	0.2196
			By series	1.000	0.2502	1.0623	0.2195
			Difference	0.1%	0.1%	0.0%	0.0%
10.0 Mev ($\eta=0.0500$)	$r=e^2/mc^2$ ($\rho=0.9772$)	12 Intervals $t=0.0001$ to $t=5$	By integral	0.804	0.628	1.022	0.590
			By series	0.805	0.628	1.021	0.590
			Difference	0.1%	0.0%	0.1%	0.0%

* The first column gives the energy of protons impinging on hydrogen atoms at rest. The second column gives the distance r between the protons for which the Coulomb wave function has been computed. The third column describes the intervals used in the evaluation of the definite integrals. The series computations are the more accurate in this case. The accuracy obtained by the integral method using relatively little arithmetical labor is seen to be sufficient for most practical purposes.

The calculation of I is often carried out more conveniently by means of

$$I_0=1+\int_0^\infty e^{-t}(e^{-\alpha}\cos\beta-1)dt. \qquad (3.2)$$

For large energies η is small and, therefore, $I_0\sim1$, $H_0\sim0$. It is convenient to evaluate H_0 and I_0-1 numerically. The same sets of quantities occur in both integrals. Similarly the derivatives $F_0'=dF_0/d\rho$, $G_0'=dG_0/d\rho$ are computed by formulas of the same type

$$\begin{aligned} F_0'&=G_0+(1/C_0)(I_0'\sin\rho+H_0'\cos\rho),\\ G_0'&=-F_0+(1/C_0)(I_0'\cos\rho-H_0'\sin\rho) \end{aligned} \qquad (4)$$

with

$$I_0'=-\int_0^\infty 2\xi\eta(t\cos\beta+2\rho\sin\beta)e^{-t-\alpha}dt, \qquad (4.1)$$

$$H_0'=\int_0^\infty 2\xi\eta(t\sin\beta-2\rho\cos\beta)e^{-t-\alpha}dt, \qquad (4.2)$$

where $$\xi=(t^2+4\rho^2)^{-1}. \qquad (4.3)$$

For comparison with Wheeler's phase-amplitude method one has

$$\begin{aligned} C_0^2AdA/d\rho&=C_0^2(F_0F_0'+G_0G_0')\\ &=I_0I_0'+H_0H_0', \end{aligned} \qquad (5)$$

$$1=F_0'G_0-F_0G_0'=A^2+(I_0H_0'-I_0'H_0)/C_0^2, \qquad (5.1)$$

$$A^2=F_0^2+G_0^2. \qquad (5.2)$$

These formulas are also useful for checking the calculations.

The calculation of G_0, G_0' by the definite integral method is no harder than that of F_0, F_0' in contrast to the series method. The phase-amplitude method has the same advantage.

In Table I calculations by series are compared with those by means of Eqs. (2) and (4). The definite integrals were evaluated relatively crudely. The range of integration was divided into intervals. The integral in an interval $t_1<t<t_2$ was evaluated by calculating all the factors for $t=t_1$ and for $t=t_2$, then multiplying $e^{-t_1}-e^{-t_2}$ by the average value of the other factors.

The Potential Energies of the Alkali Halides: Errata and Extension of the Semi-Empirical Formula

ALBERT MAY
The Catholic University of America, Washington, D. C.

(Received August 17, 1938)

A correction is first made of the author's previous calculations for CsCl, in which an incorrect empirical value was used. By extending the method of Born and Mayer, six constants in the potential energy expression for CsCl are evaluated from available measurements on the lattice and vapor. The results so obtained are then applied to other alkali halides, and permit the determination of the interionic distances in the gas, the lattice energies and heats of sublimation. The agreement with empirical data is satisfactory for the interionic distances, but is otherwise poor.

INTRODUCTION

SEVERAL attempts have been made to approximate the potential energy curves of the alkali halides by the method of Born and Mayer[1] in which constants in the energy expression for the crystal are evaluated from experimental data. Born and Mayer, and Huggins and Mayer[2] evaluated two such constants but their expressions for the potential energy failed to show why CsCl, CsBr and CsI crystallize normally in the body-centered CsCl-type lattice, and not in a simple lattice of the NaCl type, the form assumed by most of the alkali halides.

The author obtained[3] the proper stability for CsCl by inserting two additional constants in the energy expression and evaluating these from experimental data. The four empirical constants required for this evaluation were the heat of transition of CsCl in passing from the body-centered type, which is stable below 445°C, to the simple lattice type, stable at higher temperatures; the compressibility β and other P-V-T data for the normally stable body-centered type; the lattice constant r_0, i.e., the distance between nearest ions, for the body-centered type at 273°K and for the simple lattice at absolute zero.

The lattice energy U was assumed to be of the form

$$U=\alpha e^2/r_0+cC/r_0^6+cD/r_0^8-B(r_0). \quad (1)$$

The components of energy are respectively, the electrostatic energy, the energies of the dipole-dipole and dipole-quadrupole van der Waals interactions and the repulsion components. α is Madelung's constant; e, the electronic charge; and C and D, the van der Waals constants as computed theoretically by Mayer.[4] The repulsion components were taken as

$$B(r_0)=b_1M\exp(-r_0/\rho)+b_2M'\exp(-ar_0/\rho). \quad (2)$$

M and M' are the numbers of nearest and next nearest neighbors of an ion, and a is the ratio of the distances of these second and first neighbors. The four constants to be evaluated are c and the three repulsion constants, b_1, b_2, and ρ. The values of α, M, M' and a, which depend only on the lattice type, are given in Table I.

The four equations necessary for the evaluation of the constants are obtained as follows. The experimental heat of transition was equated equal to the difference of the lattice energies for the body-centered and simple lattice types as given by Eq. (1). The other three relations were obtained by forming the first and second derivatives of this equation with respect to r_0

$$-r_0\frac{\partial U}{\partial r_0}=\frac{\alpha e^2}{r_0}+\frac{6cC}{r_0^6}+\frac{8cD}{r_0^8}+r_0\frac{\partial B}{\partial r_0}=R \quad (3)$$

and

$$r_0^2\frac{\partial^2 U}{\partial r_0^2}=\frac{2\alpha e^2}{r_0}+\frac{42cC}{r_0^6}+\frac{72cD}{r_0^8}-r_0^2\frac{\partial^2 B}{\partial r_0^2}=-S, \quad (4)$$

[1] M. Born and J. E. Mayer, Zeits. f. Physik **75**, 1 (1932).
[2] M. L. Huggins and J. E. Mayer, J. Chem. Phys. **1**, 643 (1933).
[3] A. May, Phys. Rev. **52**, 339 (1937).
[4] J. E. Mayer, J. Chem. Phys. **1**, 270 (1933).

TABLE I. *Constants which depend on lattice type.*

TYPE OF LATTICE	α	M	M'	a
CsCl	1.7627	8	6	1.1547
NaCl	1.7476	6	12	1.4142

where R and S are given by

$$R=(3T/N\beta)(\partial V/\partial T)_P \tag{5}$$

and

$$S=\frac{9V}{N\beta}\left[1+\frac{T}{\beta}\left(\frac{\partial\beta}{\partial T}\right)_P + \frac{T}{\beta^2 V}\left(\frac{\partial V}{\partial T}\right)_P\left(\frac{\partial\beta}{\partial P}\right)_T+\frac{2}{3}\frac{T}{V}\left(\frac{\partial V}{\partial T}\right)_P\right]. \tag{6}$$

V is the mole volume; P, the pressure; T, the temperature, and N is Avogadro's number. Eqs. (3) and (4) were applied to the body-centered type lattice at 273°K and Eq. (3) was used for the simple lattice type at 0°K. The lattice constant at 0°K was calculated by extrapolation from values obtained above the transition point.

Errata

In the calculations for CsCl previously reported[3] by the author, $\beta^{-1}(\partial\beta/\partial P)_T$ was inadvertently given a value only one-tenth that experimentally determined.[5] Those calculations have, therefore, been corrected. Most of the P-V-T data used were those recently recomputed by Huggins.[6] They are listed in Table II.

Table III gives the results of the recalculation of the lattice energies of CsCl by this method of four constants. The symbols employed are those of the previous paper except for the addition of a subscript "a," which will be explained later. For the electronic charge, Birge's value[7] 4.803 $\times10^{-10}$ e.s.u. has been used. A comparison of the values in Table III with those formerly given, shows that while the van der Waals factor, c, is practically the same, 3.5 instead of 3.6, ρ has increased from 0.365 to 0.393 and consequently b_1 has become somewhat less. The ratio b_2/b_1 has dropped from 0.7 to 0.4.

The elastic constants and frequencies, obtained as before, are given in Tables IV and V. They are lower than those previously reported. The optical frequency of 3.16×10^{12} sec.$^{-1}$ for the CsCl-type lattice is 7.5 percent higher than the value of 2.94 obtained by Barnes from the measured infra-red absorption limit of CsCl. Heckmann's correction for the electron polarization results in a value of 2.41×10^{12} sec.$^{-1}$ which is 18 percent lower than Barnes' value.

The determination of the temperature of transition between the two lattice types, by equating the free energies and using the frequencies found for 0°K, yields a value of 741°K, still in substantial agreement with the experimental value of 718°K. As before, an attempt to use, in this computation, the frequencies calculated for the transition temperature fails because of the too rapid decrease of the acoustic frequency limit for the CsCl-type lattice with increasing temperature.

THE MOLECULE

Calculations for the gaseous molecule can be made in a manner entirely similar to that already used for the crystal. Here we are confronted by a source of error, whose magnitude is difficult to estimate. The potential energy expression should contain a polarization term whose size would depend on the number of neighbors of an ion. For CaCl, Neugebauer and Gonbas[8] found the principal part of this term almost identical in form and magnitude with the first van der Waals component. In the method we have used, such a contribution would be indistinguishable from the van der Waals energy and would merely increase the value of c. Since, in the gaseous molecule, each ion has a single companion, this polarization energy should be somewhat greater

TABLE II. *Data used in calculations for* CsCl *273°K.*

P-V-T CONSTANTS	CsCl TYPE	NaCl TYPE
$C\times10^{60}$ erg cm^6	1621	1105
$D\times10^{76}$ erg cm^8	2630	1751
$r_0\times10^8$ cm (meas.)	3.553	
$\beta\times10^{12}$ barye^{-1}	5.95	
$\beta^{-1}(\partial\beta/\partial T)_P\times10^4$ deg^{-1}	8.8	
$\beta^{-1}(\partial\beta/\partial P)_T\times10^{11}$ barye^{-1}	−3.40	
$V^{-1}(\partial V/\partial T)_P\times10^4$ deg^{-1}	1.887	
R	1.79	
S	102.4	
ΔU	0.093	

$\times10^{12}$ ergs per molecule

[5] P. W. Bridgman, Proc. Am. Acad. **67**, 345 (1932).
[6] M. L. Huggins, J. Chem. Phys. **5**, 143 (1937).
[7] R. T. Birge, Phys. Rev. **52**, 241 (1937).
[8] Th. Neugebauer and P. Gombas, Zeits. f. Physik **89**, 480 (1934).

TABLE III. *Results of calculation of lattice energies of* CsCl.*

	METHOD OF 4 CONSTANTS		METHOD OF 6 CONSTANTS	
	CsCl TYPE	NaCl TYPE	CsCl TYPE	NaCl TYPE
c	3.5	3.5	2.60	2.60
ρ_a } $\times 10^8$ cm	0.393	0.393	0.380	0.380
ρ_b			0.100	0.100
b_2/b_1	0.4	0.4	0.203	0.203
$b_1\times 10^{12}$ ergs per molecule	3175	3175	3580	3580
$b_{ab}\times 10^{-8}$			3.375	3.375
$\alpha e^2/r_0$	11.44	11.75	11.44	11.67
cC/r_0^6	2.82	2.38	2.09	1.69
cD/r_0^8	0.36	0.32	0.27	0.22
$B_{1a}(r_0)$	3.00	3.08	2.49	2.42
$B_{2a}(r_0)$ } $\times 10^{12}$ ergs per molecule	0.22	0.07	0.09	0.02
$B_{1b}(r_0)$			0.00	0.01
$B_{2b}(r_0)$			0.00	0.00
U	11.40	11.30	11.22	11.13
ΔU	0.10		0.09	
$r_0\times 10^8$ cm 0°K (calc.)		3.402		3.421
$r_0\times 10^8$ cm 273°K (estimated)		3.454		3.454
	gas		*gas*	
$r_g\times 10^8$ cm (calc.)	2.94		3.07	
F dynes per cm	5.0		9.0	

* Calculations are for $T=273$°K unless otherwise specified.

than in the crystal, but calculations for the gas were made in the hope that the error might not be important.

The heat of dissociation of molecules into ions, is given by

$$U_D=\frac{e^2}{r_g}+\frac{cc_{+-}}{r_g^6}+\frac{cd_{+-}}{r_g^8}-B_g(r_g), \qquad (7)$$

where $B_g(r_g)=b_1\exp(-r_g/\rho)$; c_{+-} and d_{+-} are the van der Waals constants for a pair of unlike ions as computed by Mayer[4] and the subscript, g, denotes the gaseous molecule.

Maxwell, Hendricks, and Mosley[9] have measured the interionic distances of the alkali chlorides, bromides, and iodides in the gaseous state at approximately 1200°C by electron diffraction. Their results furnish an additional test of the correctness of the shape obtained for the potential energy curve of the ions. If it is assumed that at 1200° only a small fraction of the molecules are in excited vibration states, these interionic distances can be calculated for absolute zero by using the equation obtained by differentiating Eq. (7):

$$\frac{e^2}{r_g}+\frac{6cc_{+-}}{r_g^6}+\frac{8cd_{+-}}{r_g^8}+r_g\frac{\partial B_g}{\partial r_g}=0. \qquad (8)$$

[9] L. R. Maxwell, S. B. Hendricks and V. M. Mosley, Phys. Rev. **52**, 968 (1937).

Applying this formula to CsCl, with the constants already obtained from crystal data,

TABLE IV. *Elastic constants* $\times 10^{-11}$ *erg/cm*^{3}.

	c_{11}	c_{12}	c_{44}	ACOUSTIC FREQUENCY LIMIT $\nu_m\times 10^{-12}$
CsCl TYPE AT 273°K				
electrostatic	1.730	−1.694	−1.694	
van der Waals C	−3.357	−1.588	−1.588	
van der Waals D	−0.662	−0.368	−0.368	
repulsion	5.670	4.388	4.388	
$R/6\Delta$	0.043		0.043	
	3.424	0.738	0.781	2.622
NaCl TYPE AT 273°K				
electrostatic	−2.688	0.616	0.616	
van der Waals C	−4.034	−0.337	−0.337	
van der Waals D	−0.982	−0.038	−0.038	
repulsion	11.032	0.113	0.113	
$R/6\Delta$	0.018		0.018	
	3.346	0.354	0.372	2.086
CsCl TYPE AT 0°K	3.787	1.014	1.014	2.890
NaCl TYPE AT 0°K	3.766	0.359	0.359	2.101

TABLE V.* *Optical frequencies at 273° and 0°K. D (Born)* $\times 10^{-26}$ *erg/cm*^{5}.

	CsCl TYPE	NaCl TYPE
at 273°K		
electrostatic	−2.026	−1.484
van der Waals C	−2.055	−1.795
van der Waals D	−0.578	−0.543
repulsion	7.311	6.353
D	2.652	2.531
frequency $\times 10^{-12}$	3.161	3.338
at 0°K		
D	3.213	2.658
frequency $\times 10^{-12}$	3.411	3.379

* For explanation of notation, see reference 3.

one finds the interionic equilibrium distance to be 2.94×10^{-8} cm as compared with the measured value of 3.06 ± 0.03. The 4 percent error is rather large.

Still another check of the potential energy expression is available. From spectroscopic absorption measurements of Sommermeyer, Herzfeld has calculated[10] $2\pi^2\omega_e^2\mu$ for a number of the alkali halides. Here ω_e is the classical vibration frequency and μ the reduced mass. This quantity is one-half the force between the gaseous ions for a separation of one cm. The forces so obtained are given in Table VI.

No value is listed for CsCl, but it will apparently be in the neighborhood of 11 dynes/cm and probably less than this, say, 10 dynes/cm.

To calculate the force per unit distance from the potential energy expression we use an equation of the same nature as Eq. (4), namely

$$\frac{2e^2}{r_g^3}+\frac{42cc_{+-}}{r_g^8}+\frac{72cd_{+-}}{r_g^{10}}-\frac{\partial^2 B_g}{\partial r_g^2}=-F. \qquad (9)$$

F is the force at unit distance. Using $r_g=2.94\times10^{-8}$ cm, we find $F=5.0$ dynes/cm, approximately half the correct value.

Method of Six Constants

Since the potential energy form chosen failed to give reasonable agreement for the molecule, the form of the repulsion energy was changed so as to give two additional parameters, making a total of six constants, whose values can then be obtained from six equations, the four previously used, together with Eqs. (8) and (9). The form used for $B(r_0)$ was

$$B(r_0)=b_1M(\exp(-r_0/\rho_a)+b_{ab}\exp(-r_0/\rho_b))$$
$$+b_2M'(\exp(-ar_0/\rho_a)+b_{ab}\exp(-ar_0/\rho_b)) \qquad (10)$$

and consequently

$$B_g(r_g)=b_1(\exp(-r_g/\rho_a)+b_{ab}\exp(-r_g/\rho_b)). \qquad (11)$$

This form assumes that the repulsion energy in the range from r_0 to r_g cannot be adequately expressed by using a single exponential and attempts improvement by including a second exponential and introducing the two additional parameters, ρ_b and b_{ab}. b_{ab} is the ratio of the b-factor for the exponential containing ρ_b to that for the one containing ρ_a. The same shielding factor, b_2/b_1, is assumed for the contributions of the two exponentials.

[10] K. F. Herzfeld, *Handbuch der Physik*, Vol. 24/2 (Berlin 1933), p. 102.

Table VI. *Forces between ions in dynes/cm from spectroscopic measurements.*

	Cl	Br	I
Na			9.0
K		12.4	10.8
Rb	10.2		9.6
Cs		11.0	7.6

The labor involved in the calculations is, of course, tremendously increased. The method employed was first to assume values of ρ_a, ρ_b and c. Next, from data for the CsCl-type lattice, and by use of Eqs. (1), (3) and (4), we solve for b_1, b_2 and b_{ab}. Having, now, values for the six constants, we applied Eq. (3) to the NaCl-type lattice at absolute zero, and determined its equilibrium distance. In general, the distance so found was not a reasonable one. With the same values of ρ_a and ρ_b as before, c was then changed until a suitable result was obtained. Finally the six constants so determined were substituted in Eqs. (8) and (9) for the gas to find what force F and what equilibrium separation r_g result. This whole process was then repeated with new values of ρ_a and ρ_b until all six equations were reasonably satisfied. The results for CsCl are given in Table III. The subscripts 1 and 2 refer to the first and second neighbors of an ion, the subscricipts a and b to the two values of ρ. Thus B_{1a} is the repulsion component containing ρ_a, for the nearest neighbors.

The experimental lattice constant for the NaCl-type lattice has been estimated now at 3.454, while 3.430 was given in the previous paper. This new value appears to be equally justified by the necessary extrapolation and agrees somewhat better with the calculated results.

The question naturally arises as to whether the determinations made for CsCl can be applied to the other alkali halides. A verification of this was attempted by assuming that ρ_a, ρ_b, b_2/b_1 and b_{ab} remain the same throughout the group. The two remaining constants, c and b_1, were then obtained from the lattice constant and com-

TABLE VII. *Constants for various alkali halides.*

CONSTANTS	NaI	KBr	KI	RbCl	RbI	CsCl	CsBr	CsI
c	0.33	2.28	2.94	2.19	2.82	2.60	2.30	3.78
$b_1\times10^{12}$ ergs per molecule	1110	1980	3800	2000	6800	3580	4800	9780
lattice energy kcal. per mole (meas.)	166.4[11]		153.8[12]					141.5[12]
lattice energy kcal. per mole (calc.)	118.2	140.0	159.0	140.5		162.5		184.0
interionic distances $\times10^8$ cm (meas.)[9]	2.90	2.94	3.23	2.89	3.26	3.06	3.14	3.41
interionic distances $\times10^8$ cm (calc.)	2.83	2.96	3.13	2.95	3.36	3.07	3.18	3.43
forces between ions dynes per cm (spect.)[10]	9.0	12.4	10.8	10.2	9.6		11.0	7.6
forces between ions dynes per cm (calc.)	20.1	12.4	7.3	13.1	4.8	9.0	6.6	4.8
heat of dissociation $MX_{gas}\rightarrow M^+_{gas}+X^-_{gas}$ kcal. per mole (calc.)	83.8	92.3	97.0	92.9	96.4	98.9	99.0	100.0
heat of sublimation kcal. per mole (meas.)	49.1[13]	53.3[14]	47.8[13]	51.3[14]				
heat of sublimation kcal. per mole (calc.)	34.4	47.7	62.0	47.6		63.6		84.0

pressibility data of the various salts as given by Huggins.[6] The values of these constants found for some of the alkali halides are listed in Table VII, together with the corresponding lattice energies, heats of dissociation from molecules to ions, equilibrium interionic distances and the interionic forces.

The computed interionic distances check with the measured values to within 1.3 percent for the salts which crystallize in the CsCl type, and within about 3 percent for those of the NaCl type, given in the table. For very small values of r_0, the method fails to give reasonable results, for example, for NaCl the van der Waals factor c is found to be -4. On the whole, the agreement is good for the values of r_0 listed. With few exceptions the computed values are too high.

The calculated interionic forces do not check well with those measured, varying from one-half to double these. In general the values found are too low for those cases where the interionic distance is greater than for CsCl, and too high where the distance is less. The large error in a few cases may be due, at least partially, to insufficient accuracy in the experimental compressibility data.

The heats of sublimation have been computed by subtracting the calculated heats of dissociation of molecules into ions, from the lattice energy. The agreement of calculated with measured values of the lattice energies and heats of sublimation is quite poor.

In conclusion the author wishes to express his appreciation to Professor K. F. Herzfeld for helpful discussions during the progress of this work.

[11] A. N. Tandon, Nat. Acad. Sci., India, Proc. **7**, 102 (1937).
[12] J. E. Mayer, Zeits. f. Physik **61**, 798 (1930).
[13] Landolt-Börnstein, *Physikalisch-Chemische Tabellen* (Berlin 1936) Eg IIIc, p. 2709.
[14] J. E. Mayer and I. H. Wintner, J. Chem. Phys. **6**, 301 (1938).

The Rate of Vaporization of Mercury from an Anchored Cathode Spot[1]

L. TONKS
Research Laboratory, General Electric Company, Schenectady, New York
(Received July 22, 1938)

Two major difficulties which interfere with the measurement of the vaporization of mercury at a free cathode spot are the spray and the normal evaporation from the free surface. By anchoring the spot the spray has been eliminated, and by a specially designed, water-cooled cathode structure the free surface has been limited to small areas of controllable size. By means of a calibrated feed mechanism, mercury was fed to the cathode as fast as it vaporized. Measurements were made over a range of arc current, cooling water temperature, and exposed area. The rate of vaporization (g/coulomb) increased with arc current, temperature, and exposed area, all due to increased normal evaporation. The rate may also increase with arc current, because of cumulative effects within the spot itself. Extrapolated to zero arc current the rate was found to be approximately 2.5×10^{-4} g/coulomb. This lies within the limits set by von Issendorf. It means that eight elementary charges pass through the arc for every atom evaporated.

THE determination of the rate of vaporization of Hg at the cathode spot of a Hg pool cathode is of considerable technical as well as scientific interest. Several attempts have been made to measure this quantity,[2-4] but the inherent difficulties have made the results inconclusive at best.

It is easily observed that the spot on a Hg surface throws up a spray of droplets whose diameters range from about 0.2 mm down. These constitute the first obstacle to a determination of the vaporization rate, because there is no way of separating the mercury transferred from the pool in this way from that transferred by evaporation. No arrangement of baffles can be devised to do this, for the baffles would either cause vaporization of droplets striking them, thus adding an unknown amount to the vapor, or else they would condense vapor from the stream passing by. It is impossible to control their temperature so that neither occurs.

Guntherschulze made no attempt to separate the spray from the vapor in his pioneer determination. That explains his high result of 22×10^{-4} g/coulomb. Von Issendorf recognized the difficulty and tried to separate the two by dividing his arc tube into two sections, in the first of which the spray collected, in the second of which the vapor condensed. Further, he varied the wall temperature of the first section. Even so he was able only to set rather wide limits for the true vaporization, namely -3×10^{-4} and $+13\times10^{-4}$ g/coulomb. Finally, Kobel's arrangement of a small pool at the bottom of a narrow, cooled tungsten funnel assured that little, if any, of the spray would escape, but also must have resulted in the condensation of an appreciable fraction of the vapor itself. His value of 0.17×10^{-4} g/coulomb is certainly low.

A second difficulty lies in the normal evaporation from the exposed surface which, though not exposed at any given instant to the cathode spot mechanisms, is heated by the momentary passages of the spot over it and by the continual flow of energy from the arc stream to it. Because of this factor von Issendorf minimized the area of his pool, but it still was about 4 cm² in extent. The low thermal conductivity of the Hg prevents the easy escape of this energy by conduction. In fact rough calculations indicate that in some practical cathode pool constructions the loss of heat by vaporization is comparable with that lost by conduction.

The anchored cathode spot offered an escape from both difficulties, for it gives no spray, and, since the spot is confined to an extremely small area, the exposed Hg surface can be made very small. Whether or not the anchoring of the spot alters the vaporization from it is a question which can be raised but which it is hardly worth while to attempt to answer, as long as there is no adequate theory of the cathode spot, or as long as the rate of vaporization, force, or current density at the free spot cannot be satisfactorily

[1] The subject matter of this paper was reported at the Washington Meeting of the American Physical Society, April 29, 1938, Phys. Rev. **53**, 936 (1938).
[2] Guntherschulze, Zeits. f. Physik **11**, 74 (1922).
[3] J. von Issendorf, Physik. Zeits. **29**, 857 (1928).
[4] E. Kobel, Phys. Rev. **36**, 1636 (1930).

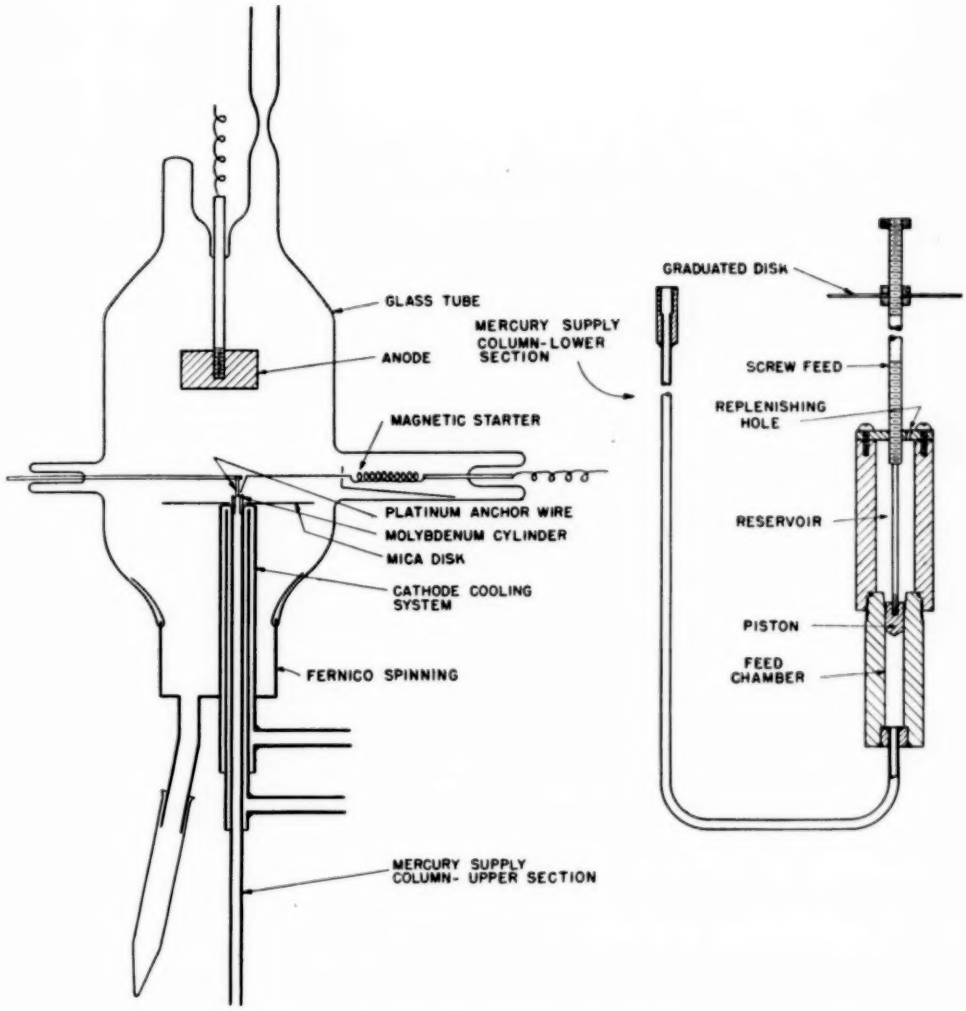

FIG. 1. Arc tube and mercury feed system.

determined. At least, the rate of vaporization from an anchored spot can help in building the theory of the fixed spot, which, in turn, must be the same in its essentials as for a free spot.

The experimental discharge tube and mercury feed system used in the present experiments are shown in Fig. 1. The central feature of the tube is the cathode structure which is shown in detail in Fig. 2. It consists of a Mo cylinder, drilled axially for flow of mercury to the cathode surface, welded to the upper end of the steel mercury feed tube, and arranged to be in good thermal contact with the cathode cooling system. The mica disk was intended to prevent the cathode spot from going to the steel of this system, but despite the shielding which it furnished, the spot would jump to the mercury accumulated on the floor of the fernico spinning, if the mercury at the tip of the cathode became exhausted. The top face of the Mo cylinder was tapered slightly instead of being turned off flat, with the idea that the cathode spot would anchor there. With the special conditions of small free surface and restricted mercury flow which existed here, it was found to be impossible to maintain a free spot for the time necessary to induce wetting of the Mo. Accordingly, the design was modified by the introduction of the vertical Pt wire dipping into the cathode Hg, for reasonably clean Pt is wet spontaneously by Hg.

Matched thermometers were placed one at the inlet and the other at the outlet of the cooling

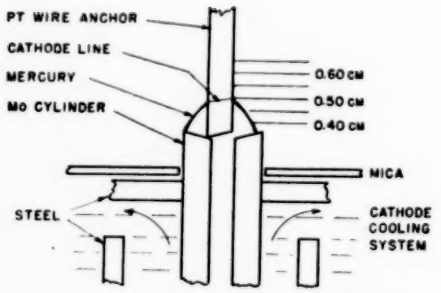

FIG. 2. Detail of cathode structure.

system. The other feature of the apparatus which requires special mention is the arrangement for feeding known quantities of Hg to the cathode spot. It also is shown in Fig. 1. The piston, working in the feed cylinder, controls the supply of Hg to the cathode. The nonwetting of the steel by the mercury made a reasonably close fit, without packing, between piston and cylinder, all that was necessary to assure a positive feed without leakage. The reservoir was designed to permit the replenishment of the Hg in the feed cylinder without the introduction of air between piston and Hg. With the surface of the mercury in the reservoir slightly less than the barometric height below the cathode surface, it was only necessary to raise the piston just out of the feed cylinder to allow fresh Hg to flow down from the reservoir. This arrangement of levels had the further advantage that the pressure tending to force Hg past the piston was small.

The height of the piston was regulated by a screw furnished with a disk graduated in degrees. As the piston diameter was 0.635 cm and the screw pitch 0.106 cm, the constant of the feed system was 1.265×10^{-3} g of Hg per degree.

Before the feed mechanism, as illustrated, was joined to the tube, all parts that were to come into contact with Hg were thoroughly washed with alcohol. The part of the feed system which was connected to the tube had been "pickled," but became oxidized in the heating attendant upon the final sealing process in the making of the fernico seal. No difficulty was foreseen as a result, and none appeared. When the two parts of the system were joined, the junction was made tight with de Khotinski cement.

The attempt was made to prevent the trapping of any air in the feed system when the Hg was introduced, by holding back the Hg in the reservoir with the piston until the tube, barometric column, and feed cylinder had been exhausted, then allowing the Hg to flow in by raising the piston out of its cylinder. This was, apparently, not completely successful, for the first runs made with the tube showed a varying rate of vaporization in the course of a single determination, but this variability disappeared as experimentation proceeded.

The anode had been fired in vacuum before the tube was assembled. In the tube, which was run on the pump, it was heated briefly by induction, but no special precautions were taken to get the tube gas-free, since small residual pressures of a micron or so would not affect the present cathode phenomenon.

A preliminary experiment in a different type of tube had shown an important effect of exposed mercury surface on the rate of vaporization. In order to maintain a constant exposed area during each determination with the present tube, a cathetometer was sighted on the cathode and the cathode line was held at a fixed level within 0.1 to 0.2 mm by manipulating the feed mechanism.

No special provisions were made for cooling the tube surface upon which the Hg condensed, beyond directing an electric fan upon it. Its temperature never rose above 40°C. Hg vapor at the corresponding saturated vapor pressure, condensing on the small exposed cathode surface, would have no appreciable effect on the experimental results.

The rate of vaporization was measured as a function (1) of arc current, (2) of meniscus height, i.e., exposed Hg surface, and (3) of

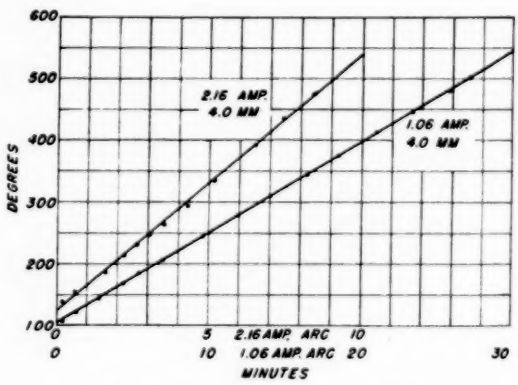

FIG. 3. Plots of experimental data.

cathode cooling water temperature. In making a determination the cooling water temperature was adjusted. The arc was then started and the current was set at the desired value. Finally, the cathode line was set slightly above the chosen height, and at the instant when the line became centered on the cross-hair of the cathetometer a stop watch was started. It was impossible to feed the Hg so evenly that the cathode line remained always at the predetermined height; accordingly, the feeding was manipulated to keep the average height at the desired value. In the early runs, until it became evident that the irregularities in feeding rate which have already been mentioned had disappeared, the elapsed time was noted for approximately every 30° rotation of the feeding head. Later only the total elapsed time was recorded. Fig. 3 shows the results of two runs made in this way. Some deviations from a straight line appear in the measurements at the larger current, but there is little latitude in drawing the best straight line.

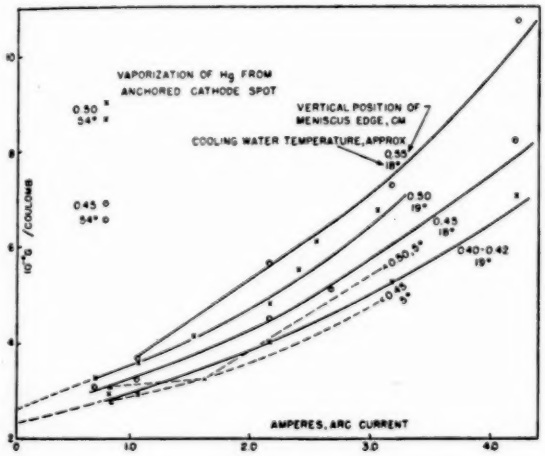

FIG. 4. Rate of vaporization of Hg as a function of arc current.

The results of the measurements are shown in Figs. 4, 5 and 6, which correlate the rates of vaporization with arc current, exposed Hg surface, and cooling water temperature, respectively. It is immediately evident that the vaporization increases significantly as each of these three parameters increases, yet that, extrapolated to zero current or low cooling water temperature, the sequences of values lead to a fairly definite rate of vaporization. From Fig. 4 we find $2.3-2.6$ $\times 10^{-4}$ g/coulomb, from Fig. 6, $2.7-3.0\times 10^{-4}$ g/coulomb. It will be noted that these values are an order of magnitude greater than Kobel's, an order of magnitude less than Guntherschulze's, and lie within the range specified by von Issendorf.

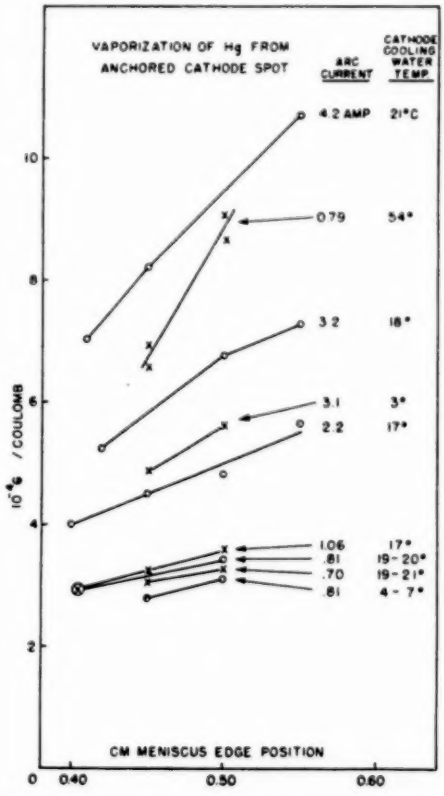

FIG. 5. Rate of vaporization of Hg as a function of exposed Hg area.

Besides the natural evaporation from the free surface, two other factors may contribute to an increase in vaporization rate. The one is an increase from the cathode line itself with increasing current density. This would only become evident as a residual effect after other causes had been considered. The other factor is condensation on the cathode Hg of Hg vaporized at the spot. It is to be expected that this effect will be the greater the more confined the cathode line is by the liquid Hg, that is, the lower the meniscus edge. The consequence would be an increase of vaporization with meniscus height, that is, an effect similar to that of natural evaporation, except that now the "true" rate is more closely approached as the meniscus is raised.

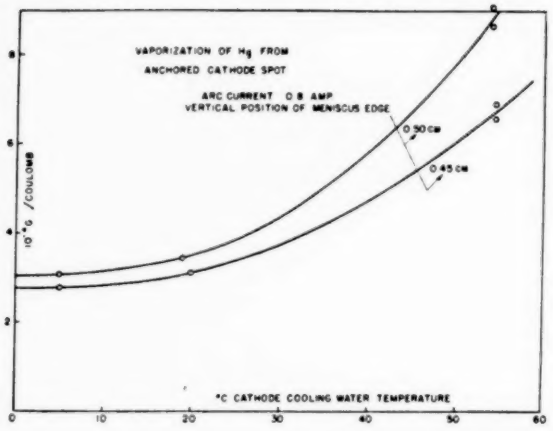

FIG. 6. Rate of vaporization of Hg as a function of cathode cooling water temperature.

We should expect the true evaporation to take place into the hemispherical solid angle above the plane over which the cathode spot is playing. If the liquid Hg cuts off one-half this angle, as it would in the present case, if the meniscus edge lay slightly below 0.4 cm, then only one-half of the vaporized Hg would escape. If the angular opening between anchor and surface is increased to 135°, then 85 percent or more would escape. No increase comparable with this is seen at the low current values where the effect should be looked for uncomplicated by the other factors. We conclude that the effect is small here, although it probably exists.

If we assume that the whole increase in vaporization with meniscus height and current is due to natural evaporation, we can make an estimate of the surface temperature of the cathode mercury for a particular value of current, say, 2.15 amp. Fig. 4 shows a difference of vaporization rate ΔR of 1.6×10^{-4} g/coulomb between the 4.1 mm and 5.5 mm meniscus positions. If the free surface be assumed to have the area of the conical surface of the frustum of a cone in the two cases, we find 0.06 cm^2 and 0.13 cm^2, respectively. If we further suppose the surface temperatures to be the same, we have to calculate the temperature at which Hg vaporizes at the rate

$$\frac{1.6\times10^{-4}\times2.15}{0.13-0.06}=4.9\times10^{-3}\ \text{g/cm}^{-2}\ \text{sec.}^{-1}.$$

This mass-transport of Hg vapor, expressed in terms of pressure (assuming 300°K) is, from the kinetic theory relation, $3.58\times10^{-5}p$ (bars), so that

$$p=137\ \text{bars},$$

corresponding to saturated Hg vapor at 83°C. This is not an unreasonable temperature in view of the low heat conductivity of Hg.

It is important to note that even the small free surfaces met with here can evaporate as much or more Hg than the cathode spot itself.

Table I shows the results of previous determinations of vaporization rates in vacuum for Cu and Zn. The spread in values between the Easton-Lucas-Creedy, the Tanberg, and the Robertson results cannot be accounted for in terms of gas pressure, for Robertson found only a small effect—and that a decrease—from increasing nitrogen pressure.

The present result for Hg fits well with Robertson's Cu value. This is particularly striking if we compare the net rate at which atoms leave the metal to the rate of transfer of elementary charge. The rate of 2.5×10^{-4} g/coulomb for Hg corresponds to 0.12 atoms/elementary charge. Similarly, 0.87×10^{-4} g/coulomb for Cu gives 0.13 atom/elementary charge. Reasoning rigorously, the Cu value should also be extrapolated to zero current instead of using the 15 amp. value. Since, however, the vapor pressure of the Cu is negligible, it will not contribute to an increase of vaporization with current. Thus, the comparison, as made, fails only to take into account a possible intrinsic increase of vaporization with current for the Cu spot. It is interesting that there is a small number ratio between the elementary charge transfer and the number of atoms which escape without immediate recondensation as either atom or ion. Thus, if the current is carried chiefly

TABLE I. *Results of previous determinations of vaporization rates in vacuum for Cu and Zn.*

MATERIAL	PRESSURE (MICRONS)	GAS	CURRENT (AMP.)	RATE (10^{-4} g/COULOMB)	REFERENCE
Cu	40–50	Residual	70–150	0.07	(1)
Zn	40–50	Residual	40	0.1	(1)
			75	0.13	(1)
Cu	0.2–10	Residual	11–32	0.15	(2)
Cu	0, extrapolated		15	0.87	(3)

[1] Easton, Lucas Creedy, Elec. Eng. **53**, 1454 (1934).
[2] Tanberg, Phys. Rev. **35**, 1080 (1930).
[3] R. M. Robertson, Phys. Rev. **53**, 578 (1938).

by electrons, some 8 electrons evaporate for every atom.

Table I makes it apparent that an important factor contributing to the high velocity of the vapor stream which Tanberg calculated is a low value of the rate of evaporation. As I have pointed out,[5] the rate of vaporization for Hg found in the present experiment is consistent with the force on the cathode which has been observed. A potential maximum of about 3 volts above space, i.e., about 13 volts above cathode, in the cathode spot plasma with complete ionization of the vapor there would account for the observed force.

[5] Tonks, Phys. Rev. **50**, 226 (1936).

The smallest current maintained by a spot anchored on a tungsten "Schwamm" is given by von Engel and Steenbeck[6] as 50 ma. The smallest currents I have observed from a porous body of Mo saturated with mercury have been in the neighborhood of 0.5 amp. The present result shows that in these cases the vaporization was at the rate of 1.2 and 12×10^{-5} g/sec., respectively. It may be that vaporization rates lower than these would give a density of gas immediately above the cathode spot which is insufficient to establish the electron emission condition.

[6] Von Engel and Steenbeck, *Elektrische Gasentladungen*, Vol. II, p. 263.

OCTOBER 15, 1938 PHYSICAL REVIEW VOLUME 54

The Effective Cross Section of Positive Alkali Ions with Respect to Gas Molecules

KENT H. BRACEWELL
Indiana University, Bloomington, Indiana
(Received July 20, 1938)

The absorption of positive sodium ions with velocities of 40 to 400 equivalent volts has been studied in hydrogen, nitrogen and oxygen. The nature of the collision processes has, in each case, been studied to determine the relative importance of neutralization, retardation or small angle scattering. The mean free paths and effective cross section of the sodium ions with respect to the gas molecules is found to be a function of the pressure of the gas, the velocity of the ion and the nature of the gas-ion combination. The effective cross section of each gas-ion combination approaches the kinetic theory value at low velocity of the ion while at high velocities it approaches a minimum considerably smaller than the kinetic theory value. At any given velocity over the range studied, the effective cross section of the gas-ion combination increases in the order hydrogen, nitrogen, oxygen. The values for nitrogen and oxygen are essentially, within experimental errors, equal. An improved furnace for the production of positive ions has been developed.

A NUMBER of investigations have been made on the absorption of slow positive ions in gases. The absorption may be due to small angle scattering, retardation or neutralization. The method of investigation generally used has been to bend a beam of positive ions in a magnetic field and measure the rate of absorption of the ions over a fixed length of path. The rate of absorption has been found to be a function of the pressure of the gas, the nature of the gas-ion combination and the speed of the ion. G. P. Thompson[1] found considerable small angle scattering of H^+ ions in H_2, He and A. Dempster[2] passed H^+ ions, accelerated between 14 and 1000 volts, into helium. Little, if any, retardation was observed, but considerable scattering of the bundle of protons was found at high pressures. Durbin[3] measured the rate of absorption of K^+ ions in He, H_2, A, N_2 and O_2. He found the absorption of the ions to increase with the pressure of the gas and with a decrease of velocity of the ions. In all cases, the mean free path was found to be greater than the kinetic theory mean free path, but it approached the

[1] G. P. Thompson, Phil. Mag. [7] **1**, 961 (1926); Phil. Mag. [7] **2**, 1076 (1926).

[2] A. J. Dempster, Phil. Mag. [7] **3**, 115 (1927).
[3] F. M. Durbin, Phys. Rev. **30**, 844 (1927).

latter at low speeds of the ions. Kennard[4] found the collisions of Cs^+ in A to result largely in neutralization, while with Cs^+ in H_2 and He the essential phenomenon was that of retardation. Cox[5] passed slow Li^+ ions through Hg vapor and measured the resulting mean free path. The collisions were found to result largely in small angle scattering of the Li^+ ions. Thompson[6] found collisions between slow Cs^+ ions and H_2 and He

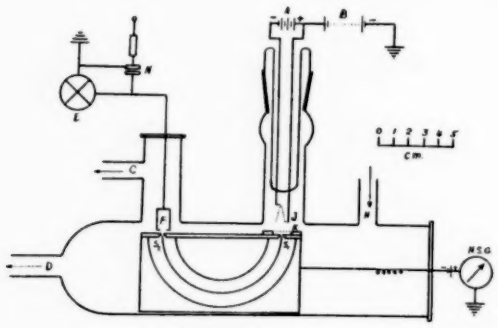

FIG. 1.

to result for the most part in retardation of the ions while for Li^+ in He, the chief factor involved was that of scattering. In a theoretical paper Beeck[7] concludes that the correction for the effective cross section of the gas-ion combination, due to the dimensions of the apparatus, varies with the angular aperture of the system of slits but is negligible for very small angular apertures. Holzer[8] found the absorption coefficient of H_3^+ in H_2 to be greater than that of H^+, but less than that of H_2^+.

The present investigation was undertaken to determine the mean free path and effective cross section of Na^+ ions in H_2, N_2 and O_2 and to determine, if possible, the type of collision occurring in each case.

APPARATUS

A modification of a Dempster mass spectrograph, Fig. 1, was chosen as the most suitable means of studying the phenomena involved. Before admission to the chamber at H, the pressure of the gas was reduced in a reservoir to a value only slightly higher than the working pressure of the gas in the analysis chamber. The gas was admitted by means of a fine capillary leak, so that a continuous flow was maintained throughout the system. Various pressures could be obtained by adjustment of the leak. The gas was pumped out at D through a liquid-air trap. Pressures were measured by a McLeod guage connected at C. Ions were produced in the furnace J which was heated by a 6-volt storage battery. The ions were accelerated to the pole shoe through a screen consisting of a brass ring having a hole 12 mm in diameter, across which were soldered fine parallel wires having a spacing of 24 to the inch. The armature, entirely enclosed in glass, contained an internal slot in the form of a semi-circular aperture of 4 cm radius. The width and depth of the slot were 0.3 and 1.7 cm respectively. After passing the slit S_1 of 2 mm width, the ions were bent in a semicircle and those passing through S_2, of 1 mm width, were captured by a Faraday cylinder connected to a Compton electrometer, adjusted to a sensitivity of 1120 mm per volt.

Let Q_0 positive ions be incident upon one end of a column of gas, and be moving parallel to the axis of the cylinder. In general, collisions will occur, and a reduction in the density of positive ions results. Let (R_i+R_m) be the maximum distance from center of ion to center of molecule, which results in a collision. Then $\pi(R_i+R_m)^2$ is called the effective cross section of the positive ion with respect to the gas molecule. The probability of collision is directly proportional to $\pi(R_i+R_m)^2$, to the number of molecules per cc, to the distance x traversed, and to the number of ions Q_0 incident upon the column. Let Q be the number of ions remaining after traversing a distance x. Then

$$Q=Q_0 \exp\left[-PN\pi(R_i+R_m)^2x\right]/760. \quad (1)$$

The quantity $N\pi(R_i+R_m)^2$ is the reciprocal of the mean free path L. Hence, at a pressure P_1 mm of Hg we have

$$Q_1=Q_0 \exp\left[-P_1x/760L\right].$$

With the same initial current Q_0 and a pressure P_2, we have

$$Q_2=Q_0 \exp\left[-P_2x/760L\right].$$

[4] R. B. Kennard, Phys. Rev. **31**, 423 (1928).
[5] I. W. Cox, Phys. Rev. **34**, 1426 (1929).
[6] J. S. Thompson, Phys. Rev. **35**, 1196 (1930).
[7] Otto Beeck, Zeits. f. Physik **61**, 251 (1930).
[8] R. E. Holzer, Phys. Rev. **36**, 1204 (1930).

Then

$$Q_1/Q_2 = \exp\left[x(P_2-P_1)/760L\right]$$

and

$$L = x(P_2-P_1)/(760 \ln Q_1/Q_2). \qquad (2)$$

Hence, by maintaining the emission current Q_0 constant and measuring the electrometer currents Q_1 and Q_2 of the ions passing through S_2, the mean free path L and effective cross section C may be computed at once.

The positive ions were obtained by heating an alkali-iron catalyst kindly supplied by Dr. Kunsman.[9] It was found that the materials, after being finely powdered and mixed with paraffin to act as a binder, would fuse nicely onto resistance wire. By winding the wire into a cone, it was possible to obtain a concentrated emission from a relatively large mass of material. After fusion to the coil, the catalysts were reduced in an atmosphere of hydrogen at about 400°C for a period of about five hours. Such a source was found to continue to emit very homogeneous ions after 200 hours of service.

The procedure in making measurements was as follows. The heating coil of the furnace was filled with material and reduced in hydrogen. The mass spectrograph was then evacuated, and after the impurities had been burned out of the furnace, the chamber was flushed with the gas to be studied. The chamber was then again evacuated, and the furnace heated to the proper temperature to yield a sufficient emission of ions, and run in this state for a number of hours before measurements were made. The rate of ion emission was measured by a galvanometer G, having a current sensitivity of 10^{-11} amp./mm. Eq. (2) depends upon the condition that the initial ion emission Q_0 remains constant. While this condition is difficult to obtain in practice, one may assume that, as long as the galvanometer current remains constant, Q_0 remains constant. This is true, provided the composition of the beam remains homogeneous, and if there is no spreading of the beam as the pressure in the chamber is raised.

After reducing the pressure to a low value, the magnet current was adjusted to bend the ions around the circle to S_2 and the rate of ion emission adjusted to give a large but readable electrometer current. After determining the electrometer current and corresponding pressure, the pressure was quickly raised to a higher value and the new pressure and corresponding electrometer current measured as before. In this manner, the electrometer and galvanometer currents were determined for from three to five different pressures. Several such runs were made for each accelerating potential. From each possible combination of two different pressures (P_2-P_1) in a given run a determination of the mean free path L was made. From the average L for a given accelerating potential, the effective cross section C was determined from the equation $C=1/(NL)$.

Discussion of Results

Kennard has pointed out that the type of collision between ion and molecule can, in general, be determined by the appearance of curves showing electrometer current against magnet current for various pressures. Three types of collision may occur. In case of pure neutralization, an ion is simply removed from the beam by collision; hence the maximum electrometer current occurs at the same field strength, but decreases in value as the pressure is raised, the base line remaining constant. In case of pure retardation, however, an ion is merely slowed up by collision, and may accordingly be brought back to the slit S_2 by weakening the field H. The maximum of the curve is thus shifted toward lower values of field strength without a decrease

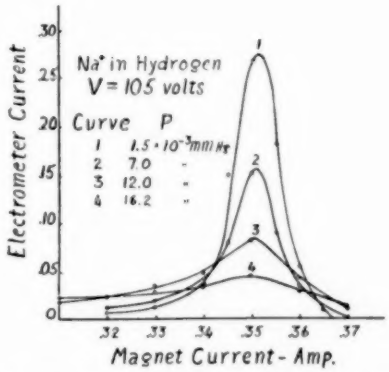

FIG. 2. Curves showing the relation between electrometer current and magnet current for 105 volt Na^+ ions in hydrogen. The essential factor involved is that of neutralization. The curves show, too, a small amount of retardation and small angle scattering.

[9] C. H. Kunsman, Science **62**, 269 (1925).

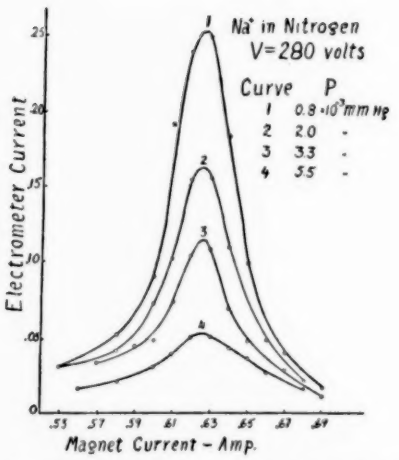

FIG. 3. The curves show the absorption of 280 volt Na^+ ions in nitrogen to be due to pure neutralization.

in area of the curve. If the collision results in scattering, however, there will occur a decrease in area of the curves and a symmetrical broadening of the base line to each side of the maximum, since the scattered ions may be deflected into the walls of the pole shoe. In case the collisions consist of two or more of these phenomena, the analysis of the phenomena is difficult to make. Fig. 2 shows such a set of curves for 105 volt sodium ions in hydrogen. From the appearance of the curves, it is apparent that the essential factor involved is that of neutralization. The curves show, too, a small amount of retardation and small angle scattering. This is in good agreement with a similar set of curves made by Kennard for the single accelerating potential of 455 volts. Fig. 3 shows a similar set of curves for Na^+ ions in nitrogen. Here we find a case of pure neutralization. In Fig. 4 we find the collisions between Na^+ ions in oxygen to result in both neutralization and small angle scattering.

Curves showing the variation of the mean free path of Na^+ ions in H_2, N_2 and O_2 are shown in Fig. 5. For 385 volt Na^+ ions in H_2, a mean free path of 15.8×10^{-5} cm was obtained. Kennard reports a mean free path value for 455 volt Na^+ ions in H_2 of 27×10^{-5} cm. Measurements made on his curves, however, show this value to be only 18.4×10^{-5} cm in excellent agreement with the determination made above. Unfortunately, Kennard's measurements were made for only one accelerating potential and his paper gives no data to support his measurement of 27×10^{-5} cm. It is probable, then, that his set of curves is correct but that his measurements, based upon the curves, are incorrect.

If the radius of the sodium ion be taken as that of the neon atom, data from viscosity measurements give $R_{Ne}=1.17\times10^{-8}$ cm and $R_{H_2}=1.09\times10^{-8}$ cm from which the kinetic theory mean free path L_0 is found to be 2.3×10^{-5} cm. From Fig. 5 it is seen that, as the accelerating potential decreases, the value of the observed mean free

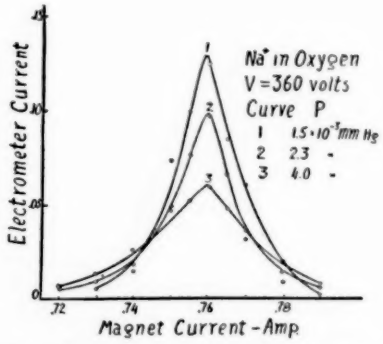

FIG. 4. The absorption of 360 volt Na^+ ions in oxygen is largely due to neutralization with some small angle scattering.

path also decreases, apparently approaching the kinetic theory value at zero accelerating potential.

The results for the mean free path of Na^+ ions in N_2 and O_2 for various accelerating potentials are also shown in Fig. 5. The closeness of the two curves came somewhat as a surprise to the author and, to make sure that avoidable errors in measurement had not been made, the curves were carefully rechecked, and found to be almost identical with the original ones. Care in obtaining pure gases was also observed. Oxygen and hydrogen were produced by electrolysis while nitrogen was obtained by heating a 10 percent solution of NH_4Cl and $NaNO_2$. The nitrogen gas was bubbled through NaOH before admission to the drying trains. The capillary leak gave continuous flow of the gases through the mass spectrograph, and the pressure was controlled by continuous pumping and adjustment of the leak. In this way, any foreign gas given off by the furnace was swept out as quickly as formed.

The closeness of the two curves is of special interest. Durbin, working with K^+ ions in H_2, N_2 and O_2, found the ratio of the observed mean free

path to the kinetic theory mean free path to decrease in the order stated, the values for nitrogen lying about halfway between those for hydrogen and oxygen. On the other hand, Ramsauer and Beeck,[10] working with the same combinations, report the absorption coefficients for the gases to increase in the order hydrogen, oxygen and nitrogen, the values for oxygen lying about halfway between those for hydrogen and nitrogen. These results for nitrogen and oxygen are, of course, contradictory. In the present work, it has been found that, within experimental error, the two curves for nitrogen and oxygen are practically identical. The present work supports the measurements of Durbin more than those of Ramsauer and Beeck. Perhaps the short life of the source of positive ions used by Ramsauer and Beeck and the necessity for rapid measurements mentioned in their paper is a cause of the discrepancy.

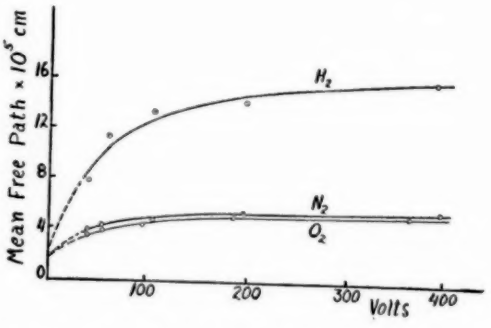

FIG. 5. The mean free path of Na^+ ions in the gases H_2, N_2, and O_2 decreases in the order stated for a given pressure and speed. The closeness of the two curves for N_2 and O_2 is of special interest. The mean free path for a given gas-ion combination decreases with an increase of the pressure of the gas and a decrease in speed of the ion. It approaches the kinetic theory value at zero accelerating potential of the ion.

[10] Ramsauer and Beeck, Ann. d. Physik **87**, 1 (1928).

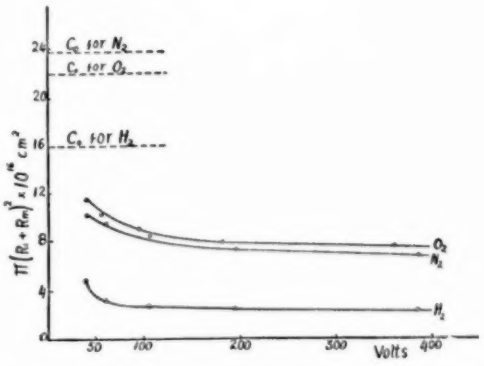

FIG. 6. The effective cross section of Na^+ ions with respect to H_2, N_2 and O_2. The curves turn sharply upward at speeds less than 50 volts and apparently approach kinetic theory values at zero accelerating potential.

Curves showing the variation of the effective cross section of Na^+ ions with respect to H_2, N_2 and O_2 are shown in Fig. 6. The effective cross sections were computed from the equation $C=1/LN$. It appears from the curves that the effective size of an ion depends not only upon its dimensions but upon its speed as well, and at high speeds it is capable of making many kinetic theory collisions without removal from the beam. Thus, 385 volt Na^+ ions are capable of making 6.8 kinetic theory collisions in hydrogen before being removed from the beam.

In conclusion the author wishes to acknowledge his indebtedness to Professor Mason E. Hufford under whose supervision the above investigation has been made and for his kindly interest and suggestions during the progress of the study.

Photographic Effects Produced by Cadmium and Other Elements Under Neutron Bombardment

J. G. HOFFMAN AND R. F. BACHER
Cornell University, Ithaca, New York
(Received September 2, 1938)

IT has been found that when a duplitized x-ray film has Cd placed next to it and is then surrounded by paraffin and exposed to a neutron source, the film shows blackening under the cadmium. Under these conditions the film also shows some general blackening which is rather weak. The neutrons used in these experiments were obtained by bombarding either Li or Be with about 10 microamperes of 1.2 Mev deuterons furnished by a cyclotron. There are, of course, also γ-rays incident on the Cd and the photographic film, and it was necessary to establish the blackening under the cadmium as due to slow neutrons and not to these radiations.

The photographic film was wrapped in heavy black paper to avoid exposure to light and a piece of Cd sheet was bent around the edge of the film so that the film was partially covered by Cd on both sides. It has been found that the Cd can be placed either outside or inside the black paper. Somewhat sharper images are produced with the Cd inside. Half of the film was then covered on both sides with paraffin and it was found that the blackening produced by the Cd was more intense under the paraffin. It is well known that the slow neutrons which are strongly absorbed in Cd are much more numerous in the paraffin. This is one indication that the photographic effect is due to slow neutrons. Several experiments have been carried out to test this point further. It has been found that appreciable photographic blackening can be obtained with thin Cd foils of thickness 0.0013 cm (0.011 g/cm^2). This indicates that the blackening is due to some action which has a large cross section in Cd. This fact also points to the slow neutron absorption. Furthermore, to test a neighboring element in the periodic table, the experiment was carried out with Sn, which gave little blackening compared to Cd. In order to test the origin of the photographic effect still further, the experiment was carried out in a cadmium box and under these conditions the blackening was greatly reduced.

Cd has been compared to various other elements, C, Al, Ni, Mo, Sn, W and Pb. The foils of these elements were compared in thicknesses which contained the same number of atoms per cm^2. These preliminary results indicate that there is some blackening produced by every element when so irradiated. This blackening increases with atomic number (elements which show strong artificial radioactivity are excluded) and is practically negligible for light elements and quite appreciable for Pb, though not nearly as strong as that produced by Cd. This blackening produced by other elements appears not to be a slow neutron effect since it is also produced in a cadmium box. In this connection it was observed that in the cadmium box, tin and cadmium behave in approximately the same way. It seems then, that the photographic effect produced by cadmium is due in part to some process which is not much different for neighboring elements but is mainly due to some action under slow neutron bombardment.

It has been found possible also to produce photographic blackening by the β-particles emitted by radioactive elements. Ag has been investigated in this respect and blackening produced by placing the Ag on the photographic film after the irradiation. Photographic blackening produced in this way by placing activated Ir next to a film, has been described by Groven, Govaerts and Guében.[1] In our experiments it was sufficient to leave the Ag next to the photographic plate for a few minutes only. Under these circumstances Ag naturally produces a considerable blackening when placed next to the plate and irradiated with neutrons. It is perhaps interesting to note that the blackening produced by thicknesses of Cd and Ag which contain the same number of atoms, produce comparable blackening if the

[1] Ch. Groven, J. Govaerts, G. Guében, Nature **141**, 916 (1938).

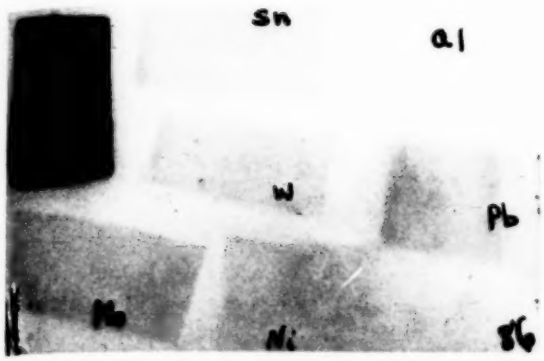

FIG. 1. Photograph taken with various thicknesses of Al, Ni, Mo, Cd, Sn, W and Pb containing the same number of atoms per cm². The sheets were placed on one side only of the photographic film and the film was then covered with paraffin on both sides. Exposure, 225 microampere minutes at 60 cm from Be target with 1.2 Mev deuterons. Cd thickness 0.028 cm.

radiators are removed at the end of a five-minute exposure. In the case of Cd, the radioactivity produced under short bombardment by neutrons is negligible, if any, and the effects produced cannot be explained in this way.

In order to determine the nature of the "radiation" from cadmium, which blackens the film, various absorption experiments have been carried out. With the Cd radiator a fixed distance from the film absorbers of C, Al and Ni which contain the same number of atoms per cm², have been used. Of these absorbers it is known that Al becomes artificially radioactive under slow neutron bombardment with a period of 2.36 minutes. This artificial radioactivity is apparently of no importance in this photographic work since it was continually observed that the blackening produced directly by the absorbers was negligible. Preliminary estimates indicate that there is little increase in the atomic absorption coefficient with atomic number. If the blackening were produced by electromagnetic radiation its atomic absorption coefficient would be expected to increase as Z^4. The small increase of the atomic absorption coefficient indicates that the blackening is produced by electrons. Furthermore, rough estimates of the absorption coefficient in aluminum indicate that the Cd "radiation" would have to be less than 20 kev and the "radiation" from lead less than 5 kev if electromagnetic in nature.

It seems unlikely that these electrons can come from any direct interaction with the neutrons. If they are produced as a result of nuclear neutron absorption, they may come either directly from a radioactive disintegration or from the internal conversion of the γ-rays emitted by the Cd nucleus or possibly by ejection of electrons from other atoms by these γ-rays. The large absorption of Cd for slow neutrons is not, however, known to be connected with any radioactivity. This point was examined briefly with cadmium in a cloud chamber, making the expansion just after the cyclotron beam had been cut off. No indication of a strong short period activity was found. This does not preclude the possibility of an extremely short period. For the other possibilities, it is well known that Cd sends off hard γ-rays under slow neutron bombardment and the possibility of electron ejection seems likely. From the increase and later decrease in blackening as the thickness of cadmium is increased, as well as from similar experiments in which part of the cadmium thickness was replaced by tin, it seems unlikely that the electrons are ejected from atoms other than the ones in which the γ-rays are produced. The possibility of internal conversion seems most likely since it is probable that some of the γ-rays produced when a Cd nucleus radiates energy upon neutron capture, are multipole radiation and the probability of internal conversion may thus be large.

In the case of the blackening produced by Pb and other elements it is likely that the mechanism is much the same, since, at least in the case of Pb, the "radiation" is probably electron in nature. In this case there is no strong absorption of slow neutrons and possibly the nuclear excitation is produced by the inelastic scattering of fast neutrons.

LETTERS TO THE EDITOR

Prompt publication of brief reports of important discoveries in physics may be secured by addressing them to this department. Closing dates for this department are, for the first issue of the month, the eighteenth of the preceding month, for the second issue, the third of the month. Because of the late closing dates for the section no proof can be shown to authors. The Board of Editors does not hold itself responsible for the opinions expressed by the correspondents.

Communications should not in general exceed 600 words in length.

The Transmission of Damped Electromagnetic Waves Through Small Hollow Metal Tubes

Barrow[1] and Southworth[2] have published experimental results on the transmission of progressive harmonic electromagnetic waves through hollow metal tubes. Theory and experiment agree that in order freely to transmit waves of the type studied through a given metal tube of circular section, the impressed frequency must exceed a certain frequency which is a characteristic of the wave type. For a tube of circular section filled with air the so-called H_1 magnetic wave[2] has the lowest critical frequency. This is given by $f=0.585c/d$, where c is the velocity of light in air and d is the internal diameter of the tube. Because of the necessity for producing oscillations of increasingly high frequency as the tube diameter is decreased, it has not been feasible thus far to observe the phenomenon in air-filled tubes of diameters much less than 15 cm. The writers have succeeded in extending the range of the observations by the simple expedient of employing spark-excited Hertzian doublets to produce damped oscillations. Such waves with wave-length as short as 1.8 mm have been reported.[3]

Upon trial it was found that damped waves were readily transmitted through metal tubes. Observations were made with tubes varying from 15 to 0.8 cm in diameter. A small doublet receiver with an iron pyrite crystal rectifier and microammeter was used for the detection of the transmitted waves and for the investigation of the wave pattern. In most cases it was found that the transmitted wave was definitely polarized in a manner characteristic of one component of the H_1 magnetic wave. It had been previously observed by one of the writers[4] in an analogous acoustic phenomenon that when the transmitting tube was made effectively elliptical a second quadrature component of the H_1 wave could be made to appear. In a tube with a diameter of 8.7 cm this phenomenon was also observed in the electromagnetic case. A quadrature component with maximum amplitude nearly as large as the direct component could be produced by inserting in the transmitting tube a copper rod 2.5 cm in diameter and skewed with respect to the tube axis.

It was found that it was not necessary for the fundamental frequency of the damped oscillator to be higher than the lowest critical frequency determined by the tube diameter, since the harmonics generated were sufficient strongly to excite the tube. Because of the filtering properties of the tube an estimate of the harmonics present in a given oscillator could be made by using a series of tubes with different diameters. Amplitude attenuation due to dissipation has not been observed, although this is to be attributed to the comparatively short tubes (700 cm) thus far employed.

HENRY E. HARTIG
ARTHUR W. MELLON

Institute of Technology, University of Minnesota,
Minneapolis, Minnesota,
September 29, 1938

[1] W. L. Barrow, Proc. I. R. E. **24**, 1298 (1936).
[2] G. C. Southworth, Bell Sys. Tech. J. **15**, 284 (1936).
[3] Nichols and Tear, Phys. Rev. **21**, 587 (1923).
[4] Hartig and Swanson, Phys. Rev. **54**, 618 (1938).

Wave Functions for $1s2s\ ^3S$ Li^+

It is well known that a variety of variational methods can be applied in the determination of atomic wave functions. The usual method is that of adjusting parameters in a judiciously chosen function so as to extremalize the energy E or energy error ϵ of this function to all variations of the parameters. An alternative method is that of minimizing the mean-square local energy deviation, $\delta^2=\int[(H-E)\psi]^2 d\tau$. James and Coolidge[1] have discussed the criteria of goodness of approximate wave functions and their bearing on the relative merits of functions obtained by these and other methods. They point out that the second of these methods tends to produce functions of more nearly correct form where the particles are near together, but with larger errors of slowly varying long-range type. The first of these facts suggests that for such a purpose as the deduction of nuclear magnetic moments from hyperfine structures it might be advantageous to use wave functions obtained by the second method. This indication is not conclusive, however, since the essential quantity is the relative probability of an electron appearing near the nucleus, which can be affected by errors anywhere in the function. We here present results from computations on the nuclear moment of Li^7 intended to test this idea.

Breit and Doermann[2] have represented the $1s2s\ ^3S$ state of Li^+ by the function $\psi=\varphi(kr_1, kr_2)$,

$$\varphi(r_1, r_2)=C\{(r_1-c)\exp[-ar_1/2-r_2/2] - (r_2-c)\exp[-ar_2/2-r_1/2]\},$$

in which the parameters a, c, k are adjusted to minimize ϵ. We have used the same function, but have instead minimized δ^2. A comparison of the results appears below, where ρ is the ratio of the computed electronic densities at the nucleus for $1s2s\ ^3S$ Li^+ and $1s\ ^2S$ Li^{++}. The limits on

q, the root-mean square error of the function, are computed by the methods of James and Coolidge. The unit of length is $a_H/9$.

	ϵ minimized	δ^2 minimized
a	0.380	0.3675
c	3.19	3.107
K	1.00162	1.00066
ϵ (ev)	0.049	0.064
β^2 (ev)^2	$(2.884)^2$	$(2.828)^2$
ρ	1.064	1.055
	$0.017 < q < 0.071$	$0.023 < q < 0.081$

Minimization of δ^2, it will be noted, is rather ineffective in reducing this quantity, and is associated with a relatively much larger increase in ϵ.

From the computed value of ρ and the observed hyperfine splitting of the state one can compute, according to the formulas of Breit and Doermann, the magnetic moment of the Li nucleus. Using the observational results of Granath[3] and the first value of ρ we obtain for Li^7 the magnetic moment 3.28 ± 0.03 nuclear magnetons, while with the second value of ρ we obtain 3.305 ± 0.03. (The estimated uncertainties arise principally from the uncertainties in ρ, as discussed by Breit and Doermann.) These values are to be compared with the value 3.265 ± 0.016 given by the new and completely independent method of Rabi and his co-workers.[4]

These results indicate that an attempt to improve the accuracy of the determination of the nuclear magnetic moment of Li by the h.f.s. method should be based on the determination of a more accurate wave function by the conventional variational method, rather than by minimization of δ^2.

HUBERT M. JAMES
F. L. YOST

Department of Physics,
Purdue University,
Lafayette, Indiana,
October 1, 1938.

[1] H. M. James and A. S. Coolidge, Phys. Rev. **51**, 860 (1937).
[2] G. Breit and F. W. Doermann, Phys. Rev. **36**, 1732 (1930).
[3] L. P. Granath, Phys. Rev. **42**, 44 (1932).
[4] I. I. Rabi, J. R. Zacharias, S. Millmann, and P. Kusch, Phys. Rev. **53**, 318, 495 (1938).

On Pre-Breakdown Phenomena in Insulators and Electronic Semi-Conductors

It is well known that insulators and electronic semiconductors display in high electric fields E (over 10^5 volts/cm for the former and a few thousand volts/cm for the latter) an increase of electrical conductivity which finally leads to breakdown, and which is approximately representable by $\sigma = \sigma_0 e^{\alpha E}$ (Poole's law). The fact that the illumination of an electronic semi-conductor results in an additional increase of the conductivity *independent of* E shows that the increase of electrical conductivity in intense fields is due to the increase of the number of free electrons, and not of their mobility.

This phenomenon can be explained very simply if the dielectric (or semi-conductor) is described not as a system of free electrons moving in a self-consistent periodic field of force, but simply as a system of neutral atoms. This refers, of course, to the normal state in which there are no free electrons. After the ionization of an atom, the electron can be described as moving freely in the surrounding medium consisting of neutral polarizable atoms and in the field of the remaining positive ion. Since this field is screened by the polarization of the surrounding atoms, the ionization energy must be decreased in the ratio $\epsilon : 1$ where ϵ is the electronic component of the dielectric constant (i.e., the square of the refractive index n for ordinary light).

In an external field E this energy is further decreased by a mechanism similar to that of the Schottky effect in the thermoelectronic emission from metals. In Fig. 1 the

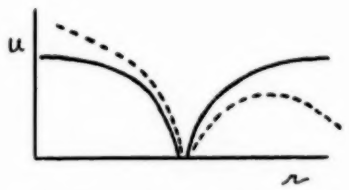

FIG. 1. Potential energy as a function of distance from the positive ion. Full line, without an external field, dotted line in the presence of the field.

full line represents the normal potential energy of the electron as a function of the distance from the positive ion while the dotted line represents the same quantity in the presence of the field. The height of the potential barrier is lowered in the field by the amount

$$\Delta U = eEr_0 + e^2/\epsilon r_0,$$

where r_0, the distance to the maximum from the ion, is given by $e^2/\epsilon r_0^2 = eE$. Thus $r_0 = (e/\epsilon E)^{\frac{1}{2}}$ and

$$\Delta U = 2eEr_0 = 2e(eE/\epsilon)^{\frac{1}{2}}.$$

Now if, in the absence of the electric field, the number of free electrons due to the *thermal* ionization of the atoms, is proportional to $\exp(-U_0/2kT)$, where U_0 is the ionization energy (decreased in the ratio $\epsilon : 1$ compared with an isolated atom), the electrical conductivity in the presence of the field will be proportional to

$$\exp[-(U_0 - \Delta U)/2kT].$$

We thus obtain

$$\sigma = \sigma_0 \exp[(e^3E/\epsilon)^{\frac{1}{2}}/kT],$$

differing from Poole's law by the substitution of $E^{\frac{1}{2}}$ for E.

This is in excellent quantitative agreement with the experiments of P. Granovskaja[1] on the electrical conductivity of mica in intense fields (over 10^6 volts/cm) as well as with the (still unpublished) experiments of Joffé on the pre-breakdown phenomena in electronic semi-conductors (up to field strengths of the order of 50,000 volts/cm). It is interesting that on the above theory the effect of the field is *reduced* by the elevation of the temperature, just as is observed experimentally. It should be mentioned that with $E = 10^6$ volts/cm, and $n = 2$, the distance r_0 is of the order of 30A; i.e., about ten times the interatomic distance. At smaller distances the electron is therefore still

attached to the parent ion, just as if there were no neutral atoms between them.

It can be shown that the mechanism of facilitated thermal ionization described above is more effective, both for dielectric and semi-conductors, than the mechanism of electrostatic ionization, which gives an additive (and not a multiplicative) effect proportional to

$$\exp\left[-4\pi(2m)^{\frac{1}{2}}U_0^{\frac{3}{2}}/heE\right]$$

unless the temperature falls below 50–60°K for insulators, or below a few degrees for semi-conductors. Further details of the theory will be published in *Technical Physics* of the U. S. S. R.

J. FRENKEL

Leningrad, U. S. S. R.
August 10, 1938

[1] P. Granovskaja, Physik. Zeits. der Sowjetunion.